ELECTROSPUN NANOFIBROUS PATCHES FOR THE DELIVERY OF CARDIAC-DERIVED C-KIT+ CELLS

A Dissertation
Presented to
The Academic Faculty

by

Benjamin William Streeter

In Partial Fulfillment
of the Requirements for the Degree
Doctor of Philosophy in the
Wallace H. Coulter Department of Biomedical Engineering

Georgia Institute of Technology & Emory University
December 2021

ELECTROSPUN NANOFIBROUS PATCHES FOR THE DELIVERY OF CARDIAC-DERIVED C-KIT+ CELLS

Approved by:

Dr. Michael E. Davis, Advisor
School of Biomedical Engineering
Georgia Institute of Technology & Emory University

Dr. Rebecca Levit
School of Medicine
Emory University

Dr. Younan Xia
School of Chemistry and Biochemistry
Georgia Institute of Technology

Dr. Joshua Maxwell
School of Medicine
Wake Forest University

Dr. Johnna Temenoff
School of Biomedical Engineering
Georgia Institute of Technology & Emory University

Date Approved: 11/01/2021

To my mom and dad, thank you for always being there for me and for always supporting me. Thank you for being great examples of how to live life with conscientiousness, kindness, and joy. I love you both.

ACKNOWLEDGEMENTS

There is no way I would've made it through my time in graduate school without the help of many incredibly caring and intelligent people. I first want to thank my advisor, Dr. Michael Davis. Mike was a match made in heaven for me as an advisor, and he constantly provided support while also giving me the freedom to use my time and scientific curiosity in a way that was best for my development as a scientist. I also want to thank my committee members, Dr. Johnna Temenoff, Dr. Rebecca Levit, Dr. Younan Xia, and Dr. Joshua Maxwell for providing thoughtful and insightful feedback on my project that really helped propel it forward and improved it tremendously.

I also would like to thank the advisors and mentors from my past who inspired me and helped me become the researcher I am today. Thank you to Dr. Gregory Underhill and Dr. Kerim Kaylan from the University of Illinois, to Dr. Jeanne Loring and Dr. Ronald Coleman from the Scripps Research Institute, and to Dr. Giovanna Tosato and Dr. Lisa Ritchey from the National Institutes of Health. You all taught me so much during my undergraduate years and continued to support me during my time as a graduate student. I want to give a special thank you to my high school biology teacher, Mr. Scott Lynn, who was the first person that truly inspired me to pursue science and whose class was one of the most enjoyable educational experiences I have ever had.

I am incredibly lucky to have the support system I have around me and want to thank everyone who has been a part of that system. To my lab mates past and present, Aline, David, Matt, Don, Sruti, Preety, Farnaz, Hyun-Ji, Jess, Kenneth, Olga, Arun, and Kimmai, thank you for always being delightful to be around, for talking reality TV with

me, and for always lending a helping a hand whenever experiments weren't working. I want to give a special thank you to our lab manager, Milton, who would do his absolute best to fix any problem I came to him with and who was instrumental in all of my animal experiments.

I want to also thank the friends I have made during my time as a graduate student, especially Andy, Mahir, and Steph. Thank you for always giving me something to look forward to on the weekend and always being there to get a beer with me to help forget an experiment gone wrong or to celebrate a big milestone. I also want to thank my friends both from back home in Morton, Illinois, and from my time at the University of Illinois. Mike and Ryan, thank you for your friendship and for being my partners in crime on group projects; I wouldn't have gotten through BIOE without you guys. Chmiel, Danny, Sam, Jake, Pelz, and Nick, thank you for always being there to make me laugh after a long night in the library. Mark, Tom, Joseph, and Christian, thank you for being the best friends I could've asked for, for always having my back, and for sticking with me through all these years. Thank you also to one of the best parts of my support system and my life, my wonderful girlfriend Mary (and our dog Gracie). Thank you for being a constant bright spot in my life and always supporting me, even when the Vols lose.

Finally, I want to thank my family for their constant support and for giving me a comfort and safety that I have carried with me my whole life. Sam, thank for being a great little brother and one of my best friends. Your hard work and kindness are a huge inspiration, and I'm so proud of the person you've become. Dad, thank you for always being a steady presence in my life and for always being a person I know I can turn to when I need help or advice. Whether it's helping with car trouble or just talking college

basketball, I know that you'll always be there to pick up the phone when I call. Mom, thank you for being so caring and being a person that I know will always be there for me no matter what the circumstances. I can't thank you enough for the comfort I get from knowing that someone is always looking out for me and for all the love that you give to me.

TABLE OF CONTENTS

LIST OF TABLES

LIST OF FIGURES

LIST OF SYMBOLS AND ABBREVIATIONS

ANG1	Angiopoietin 1
ANOVA	Analysis of Variance
ASD	Atrial Septal Defect
ATP	Adenosine Triphosphate
bFGF	Basic Fibroblast Growth Factor
BMMNC	Bone Marrow-derived Mononuclear Cell
CHD	Congenital Heart Disease
CM	Cardiomyocyte
CM	Conditioned Media
COL1A1	Collagen Type 1 Pro-α1 Chain
CPC	Cardiac-derived c-Kit^{+} Cell
CPC^{high}	High Reparative Capacity CPC
CPC^{low}	Low Reparative Capacity CPC
CTGF	Connective Tissue Growth Factor
DAPI	4′,6-Diamidino-2-Phenylindole
EC	Endothelial Cell
ECM	Extracellular Matrix
EHT	Engineered Heart Tissue
ESC	Embryonic Stem Cell
EV	Extracellular Vesicle
FFT	Fast Fourier Transform
FN	Fibronectin

Gel	Gelatin
HGF	Hepatocyte Growth Factor
HLHS	Hypoplastic Left Heart Syndrome
HSF1	Heat Shock Factor 1
HUVEC	Human Umbilical Vein Endothelial Cell
IB4	Isolectin B4
IL-2	Interleukin-2
iPSC	Induced Pluripotent Stem Cell
ITGAV	Integrin Subunit Alpha V
KI	Knock-in
KO	Knockout
LA	Left Atrium
LV	Left Ventricle
MI	Myocardial Infarction
miRNA	microRNA
MMP	Matrix Metalloproteinase
mRNA	Messenger RNA
MSC	Mesenchymal Stem Cell
PA	Pulmonary Artery
PAB	Pulmonary Artery Band
PBS	Phosphate Buffered Saline
PCL	Polycaprolactone
PDA	Patent Ductus Arteriosus
PDMS	Polydimethylsiloxane
PGS	Poly(Glycerol Sebacate)

PLGA	Poly(Lactic-co-Glycolic)
RA	Right Atrium
RCF	Rat Cardiac Fibroblast
RT-PCR	Reverse Transcriptase Polymerase Chain Reaction
RV	Right Ventricle
RVFAC	Right Ventricular Fractional Area Change
RVHF	Right Ventricular Heart Failure
RVWT	Right Ventricular Wall Thickness
SDF1	Stromal Cell-derived Factor 1
SEM	Scanning Electron Microscopy
siRNA	Small Interfering RNA
SIS	Small Intestinal Submucosa
SkMB	Skeletal Myoblasts
SMC	Smooth Muscle Cells
SSEA1	Stage-specific Embryonic Antigen 1
TAPSE	Tricuspid Annular Plane Systolic Excursion
TCP	Tissue Culture Plastic
TGF-β	Transforming Growth Factor Beta
TOF	Tetralogy of Fallot
UCB	Umbilical Cord Blood
VEGF	Vascular Endothelial Growth Factor
VIM	Vimentin
VSD	Ventricular Septal Defect
WGA	Wheat Germ Agglutinin

SUMMARY

Congenital heart disease (CHD) affects 8 in 1000 live births and is the number one cause of birth defect-related deaths. Current treatment is surgical correction of the abnormality, but these surgeries are often only palliative and lead to right ventricular heart failure (RVHF). One promising avenue to restore the contractile function of the right ventricle is cardiac cell therapy. However, cell injection is hampered by low cell retention and survival following injection into the heart. Additionally, autologous cell therapy for CHD may suffer from patient-to-patient variability in cell efficacy. To combat these issues, therapeutic cells can be combined with biomaterials that serve as a delivery vehicle to enhance cell survival and modulate reparative paracrine release *in vivo*. The aim of this dissertation is to combine electrospun nanofibrous polycaprolactone (PCL) scaffolds and cardiac-derived c-Kit^{+} cell (CPCs) to create an epicardial cardiac patch. We investigate the effects of PCL fiber alignment and inclusion of extracellular matrix (ECM)-mimicking adhesion factors gelatin and fibronectin on CPCs from different donors and develop patient-specific cardiac patches capable of restoring RV function in a rat model of RVHF.

CHAPTER 1. INTRODUCTION

1.1 Motivation

Congenital heart disease (CHD), which occurs at 8 out of every 1000 live births, is the most common group of congenital abnormalities and the leading cause of birth defect-related death[1–3]. The current gold standard of treatment is surgical palliation of the defect to improve the function of the heart. However, surgery often leads to hemodynamic changes to the heart, which often can result in impaired right ventricular (RV) function and co-morbidities, with many patients requiring heart transplantation later in life[4]. Cell-based, regenerative therapies have emerged as an alternative strategy to treat RV dysfunction brought about by surgical palliation[5–7]. Previous studies have found cardiac-derived c-Kit$^+$ cells (CPCs) to be a potential candidate for use in pediatric cardiac therapies[8–11] due to their release of reparative paracrine effectors, including growth factors and exosomes[12–14]. One major drawback of autologous cell therapy is patient-to-patient variation in cell quality. There is also low cell retention in the host tissue following cell therapy, with only 0.1−10% of the injected cells being successfully grafted to the myocardium[15–17]. If paracrine therapy is to be sustained over longer periods of time, novel methods are needed to support cell retention while enabling function in a patient-specific manner.

In order to enhance cell retention and maximize reparative paracrine secretion, cells are often incorporated into supportive material scaffolds to form therapeutic cardiac patches[18,19]. Thus, the objective of this dissertation is to develop a cardiac patch capable of treating the diseased RV. We hypothesized that patches composed of electrospun polycaprolactone (PCL) nanofibers and pediatric patient-derived CPCs can improve

cardiac function in a rat model of RVHF. Further, we investigated the effects of fiber alignment and inclusion of gelatin and fibronectin in our PCL scaffolds and hypothesized that these changes will affect CPC reparative capacity in a patient-specific manner. We tested these hypotheses by accomplishing two different specific aims.

1.2 Specific Aims

Aim 1: To determine the CPC age-dependent effects and underlying mechanisms of PCL patch parameters on CPC behavior and reparative capacity.

PCL nanofibrous scaffolds were fabricated using electrospinning, and their mechanical properties were characterized using tensile testing, scanning electron microscopy (SEM), and water droplet contact angle testing. CPCs isolated from neonatal and child patients were then initially cultured on either aligned or random electrospun PCL nanofibers for 7 days. CPCs were also cultured on random or aligned scaffolds that included gelatin, fibronectin, or both factors. CPC alignment and morphology on each patch was assessed after 7 days in culture. CPC metabolism was measured using an alamarBlue® assay at days 1, 3, and 7. To assess paracrine release from the patches, patch conditioned media was collected after 2, 3, 5, and 7 days in culture. Angiogenic and anti-fibrotic potential of patch conditioned media collected after 2 and 5 days was measured. A Luminex® assay was then performed on patch conditioned media collected after 3 and 7 days to identify reparative growth factors secreted from each patch.

We hypothesized that CPCs that are low in reparative capacity benefitted from culture on PCL patches with fibronectin (PCL + FN). To elucidate the mechanism of this benefit, partial least squares regression and linear regression modeling was used to identify

an integrin (α_V) in CPCs whose binding to fibronectin on the patch surface led to improved CPC function. CPCs from four different donors (896, 903, 924, 956), one of which (patient 956) was high in expression of α_V integrin and low in reparative capacity, were then cultured on PCL and PCL + FN patches. Endothelial marker and cardiac transcription factor transcript expression was measured using RT-PCR for each CPC patient following 3 days in culture on PCL and PCL + FN patches. The conditioned media from these different patches was also collected after 3 days, and the angiogenic and anti-fibrotic paracrine release from each patch was measured. To confirm that α_V integrin expression was responsible for improved CPC performance on PCL + FN patches, α_V integrin was knocked down in patient 956 CPCs on PCL + FN patches using siRNA transfection, and the same conditioned media experiments were performed. The α_V integrin was also overexpressed in CPCs that had inherently low α_V integrin expression (patient 896) using plasmid transfection, and CPC angiogenic and anti-fibrotic paracrine release on PCL + FN patches was again assessed.

Aim 2: To determine if a PCL/CPC patch implanted onto a failing RV improves cardiac function.

Patches were implanted onto the epicardium of juvenile athymic rats with RVHF induced through pulmonary artery banding (PAB). Our first study used patches composed of pooled lines of neonatal or child CPCs and scaffolds made of only aligned or random PCL nanofibers. The next study used patches composed of PCL or PCL + FN scaffolds loaded with CPCs from patient 956. Control groups with animals receiving a sham PAB surgery, PAB animals receiving a sham patch surgery, PAB animals receiving a cell-only injection, and PAB animals receiving cell-free patches were also assessed. Animals

received treatment at 2 weeks post-PAB, and longitudinal echocardiographic measurements taken just before PAB surgery, and at 2, 4, and 6weeks post-PAB were used to assess functional improvement. At 4 weeks post-patch implantation, histological analysis to determine fibrosis, myocyte hypertrophy, and angiogenesis were performed.

1.3 Significance

In Aim 1, we tested eight different formulations of electrospun PCL nanofibrous scaffolds as a potential delivery vehicle for neonatal and child CPCs. The preliminary results from this study informed our computational analysis later in Aim 1 that led to the discovery of α_V integrin as a mediator of improved CPC function on PCL + FN patches. With this knowledge, we were able to design a cardiac patch with the proper biomaterial formulation, PCL + FN, and a suitable CPC donor, patient 956, that was be able to improve function following implantation onto the failing RV. This study is one of the few studies that, rather than focusing on the left ventricle, develops cardiac patches for treating RVHF, and, to our knowledge, is the first study that does so in a patient-cell-specific manner. The outcomes presented here set the stage for possible translation to larger animal models of RVHF and future clinical use. Additionally, the framework outlined in this work can be used to better design cardiac biomaterials for delivering autologous cell populations to treat ventricular failure. In total, this study uncovers new insights about mechanisms of pediatric cardiac cell therapy and develops a cardiac patch that can be used to treat RVHF like that seen in CHD patients.

CHAPTER 2. LITERATURE REVIEW

2.1 Congenital Heart Disease

Congenital heart disease (CHD) is characterized by malformations of the heart at birth. CHD occurs in roughly 1% of all live births, making it the most common form of congenital disease[20,21]. Further, CHD is the leading cause of birth defect-related death[21]. However, due to surgical advances in recent years, CHD patients with both simple and complex forms of the disease have experienced improved outcomes and survival[22,23]. Still, CHD patients who receive care early in life may still experience complications associated with CHD later into adulthood, requiring further treatment and intervention[24]. In this section, we review common forms of CHD, current surgical methods of treatment and their associated outcomes, and the right ventricular heart failure (RVHF) that can occur in more complex forms of the disease.

2.1.1 Common Forms of Congenital Heart Disease

2.1.1.1 Septal Defects

Atrial (ASD) and ventricular (VSD) septal defects are the most common forms of CHD and occur when holes are present in the barrier (septum) separating the left and right sides of the hearts[21,25]. Together, ASDs and VSDs account for close to 40% of the CHD cases in the United States[21]. ASDs often result in left to right shunting of blood flow, leading to mixing of oxygenated and deoxygenated blood and, if left untreated, can lead to volume overload in the RV and right atrium (RA) as well as the pulmonary arteries[25]. Further, the volume and subsequent pressure overload in the right side of the heart can lead

to a septal shift towards the left ventricle (LV), leading to a D-shape geometry in the LV rather than the normal circular geometry[26]. These changes can lead to diminished LV filling and systemic output, which can lead to LV dysfunction if the defect is large enough[27]. Unrepaired ASDs can lead to increased risk of RVHF, stroke, and pulmonary hypertension[28]. VSDs, in contrast, do not lead to enlargement of the RV even though left to right shunting still occurs. VSDs in adults are often either not large enough to cause major complications or have been repaired earlier in life. As a result, the long-term prognoses of VSD patients are often very good with patients requiring little further intervention[25,29]. If septal defects require closure, surgery to close the hole by either a suture or a pericardial or synthetic patch is often performed[30]. When isolated ASDs are surgically treated before the age of 25, there is almost no difference in survival rate to control populations, with 98% surviving when the repair takes place when the patient is younger than 12 years-old and 93% surviving when the patient was operated on between 12 and 24 years-old[31].

2.1.1.2 Patent Ductus Arteriosus

A patent ductus arteriosus (PDA) is a piece of vasculature that connects the aorta to the roof of the pulmonary artery (PA)[32]. It is the third most common form of CHD, accounting for 14% of all CHD cases[21]. The PDA is a fetal structure that normally closes spontaneously within the first few weeks of life after birth. However, if it remains attached to the PA, left-to-right shunting can occur leading to pulmonary overcirculation. The increased flow returning to the heart from the pulmonary circulation then results in enlargement of the LV and left atrium (LA) as well as increases in end-diastolic pressures in the left heart. The LV then compensates to the volume and pressure overload by

increasing stroke volume, which at times can lead to hypertrophy[32]. Even with this left-to-right shunting in the PDA, patients with small shunts usually have normal long-term prognoses[25]. Patients with large enough shunts, though, may develop congestive heart failure, atrial arrythmias, and pulmonary hypertension[25,33]. For patients who require closure of the PDA, transcatheter closure is the preferred form of treatment. A catheter is advanced to the deliver a closure device to occlude the ductus and prevent flow. If transcatheter closure is not feasible, surgery is performed to ligate and close the PDA, restoring the normal path of circulation[32].

2.1.1.3 Tetralogy of Fallot

Tetralogy of Fallot (TOF) is the most common complex form of CHD, accounting for 6-7% of all CHD cases[21]. TOF is a defect made up of 4 different abnormalities in the heart: RV outflow tract obstruction, a VSD, overriding of the aorta, and RV hypertrophy. RV outflow tract obstruction can be caused by thickening of muscle near the pulmonary valve as well as a stenotic or hypoplastic pulmonary valve, leading to reduced blood flow to the lungs. Overriding of the aorta refers to the fact that the aorta is positioned further to the right and directly over the VSD. The blood delivered to the systemic circulation is a combination of oxygenated and deoxygenated blood due to this combination of defects. Finally, the RV experiences hypertrophy to compensate for the increased pressure caused by obstruction of the RV outflow tract[34]. Other anatomical variants of TOF exist[35], but to treat the most common form of TOF discussed here, surgery is performed at 3 – 6 months old. During this surgery, the VSD is closed with a patch to restore a normal path of circulation in the heart. The RV outflow tract obstruction is also repaired during surgery by removing thickened muscle below the pulmonary valve and either dilating or inserting

a transannular patch to repair the narrowed pulmonary valve[34]. Long-term outcomes for patients receiving surgery are excellent, but problems can arise due to pulmonary valve regurgitation caused by the implanted transannular patch. This may cause exercise intolerance, ventricular arrythmias, and increased risk of sudden death[36,37]. In adulthood, chronic pulmonary regurgitation may lead to RV dilation and subsequent RV failure. As a preventative measure, the pulmonary valve may be replaced with a tissue valve to restore normal valve function and stop the progression of RV dilation[34].

2.1.1.4 Hypoplastic Left Heart Syndrome

Despite accounting for only 2% of CHD cases, hypoplastic left heart syndrome (HLHS) is responsible for 23% and 15% of cardiac deaths during the first week and first month of life, respecitvely[38]. In HLHS, the left side of the heart is unable to support the systemic circulation, and as is true with TOF, several phenotypic variants of HLHS exist[39]. The most common form of HLHS, though, typically is a combination of four different defects: an underdeveloped LV with a thickening of the LV myocardium and small cavity size, a PDA, an ASD, and an underdeveloped aorta[40,41]. Because of the present of the PDA and the ASD, pulmonary and systemic return mix in the heart and then can be pumped out of the heart by the RV. However, if left untreated, the PDA will close soon after birth, and the dysfunctional LV will not be able to provide sufficient force to drive systemic circulation[40].

In this typical case, a three-stage surgical palliation is typically performed to reroute circulatory pathways. In the first step that is performed shortly after birth, the Norwood procedure, the remaining atrial septum is removed to allow complete flow of venous return

to the RV. The aorta is also reconstructed and a shunt from this newly constructed aorta to the pulmonary artery is implanted so that the RV ejects into the systemic circulation[42]. In stage two, performed at 4-6 months of age, the shunt constructed during the Norwood procedure is replaced with the so-called bidirectional Glenn shunt that connects the superior vena cava to the branch pulmonary arteries[43]. The Glenn shunt directs systemic venous return from the superior vena cava directly to the lungs, bypassing the heart. In the third and final stage, the Fontan procedure, the inferior vena cava is connected to the pulmonary arteries, leading to total bypass of the returning systemic circulation from the heart[44]. Following the Fontan procedure, the RV is now the sole pumping source for the entire body, pumping blood directly to the systemic circulation which is completely connected in series to the lungs.

Survival following the Fontan procedure is between 63% and 74% during the first year of life, and those children that survive to one year of life have a long-term survival of close to 90%[45]. However, several complications and comorbidities are often present later in life for Fontan patients. In one longitudinal study of Fontan patients, about 40% of them had heart failure at 15.7 years following surgery[46]. Further, hepatic dysfunction is almost universal in Fontan patients due to higher venous pressure and hypoxic tissue from decreased cardiac output[47]. In one multicenter study, 94% of Fontan patients had at least one abnormal liver-related finding with 99% having sinusoidal dilation[48]. Other comorbidities that have been observed in Fontan patients are arrythmias[49], pulmonary hypertension[50], plastic bronchitis[51], protein losing enteropathy[52], and thromboembolic events[53].

2.1.2 Right Ventricular Heart Failure in Congenital Heart Disease

2.1.2.1 Physiological Changes in RVHF

In contrast to the ellipsoidal LV, the RV has a complex shape that appears triangular from a side view and crescent-shaped from a cross sectional view[54]. Despite having about one sixth of the mass of the LV, the RV has a stroke volume nearly equal to that of the LV[55]. Under normal hemodynamic conditions, the RV is exposed to much lower impedance and pressures than the LV due to the lower resistance of the pulmonary circulation[56]. However, hemodynamic changes induced by anatomical changes from either surgery or CHD itself results in abnormal loading on the RV. Volume overload occurs often in CHDs with significant left-to-right shunting, such as ASDs, and when pulmonary valve regurgitation is present like following repair of TOF[57]. Increased pressure loading in patients with conditions such as pulmonary valve stenosis or RV outflow tract obstruction can also contribute to the development of RVHF. Further, arrythmias and dyssynchrony between electrical propagation and subsequent mechanical contraction is present in many forms of CHD. In conditions such as HLHS and corrected transposition of the great arteries, a systemic RV is responsible for all cardiac output and as a result may undergo a combination of these different hemodynamic changes[58].

2.1.2.2 Cellular Mechanisms of RVHF

The hemodynamic changes discussed above lead to RV remodeling and several changes at the cellular level that can result in the development of RVHF. Major metabolic changes occur in the RV in response to both pressure and volume overload. In response to these overloads, a metabolic switch occurs in the RV in which glucose metabolism becomes the preferred source of ATP generation rather than fatty acid metabolism that is

used preferentially under normal conditions[59]. While fatty acid metabolism yields more ATP, glucose metabolism requires less oxygen, making it favorable when metabolic demand is high and myocardial hypertrophy occurs[59,60]. Although effective in the short term, dependency on glucose metabolism in the long term is not sufficient to meet the energy demands of the RV, leading to energy starvation and contributing to RVHF[61].

In addition to metabolic changes, other maladaptive responses occur in response to abnormal loading in the RV. For example, ischemia can develop in response to stress more readily in the RV than LV. In pulmonary artery band (PAB) models of RV pressure overload, there is a marked decrease in both VEGF and no increase in capillary density to compensate for the hypertrophy of the RV[62,63]. The resulting decrease in coronary prefusion in the RV exacerbates ischemic conditions leading to the metabolic shift to glycolysis discussed above and the subsequent cascade of energy starvation and eventual RVHF[64]. The RV may also experience neurohormonal dysfunction in adrenergic receptors and in the renin-angiotensin-aldosterone system, the latter of which can lead to myocardial fibroblast stimulation and subsequent increases in myocardial fibrosis[65,66]. Other maladaptive responses to abnormal loading in the RV include adverse electrical remodeling, production of mitochondrial reactive oxygen species without increases in antioxidants in response to oxidative stress, and changes in microRNA expression (miRNA) that exacerbate many of the processes described here[65]. The combination of these dysfunctional changes makes RVHF in CHD a complex process that is difficult to treat. There is therefore a need for alternatives to conventional therapies that can address the underlying mechanisms of RVHF and improve RV function.

2.2 Cell Sources for Cardiac Cell Therapy and Cardiac Patches

One promising avenue to help treat RVHF is the use of cell therapy, administered by injection or cardiac biomaterials. Many of these strategies have been investigated for treating LV dysfunction brought about ischemic events such as myocardial infarction (MI) but may also be applied to treat the failing RV. It is estimated that cardiomyocyte (CM) turnover in the human heart is only about 0.5% to 2%[67]. Although this rate may increase following injury[68], endogenous CM renewal is not sufficient to restore contractile function after a major cardiac event such as MI. Cells from many different sources have been investigated to both replace lost CMs in the native heart as well as to galvanize cardioprotective events through paracrine signaling following their implantation[69]. Cell sources used in cardiac cell therapy include skeletal myoblasts, bone marrow-derived cells, mesenchymal stem cells, embryonic stem cells, induced pluripotent stem cells, and cardiac stem cells[70,71]. In this section, we review previous work that has utilized these different cell sources to treat the failing heart and highlight important preclinical and clinical findings.

2.2.1 Skeletal Myoblasts

The first clinical study investigating cell therapy for myocardial repair was published in 2001 by Menasché et al. The authors delivered autologous skeletal myoblasts (SkMBs) to a MI patient. Several SkMB injections were administered in and around sites of necrosis on the LV wall, and the patient's contractile function improved upon a 5-month follow-up[72]. The same group performed a much larger clinical trial in MI patients, The Myoblast Autologous Grafting in Ischemic Cardiomyopathy Trial, in 2011, but found that SkMB injection showed no improvement in cardiac function compared to a placebo control injection. Additionally, a greater number of arrythmias were reported in patients receiving SkMB patients [73]. Further pre-clinical research investigating SkMBs' potential as a

therapeutic cell type for myocardial repair has focused on *ex vivo* engineering of SkMBs to prevent arrhythmic events upon implantation and to improve their reparative paracrine signal secretion. SkMBs do not naturally express the gap junction protein connexin 43 that CMs use to propagate electrical signals through the myocardium. Therefore, several studies have investigated overexpressing connexin 43 in SkMBs to enhance electrical coupling and engraftment to host CMs. These studies have shown that this strategy leads to attenuation of arrythmias and improvement in ventricular function following treatment with connexin-43-overexpressing SkMBs[74–76]. SkMBs have also been used in tissue engineered constructs to produce functional tissue and production sources of reparative paracrine signals. Both Blumenthal et al and Siepe et al used polyurethane-based scaffolds seeded with SkMBs as a cardiac patch that was implanted onto the epicardium of MI animal models. Further, the SkMBs used in these constructs overexpressed the pro-survival gene AKT1. Implantation of these patches led to increased angiogenesis and reductions in infarct size[77,78]. Recently, scaffold-free SkMB cell sheets have been shown in clinical trials to decrease arrythmias, improve LV injection fraction, and increase angiogenesis in ischemic and dilated cardiomyopathy[79,80]. The results from these studies suggest that the use of SkMB cell sheets and SkMB-based tissue-engineered patches may circumvent some of the safety and efficacy issues that plagued earlier injection-based trials and may make them more successful in larger clinical studies.

2.2.2 Bone Marrow-derived Cells

Bone marrow-derived mononuclear cells (BMMNCs) are a heterogeneous group of cells composed of several cell types including hematopoietic progenitor cells, bone marrow mesenchymal cells, and monocytes[81]. They have been studied extensively as a candidate

to regenerate and repair the damaged myocardium and, to date, are the cell type most used in cardiac cell therapy clinical trials. The first clinical application of BMMNCs took place in 2001, when Strauer et al. delivered BMMNCs to an acute MI patient via intracoronary injection. At follow-up ten weeks later, the patient had a reduced infarct area and improved cardiac function[82]. This study set the stage for several other clinical trials that later used BMMNCs to treat acute MI, including the BOOST[83] and TIME[84] trials, and subsequent follow-ups to these trials, BOOST-2[85] and LateTIME [86]. Additionally, BMMNCs have been used in clinical trials to restore myocardial function in other cardiac disorders including ischemic cardiomyopathy[87–91] and dilated cardiomyopathy[92–95] along with others focused on addressing acute MI similar to the BOOST and TIME trials[96]. Although many of these studies report modest improvement in LV function following BMMNC injection in certain areas, these results have not often translated to improvement in clinically meaningful outcomes[97]. Because of this, other research efforts have been driven toward modifying BMMNC therapy through enhanced delivery methods. One previous study by Lin et al used self-assembling peptide nanofibers to increase BMMNC retention following injection and showed improved systolic and diastolic function in pig models of MI[98]. BMMNC populations have also been enriched by sorting cells for the stem cell marker c-Kit, and this enriched cell population has been modified via tissue and genetic engineering methods to enhance the bone marrow-derived c-Kit$^+$ cells' efficacy[99,100].

2.2.3 Mesenchymal Stem Cells

Mesenchymal stem cells (MSCs) are multipotent fibroblast-like cells have the ability to differentiate into osteoblasts, adipocytes, and chondroblasts[101]. MSCs can be derived from many different organ and tissue sources in the body, but the most common

sources are bone marrow and adipose tissue. They are an attractive cell source due to their immunoprivileged nature, as they lack major histone compatibility complex class II markers and due to their many pro-reparative functions including attenuating fibrosis, enhancing angiogenesis, and kickstarting endogenous cardiac repair mechanisms[102]. Because MSCs have limited retention at target sites when injected[103], these functional improvements are often attributed to the secretion of paracrine effectors[104].

MSCs are the most commonly used cell type in preclinical cardiac tissue engineering studies, and several clinical trials have been conducted investigating MSCs as a feasible and efficacious cell source for cardiac cell therapy[70]. The POSEIDON trial conducted by Hare et al. compared the use of allogenic and autologous MSCs as a therapy for ischemic cardiomyopathy. The authors injected MSCs transendocardially at three different doses: 20 million, 100 million, or 200 million cells. They found that both autologous and allogenic MSCs significantly reduced infarct size and that the lowest dose, 20 million cells, led to the greatest reduction in LV volume and increase in ejection fraction[105]. MSCs have also been used in combination with other cell types including BMMNCs and cardiac progenitor cells in preclinical and clinical studies[91,106,107]. MSCs may be able to enhance the proliferation and cardiac reparative capacity of these cell types, while also improving therapy through immunomodulation. Other preclinical work has used computational modeling to better understand MSCs' ability to couple to host myocardium and to elucidate the underlying mechanisms of MSC paracrine secretion that leads to functional benefit[108,109]. MSCs have been used extensively in combination with biomaterials for cardiac tissue engineering applications, and several of these studies will be discussed later in this chapter.

2.2.4 Embryonic Stem Cells

Embryonic stem cells (ESCs) are stem cells isolated from the inner cell mass of an embryo and can give rise to any cell type in the body, excluding those in placental tissue[110]. ESCs have been used both in their undifferentiated, pluripotent state as well as differentiated into many different cell types for cardiac cell therapy and tissue engineering purposes. Kofidis et al combined undifferentiated mouse ESCs with Matrigel and injected this mixture into a mouse infarct model. Injected ESCs formed colonies in the infarcted area, showed expression of connexin 43 at contact sites with host cells, and improved fractional shortening[111]. Although in this study no teratoma formation was observed, the tumorgenicity of undifferentiated ESCs, along with ethical issues, immunogenicity, and scaling up of ESC isolation and production, remains a major concern for their clinical translation[112].

To bypass some of these issues as well as produce more cardiac-like cells, ESCs are often differentiated to cardiac progenitors, CMs, and endothelial cells (ECs). A fibrin patch embedded with ESC-derived $SSEA1^+$ progenitor cells was shown to increase ejection fraction and angiogenesis when implanted onto infarcted rat hearts[113]. This same group has also scaled up the use of their ESC-derived progenitor/fibrin patches and showed them to be feasible and safe for treatment of ischemic LV dysfunction in six human patients[114]. Stem cell-derived CMs have been a highly investigated topic of cardiac cell therapy, and many studies have shown their efficacy in both rodent and non-human primate models[115–118]. ESC-derived ECs and CMs have been used together with one another to form vascularized cardiac muscle, illustrating the versatility and flexibility of ESCs as a cell source[119]. Ongoing research focuses on further maturation of ESC-CMs so that they more

closely mimic the mechanical properties of natural CMs *in vivo*. A variety of methods including modulating substrate stiffness[120], electrical stimulation[121], and delivering biochemical cues[122] are currently being explored to increase ESC-CM maturation.

2.2.5 Induced Pluripotent Stem Cells

The Yamanaka laboratory first demonstrated the creation of induced pluripotent stem cells (iPSCs) in 2007. The authors of this study retrovirally transduced human dermal fibroblasts with four key transcription factors: Oct3/4, Sox2, c-Myc, and Klf4. These "Yamanaka factors" converted human dermal fibroblasts into pluripotent stem cells with similar characteristics, including gene expression and morphology, to ESCs[123]. This landmark work set the stage for the use of iPSCs throughout the field of regenerative medicine, including cardiac tissue engineering. Because iPSCs are patient-derived from adult fibroblasts, they circumvent the immunogenic and ethical concerns associated with the use of ESCs, while still providing the versatility of a pluripotent cell source.

iPSCs have a similar differentiation potential to ESCs[124] and have been differentiated to a variety of different cardiac cells for use in cell therapy. Ye et al differentiated iPSCs into ECs, CMs, and smooth muscle cells (SMCs) and implanted this tri-lineage combination with a fibrin patch into a porcine model of MI. The iPSC-derived CMs integrated into the host myocardium, while the ECs and SMCs contributed to endogenous vessels, leading to improvements in LV function[125]. This same group later reported a similar tri-lineage cell patch approach with larger, more clinically relevant dimensions and more advanced maturation of iPSC-CMs through dynamic culture on a rocking platform[126]. Other studies have shown improvements in iPSC-CM therapy and

maturation using anisotropic scaffolds[127], naturally-derived extracellular matrix (ECM)-based materials[128,129], and 3D spheroid aggregation[130]. Recently, an innovative study by Wang et al delivered a cardiac patch with shape-memory properties composed of methacrylated elastin and gelatin and carbon nanotubes seeded with iPSC-CMs to minipigs through catheter injection. The patches were rolled up into a catheter and delivered to the infracted myocardium, where it recovered its shape after injection and improved LV fractional shortening and ejection fraction[131]. Additionally, the first in-man clinical study of an iPSC-CM cell sheet for treatment of ischemic cardiomyopathy began recently at Osaka University in Japan (jRCT2053190081). Despite their promise, issues with iPSCs, including partial reprogramming that can lead to genetic and epigenetic changes, remain a challenge for clinical translation, and are being addressed by ongoing research[132].

2.2.6 Resident Cardiac Cells and the Cardiac Stem Cell Controversy

The first population of cardiac-derived cells that were deemed cardiac "stem" cells was discovered in 2003 when cells marked by the tyrosine kinase c-Kit were isolated from the adult mammalian heart. These cells were shown to be clonogenic, self-renewing, and multipotent with the ability to differentiate into CMs, ECs, and SMCs[133]. This discovery helped launch SCIPIO, a Phase I clinical trial, which was the first in-human clinical trial using autologous cardiac-derived c-Kit$^+$ cells (CPCs). The CPCs were used to treat patients with ischemic cardiomyopathy undergoing coronary artery bypass grafting. Results from the trial showed encouraging outcomes including an increase in LV ejection fraction and a decrease in infarct size[134,135]. However, the true nature of these cells' role in cardiac biology and their contribution to the functional cardiomyocyte population *in vivo* has been hotly debated and shown to be very minimal[136–142]. This skepticism eventually led to an

investigation by Harvard Medical School and Brigham and Women's Hospital into Piero Anversa's laboratory. Anversa's lab was where the original work on CPCs was published and was also one of the groups involved in the SCIPIO trial. The investigation revealed that falsified and/or fabricated data was used in much of the work that pioneered the use of CPCs[143]. Ultimately, the institutions called for the retractions of 31 publications produced by Anversa's group including the results of the SCIPIO trial, which was eventually retracted by *The Lancet*[144]. Despite the sullied reputation of CPCs, their ability to provide therapeutic benefit in CHD patients has been shown in both preclinical and clinical studies, and these data will be discussed in a later section.

Several other resident cardiac cell populations and their ability to heal the myocardium have also been studied, including cardiosphere-derived cells (CDCs), stem cell antigen-1^+ cells, and Islet-1^+ cells[145]. CADUCEUS, a Phase I clinical trial, employed CDCs to treat patients 2 to 4 weeks following an MI. Although initial results showed no changes in LV ejection fraction with CDC therapy, CDC treatment did lead to a decrease in infarct size and an increase in viable myocardium[146]. As is true with other cell therapy, the functional benefit provided by resident cardiac cells is thought to be due largely to paracrine factor secretion. Therefore, current research has employed computational methods to elucidate the paracrine factors most important for cardiac repair[12–14]. Other arms of resident cardiac cell research have focused on *ex vivo* conditioning through hypoxic growth conditions[13], genetic manipulation[148], and combinatorial cell therapy[107,149].

2.3 Material Considerations for Cardiac Patches

While a sufficiently therapeutic cell source is vitally important to the success of cardiac tissue engineering strategies, a biomaterial that can effectively act as a carrier of this therapeutic cell source is equally essential. Further, cell-free materials that bolster the function of endogenous cells and tissue may be a similarly effective option to cell-laden patches. Because of this, research uncovering the optimal parameters of a biomaterial's formulation as well as the most therapeutic combination of material and cell source is paramount for advancing cardiac tissue engineering.

2.3.1 Material Sources

2.3.1.1 Natural Materials

Natural biomaterials are those derived from naturally occurring, biological sources, giving them many advantages for their use in cardiac tissue engineering. Most notably, because these materials are derived from *in vivo* sources, they retain much of the microenvironmental architecture cells experience in native tissue. Cues from this biomimetic microenvironment can help improve stem cell maturation and therapeutic function. Additionally, natural materials often have superior biocompatibility, allowing them to avoid immune reaction and thrombosis once implanted. Natural materials that have been used in cardiac tissue engineering applications include collagen, chitosan, fibrin, alginate, Matrigel, hyaluronic acid, gelatin, and decellularized ECM[150,151]. Decellularized ECM has been derived previously from both cardiac sources, including the myocardium[152–154] and pericardium[155–158], as well as from non-cardiac sources, including small intestinal submucosa (SIS)[159,160] and urinary bladder matrix[161,162]. Cardiac decellularized matrix was first harvested by Ott et al in 2008 when the authors delivered detergents including PBS,

SDS, and Triton X-100 through coronary perfusion to rat cadaveric hearts. This process eliminated virtually all cellular contents in each heart but retained ECM content such as collagens I and III, laminin, and fibronectin and maintained ECM fiber composition and architecture. Further, the researchers were able to repopulate the decellularized hearts with neonatal cardiac rat cells and produced hearts that displayed expected electrical and contractile responses to electrical stimulation[163]. The Christman group then expanded upon this decellularization principle and used it to process soluble porcine myocardial ECM (VentriGel) that gelled at 37°C, allowing the ECM to be used as an injectable material to treat early and late MI patients in a recent clinical trial[164,165].

Although decellularized ECM and other natural materials confer better mimicry of the native cell microenvironment, use of these materials still often faces the challenge of being too mechanically weak to successfully function as a cardiac patch. The human myocardium can range in stiffness from 20 kPa (end of diastole) to 500 kPa (end of systole), while many natural materials have stiffnesses in the tens of Pa range[150]. Moreover, batch-to-batch variation of natural materials is largely dependent on variations in material sources. Engineering natural materials to more closely mimic *in vivo* stiffnesses and creating consistent material processing practices are needed to continue to push these materials towards clinical use.

2.3.1.2 Synthetic Materials

While natural materials often provide a ready-made cell microenvironment that closely mimics that seen *in vivo*, synthetic materials offer modular building blocks that can be combined in myriad ways to create scaffolds with more clearly defined physical and

mechanical properties. Additionally, use of synthetic materials allows for more reproducible fabrication processes and often have enough mechanical strength for implantation as a patch. Synthetic materials commonly used in cardiac tissue engineering include polycaprolactone (PCL), poly(glycerol sebacate) (PGS), polyurethane, poly-(L-lactic) acid, and poly(lactic-co-glycolic) (PLGA) acid, among several others[150,166]. PCL has been used in combination with neonatal rat CMs to form cardiac grafts where CM beating was maintained, cell-to-cell contact occurred, and cardiac specific markers such as connexin 43, cardiac troponin I, and α-myosin heavy chain were expressed[167,168]. PCL has also been combined with other co-polymers, including those from synthetic sources like carbon nanotubes[169] and PGS[170] and from natural sources such as chitosan[171] and gelatin[172], to form more complex constructs. PGS is another particularly attractive synthetic polymer due its elastic nature, making it ideal for mimicking the mechanically dynamic environment of contracting CMs. Additionally, mechanical characterization of PGS scaffolds has shown its Young's modulus to more closely mimic that of native myocardium compared to several other synthetic polymers[173]. PGS has also been shown to provide a viable environment for a variety of cells including fibroblasts and ESC-CMs[174].

While synthetic materials offer many benefits for cardiac tissue engineering, there are also problems with their use that still need to be solved. Synthetic materials provide a great deal of mechanical support, but this often means that their stiffnesses can be orders of magnitude greater than that seen in the native myocardium. This may cause a mechanical mismatch with the heart upon implantation and could induce additional burden on the pumping function of the heart. Additionally, due to many of these materials' bioinert nature, they may not be able to fully propagate electrical signals to the heart and could

cause arrythmias when implanted. Continuing research into properly tuning the properties of synthetic polymers and co-polymers is needed to address these issues.

2.3.2 Material Fabrication Techniques

2.3.2.1 3D Bioprinting

Several different techniques for fabricating biomaterials exist, and each technique can significantly impact material properties. 3D bioprinting, one such technique, is the process of depositing sequential layers of biological materials (often a biomaterial/cell mixture) on top of one another to form 3D structures. Utilizing this technique allows for precise control of cardiac patch geometry and modulation of properties such as strand diameter and pore size[175]. Further, one major issue with cardiac patches is delivery of a clinically relevant number of cells. Patches may suffer from either low proliferation of cells or insufficient oxygen and nutrient delivery to cells within the patch, leading to a high degree of cell death. 3D printing allows for the creation of complex porous networks that permit efficient nutrient delivery, and ensures a uniform distribution of cells throughout the patch[176].

3D printing has been used with many combinations of materials and different cell types, often termed “bioinks”, for cardiac applications. Gao et al recently printed a methacrylated gelatin-based patch with CMs, SMCs, and ECs, all differentiated from iPSCs. To precisely control the architecture of their patch, the authors used multiphoton-excited 3D printing and mapped the blueprint for the printed scaffold to the distribution of fibronectin within the mouse myocardium. This technique produced printing with a resolution of <1 μm, giving a highly accurate approximation of native ECM structure.

Following printing and seeding with the three cell types, the patch beat synchronously after just 1 day and improved cardiac function, infarct size, and vessel formation when implanted into a mouse model of MI[177]. Another recent study used 3D printing to print gelatin microchannels to improve MSC differentiation and CM alignment and beat synchronicity. MSCs aligned and elongated at a higher rate in microchannel constructs than unpatterned constructs, leading to a higher expression of cardiac specific proteins. CMs also showed more pronounced alignment and display synchronous beating on microchannels[178]. These studies highlight the ability of 3D bioprinting to produce complex and highly defined architectures to influence cell behavior and function.

2.3.2.2 Electrospinning

Electrospinning is another fabrication process that has garnered a great deal of attention recently in cardiac tissue engineering. During scaffold fabrication, a high voltage (~1 – 30 kV) is applied to the needle of a syringe containing a polymer of choice. As the polymer is extruded out of the needle, the electrostatic force at the surface of the polymer droplet and the Coulombic force from the surrounding electric field overcome the surface tension of the droplet, leading to the formation of a polymer jet that is deposited onto a grounded collector[179]. Electrospinning produces polymer patches with nanoscale fibers and high porosity, mimicking the fiber composition of native ECM and allowing for efficient nutrient diffusion throughout the patch[180]. Additionally, electrospinning is a highly reproducible, tunable, and cost-effective process. Electrospinning was first used in cardiac tissue engineering by Shin et al to create PCL patches seeded with neonatal rat CMs[168]. Since this initial study, electrospinning has been used expansively with both natural and synthetic materials for cardiac applications[181]. Notably, electrospinning has been employed

to create patches with highly aligned fibers to align cells, more closely mimicking CM morphology and spatial organization in the myocardium. For example, neonatal rat CMs seeded on aligned PGS/gelatin electrospun patches showed greater anisotropic sarcomere formation and synchronized beating compared to random patches[182]. Electrospun scaffolds are also easily modifiable with other components to improve cell attachment, survival, and reparative function. These components include gold nanoparticles[183–185], growth factors such as VEGF [186,187], and ECM proteins such as fibronectin[188,189] and laminin[190].

2.3.2.3 Engineered Heart Tissues

While 3D bioprinting and electrospinning precisely control material architecture to mimic *in vivo* tissue, creating engineered heart tissues (EHTs) capitalizes on cells' inherent ability to self-assemble and form tissue. The first EHT was created by Eschenhagen et al. in 1997 when CMs from chick embryos were blended with a collagen matrix and seeded between two Velcro-coated glass tubes. The EHT that formed was able to beat in response to electrical pacing and increased contractile strength with increased pacing frequency[191]. Since this initial work, EHTs have been produced in a variety of geometries with an abundance of different cell types. For instance, one study generated EHTs from a combination of Matrigel and a mixed population of cardiac cells including CMs, fibroblasts, ECs, and SMCs. These EHTs were then formed into many different shapes including stars, horizontal tubules, a mesh network, and a "rope" structure[192]. EHTs have also been investigated as a therapy for chronic MI. Loop-shaped EHTs formed from ESC-CMs and collagen I matrix were mechanically stretched and implanted into a rat model of MI. The EHTs showed high engraftment rates and significantly improved the ejection fraction of rat hearts[193]. More recently, a square patch EHT generated from neonatal rat

ventricular cells and a gel mixture of thrombin, fibrinogen, and Matrigel was formed using a large (18 mm X 18mm) PDMS mold. The patches were epicardial implanted onto rat ventricles and electrically coupled to healthy host myocardium without altering any electrophysiology of the heart[194]. Because it is very difficult to couple EHT patches to unexcitable, damaged myocardium, ongoing research will continue to work towards more effectively forming effective cell-cell contacts between patch and native cells to allow for more functional integration of patches into hearts.

2.3.2.4 Hydrogels

Hydrogels are water-insoluble polymers that are formed through crosslinking of synthetic and/or natural precursor polymers. These gels are often at liquid phase *in vitro* but, following injection to a site *in vivo*, will gel and can help replace damaged ECM and deliver therapeutic cells[195]. Hydrogels used in cardiac tissue engineering have been both in cell-free and cell-laden forms. Cell-free alginate hydrogels were implanted into rat MI models and were shown to replace up to 50% of the scar tissue area. Additionally, alginate gel injection attenuated LV dysfunction and achieved similarly therapeutic outcomes to neonatal rat CM injection[196]. Another acellular approach used a cell-free collagen I patch and found that when implanted, the collagen patch attenuated remodeling and fibrosis and enhanced angiogenesis in infarcted LVs[197]. Hydrogels have also been utilized to facilitate differentiation of stem cells into more mature cardiac phenotypes through methods such as cellular aggregation[198] and incorporation of important signaling molecules such as Notch1[199]. Continuing research focuses on finding the right combination of cells and hydrogel polymer and introducing components to hydrogels to modulate their mechanical and bioactive properties.

2.4 Current Outlook for Cardiac Patches

2.4.1 Strategies for Advanced Cardiac Maturation

While maturation of cells on cardiac patch constructs has improved greatly over the years, more techniques to further advance this maturation are needed to produce true-to-form CMs *in vitro.* Research has focused on primarily on subjecting immature pluripotent cell-derived or primary CMs to similar physical forces native CMs experience in the myocardium, namely mechanical strain and electrical stimulation. This phenomenon has also been seen in neonatal rat CMs, where electrical stimulation induced calcium handling once again and increased CMs' expression of cardiac differentiation markers, independently of contractile effects[121]. While both of these maturation techniques can have profound effects on their own, they are often used in combination with one another[200] and with other techniques, including perfusion culture[201] and cellular coculture with cell types such as ECs and fibroblasts[202].

Importantly, these techniques not only induce increased maturation and cardiac differentiation, but also confer enhanced cardiac benefit *in vivo*. Tissues engineered from hESC-CMs and ECs and pre-conditioned with mechanical stress showed increased engraftment into the hearts of athymic rats[202]. A similar patch using the elastic polymer poly(lactide-co-caprolactone) and hESC-CMs preconditioned with cyclic strain attenuated fibrosis in a rat infarct model[203]. Following mechanical preconditioning, SkMBs were also shown to electrically couple to host myocardium upon implantation and expressed the cardiac-specific gap junction protein connexin 43[204]. More recently, Ronaldson-Bouchard et al achieved the greatest degree of maturation in engineered cardiac tissue to date using

iPSC-CMs and physical conditioning with increasing intensity. Specifically, tissues formed from early iPSC-CMs, just after the cells began to beat, were subjected to electrical stimulation from 2 Hz to 6 Hz, with the stimulation increasing 0.33 Hz each day. Following 4 weeks of stimulation, the engineered tissues showed sarcomere length and mitochondria density at physiological levels, had formed transverse-tubules, and had functional calcium handling[205]. Continuing optimization of electrical and mechanical stimulation techniques and fabrication of complex bioreactors combing these techniques may be needed to more effectively mature stem cell-derived CMs and tissue-engineered grafts.

2.4.2 Cell-free Products

While cell therapy has been shown to provide functional benefit in the injured heart, exogenous cell engraftment into host myocardium is very low[70]. These observations have led researchers to believe that the benefit exhibited following cell therapy must be attributable to paracrine mechanisms from implanted cells, prior to the cells being washed away from the site of injection. Therefore, a recent push has been made to both define the secretory factors responsible for cardiac improvement and to use these reparative factors as their own therapy, separate from the cells that produce them. Informatics and systems biology methods have proved to be powerful tools for elucidating the functional units of many different cell types. Sharma et al used informatics techniques to identify upregulated growth factors and signaling pathways in the secretome of CPCs from adult and neonatal patients. Using this analysis, the authors were able to pinpoint heat shock factor 1 (HSF1) as a crucial regulator of the secretome of CPCs and demonstrated that knockdown of HSF1 led to decreased secretion of important pro-reparative factors such as VEGF, ANG1, and SDF1[12].

While growth factors certainly play an important role in the reparative secretome, other research has focused on characterization of another important player in the secretome: exosomes. Exosomes are small (30-120 nm in diameter) extracellular vesicles that form within larger multivesicular bodies and release from the cell upon fusion with the cell membrane. Exosomes can contain proteins, lipids, RNA, and/or DNA, and it is this cargo that can provide reparative effects to the heart[206]. The Cheng laboratory has developed innovative methods to deliver exosomes to treat MI, including injection in a hyaluronic acid hydrogel into the pericardial cavity[207] and an exosome "spray" composed of thrombin and fibrinogen[208]. It has also been shown that one of the most important pieces of exosomal cargo, miRNAs, can alone improve heart function. A recent study identified miR-21-5p as the functional miRNA of the MSC secretome and showed that delivery of miR-21-5p alone was enough to increase expression of calcium handling genes and, consequently, contractility in EHTs[209]. To avoid the issues with implantation of cells, other cell-free delivery methods have been explored to deliver reparative secretome products. In one study, the complete secretome from adipose-derived stem cells was loaded into a gelatin and Laponite® hydrogel and injected into a rat acute MI model and shown to reduce scar area, increase angiogenesis, and improve several cardiac functional parameters[210]. Another innovative method to deliver therapeutic secretome components are the use of "synthetic stem cells", a method created by Tang et al. Synthetic stem cells are PLGA microparticles loaded with stem cell conditioned media and coated with stem cell membranes. They have been fabricated using the secretomes and membranes from both MSCs and CDCs, and both sets of synthetic stem cells have been shown to repair the heart in mouse models of MI[211,212]. The same group has further developed this technology by

combining their synthetic stem cells with decellularized ECM to create an "off-the-shelf" cardiac patch[213]. Future work on cell-free products will continue to identify the functional units of different therapeutic cells' secretomes and will work to find efficient ways to deliver and scale up the production of these factors.

2.5 Cardiac Cell Therapy and Cardiac Patches for Congenital Heart Disease

The bulk of cardiac cell therapy research that has been conducted and that has been discussed in this dissertation thus far has focused on treating ischemic conditions in the LV, specifically MI. However, while many of the therapies developed through this research may also be applicable to the RV, there remains a need to conduct studies to measure specifically the efficacy of cell therapy and cardiac patches in treating RVHF brought on by CHD. In this section, we review preclinical and clinical studies of cardiac cell therapy and tissue engineered approaches for treating RVHF in CHD.

2.5.1 Preclinical Studies

2.5.1.1 c-Kit$^+$ Cardiac-derived Cells

Even though multiple studies have shown that endogenous CPCs do not differentiate to CMs *in vivo*[139,140], there is a growing body of evidence that suggests these cells exhibit therapeutic effects once injected and can be used to heal the myocardium in RVHF conditions[214,215]. It is important to distinguish the difference between those CPCs used in the retracted SCIPIO trial and those being studied in the context of CHD; the CPCs from SCIPIO were isolated from adult patients who had undergone coronary artery bypass, while the pediatric CPCs used by our laboratory and others are isolated from young patients

(<5 years old) undergoing surgery for CHD[135,216]. Several studies have shown that younger CPCs have increased reparative capacity compared to cells isolated from older donors. Agarwal et al injected neonatal (0–1 month old), infant (1 month – 1 year old), or child (1–5 years old) CPCs and found that only the younger neonatal CPCs were able to improve both RV ejection fraction and tricuspid annular plane systolic excursion (TAPSE) in a rat PAB model[147]. This age-dependence has also been shown by Simpson et al, who found that neonatal atrial appendage biopsies have increased numbers of cardiac progenitor cells[217].

To elucidate the underlying mechanisms of these donor-specific differences, computational methods have been employed to examine intracell gene expression and the contents of factors secreted by CPCs. Gray et al and Agarwal et al used systems biology methods to distinguish what exosomal cargo from rat and human pediatric CPCs, respectively, correlated most strongly with improvement in functional outcomes such as angiogenesis, fibrosis, and ejection fraction[13,14]. Computational methods have also been used to examine differences in CPC gene expression measured by RNA-seq data to identify genes whose upregulation may be most important for improved functional outcomes. Importantly, in these studies, there was clustering of CPC gene expression and exosomal cargo based on age, further highlighting the age-related differences in their reparative capacity[14,218,219]. Autologous cell therapy also may be affected by other donor characteristics, including what type of CHD the CPC donor is experiencing[220,221].

As with other therapeutic cell types, there has been great interest in using *ex vivo* conditioning methods to improve pediatric CPC function. French et al cultured CPCs on various ECM proteins and subjected the CPCs to cyclic strain. The CPCs aligned more efficiently when subjected to higher strain, and this led to an increase in angiogenic

paracrine factor production on many of the ECM substrates[222]. Similar maturation of CPCs and induced calcium handling was also seen following electrical stimulation, and these electrically stimulated CPCs were able to increase TAPSE in a PAB rat model[223,224]. Injection of spherical aggregates of CPCs also led to improved functional outcomes in PAB rats compared to CPCs from simple 2D culture[225].

2.5.1.2 Other Cell Types

Cell types other than pediatric CPCs have also been investigated for treating RVHF in CHD, primarily through injecting these cells into animal models with pressure-overloaded RVs. Human umbilical cord blood (UCB) cells have been implanted to both a sheep and mouse PAB model and, these UCB cell injections improved RV function, decreased fibrosis, and increased angiogenesis[226,227]. As with treatment for MI in the LV, bone marrow-derived MSCs have been explored as candidate for cell therapy for RHVF. Similarly to studies using CPCs, Liufu et al injected MSCs derived from neonatal, infant, and child patients into a mouse model of PAB and also found that only neonatal MSCs decreased RV dimension and hypertrophy following injection[228]. The use of bone marrow-derived MSCs has also been explored in a neonatal swine PAB model, where intramyocardial injection of the MSCs led to increased RV function, increased angiogenesis, and decreased RV hypertrophy[229].

2.5.2 Clinical Trials

Many of the preclinical studies mentioned above paved the way for cell therapy clinical trials in CHD patients. The Transcoronary Infusion of Cardiac Progenitor Cells in Patients With Single Ventricle Physiology (TICAP, NCT01273857) was the first clinical

study in which the use of cell therapy to treat CHD was used. Initial results from this phase 1 trial showed that intracoronary injection of CDCs improved RV ejection fraction and rescued heart failure status in patients with single ventricle physiology[230,231]. After these promising outcomes in TICAP, a phase 2 (PERSEUS, NCT01829750) and phase 3 (APOLLON, NCT02781922) were conducted by the same group using the same CDC injection[232,233]. The APOLLON trial is still ongoing, and results have yet to be reported. The next cell type that was explored clinically was autologous UCB mononuclear cells, injected into the RV of HLHS patients during the bidirectional Glenn procedure (NCT01883076). The phase 1 results showed that intramyocardial injection of UCB mononuclear cells was safe and did not lead to any reductions in cardiac function, setting the stage for a phase 2 follow-up study[234]. The same group is also investigating using autologous BMMNCs for treating RV dysfunction in patients with Fontan circulation (NCT02549625). Other cell types being explored to treat RV dysfunction in CHD include allogeneic MSCs (ELPIS, NCT02398604)[235] and autologous CPCs (CHILD, NCT03406884). In total, cell therapy has shown promise in treating CHD, primarily for RV dysfunction in patients with single ventricle physiology. However, there is still further work to be done including identifying which cell source is most effective and how to account for patient-to-patient differences in cell quality before cell therapy for CHD will become common practice in the clinic.

2.5.3 Biomaterial-based Treatments for Right Ventricular Heart Failure

As is true with cardiac patches for LV failure, the use of biomaterials in combination with cells may overcome some of the issues with cell therapy for the RV, namely low cell retention. However, the bulk of tissue engineering studies geared towards

CHD involve fabricating patches and vascular conduits to be used during reconstructive CHD surgeries, such as patches for ASD and VSD closure[236,237]. Few studies have investigated the use of cardiac patches to repair the failing myocardium like has been done in the MI studies discussed earlier in this chapter. Some of the first and only cardiac patches for treating RVHF have been developed by our laboratory, where 3D-printed and electrospun patches have been used to deliver pediatric patient-derived CPCs for treatment of RVHF[9,10]. There is still a dearth of cardiac patch studies for treating CHD and RVHF, and more research is required to uncover if cardiac patches can, as they have been in the failing LV, be successful in repairing the failing RV.

CHAPTER 3. CHANGES IN PCL PATCH PARAMETERS AFFECT CPC REPARATIVE CAPACITY IN A CPC AGE-DEPENDENT MANNER

3.1 Abstract

Congenital heart disease (CHD) is the number one cause of birth defect-related death because it often leads to right ventricular heart failure (RVHF). One promising avenue to combat this RVHF is the use of cardiac patches comprised of stem cells and scaffolds. Herein, we demonstrate a reparative cardiac patch by combining neonatal or cardiac-derived child c-Kit$^+$ cells (CPCs) with a scaffold comprised of electrospun polycaprolactone (PCL) nanofibers. We examined different parameters of the patch, including the alignment, composition, and surface properties of the nanofibers, as well as the age of the CPCs. The patch based on uniaxially aligned nanofibers successfully aligned the CPCs. With the inclusion of gelatin in the nanofiber matrix and/or coating of fibronectin on the surface of the nanofibers, the metabolism of both neonatal and child CPCs was generally enhanced. The conditioned media collected from both patches based on aligned and random nanofibers could reduce the fibrotic gene expression in rat cardiac fibroblasts following stimulation with transforming growth factor beta (TGF-β). Furthermore, the conditioned media collected from the nanofiber-based patches could lead to the formation of tubes of human umbilical vein endothelial cells, indicating the pro-angiogenic capability of the patch. Taken together, the electrospun nanofiber-based patches are a suitable delivery vehicle for CPCs and can confer reparative benefit through anti-fibrotic and pro-angiogenic paracrine signaling.

3.2 Introduction

Congenital heart disease, which occurs in about 1 in every 100 live births, is the most common group of congenital abnormalities, and the leading cause of birth defect-related death[1–3]. The current gold standard of treatment is surgical palliation of the defect to improve the function of the heart. However, these surgeries often lead to right ventricular (RV) hemodynamic changes to the heart resulting in impaired RV function and co-morbidities, with many patients requiring heart transplantation later in life[4]. Even with transplantation, the 5-year survival for patients who, for example, undergo the Fontan procedure is only about 60%[238]. Transplantation effectiveness is also often hampered by immune rejection and severe infection due to administration of immunosuppressants[239]. Finally, there is also a great economic and social cost to treating CHD patients including more frequent surgical intervention and enormous strain on the family of the patient[57]. Because of these many problems, CHD is an immense and significant public health issue.

Stem cell-based and regenerative medicine therapies have emerged as alternative strategies to treat CHD and to potentially repair dysfunction brought about by surgical palliation[5–7]. Previous studies have found cardiac-derived c-kit$^+$ cells (CPCs) to be a potential candidate for use in pediatric stem-cell therapy[8,9,147,225]. While CPCs do not directly contribute to the endogenous cardiomyocyte population[139–141], several studies have shown their ability to improve cardiac function by the release of reparative paracrine effectors[12–14]. Further, clinical trials using CPCs in both adult and child patients have demonstrated safety and modest cardiac improvements in heart failure patients[134,230]. Notably, our laboratory has previously demonstrated the age-dependent therapeutic effects of CPCs and that at early as 1 year old, CPCs' reparative capacity can begin to decline[147].

One major drawback of stem cell therapy is low cell retention within the host tissue, with only 0.1-10% of injected cells successfully grafting into the myocardium following injection[15–17,240]. If paracrine therapy is to be sustained over longer periods of time, novel methods to support cell retention while enabling function are needed. These limitations highlight the need to augment stem cell therapy to improve its efficacy as a treatment for CHDs.

In order to enhance cell retention and maximize reparative paracrine secretion, scaffolds are often used for the implantation of a therapeutic stem cell source[18,19]. Electrospinning has been used in many different regenerative medicine applications over the past several decades because of its capability to generate scaffolds that mimic the *in vivo* cell microenvironment[181,241]. Electrospinning can produce scaffolds made of a highly porous network of fibers in the nanometer range, allowing for the effective transportation of nutrients and wastes while mimicking the collagen nanofibers in the extracellular matrix (ECM). Importantly, the electrospun fibers can be oriented parallel to each other along one specific direction, giving the fiber-based scaffold an anisotropic structure like that of the myocardium. The scaffolds can also be readily functionalized with other components to help improve cell adhesion and survival[180]. Because of these advantages, we have fabricated nanofiber-based scaffolds made of polycaprolactone (PCL), an FDA-approved biocompatible and biodegradable polymer, and evaluated their use as a carrier for CPCs. Gelatin has been previously shown to modulate the mechanical properties of nanofiber-based scaffolds[172,182] and the differentiation profile of stem cells[242], while fibronectin has been shown to increase CPC alignment[222] and to be necessary for CPC repair following cardiac injury[243]. In the present work, we systematically investigated the metabolism and

morphology of CPCs at different ages when cultured on the nanofiber-based scaffolds with different alignments and with the inclusion of adhesion factors such as gelatin and/or fibronectin (Figure 1). We further demonstrated the effect of the conditioned media collected from the different patches with CPCs on the fibrotic gene expression in rat cardiac fibroblasts (RCFs) and tubular formation of the human umbilical vein endothelial cells (HUVECs) to validate the anti-fibrotic and pro-angiogenic potentials of the nanofiber-based patches, respectively.

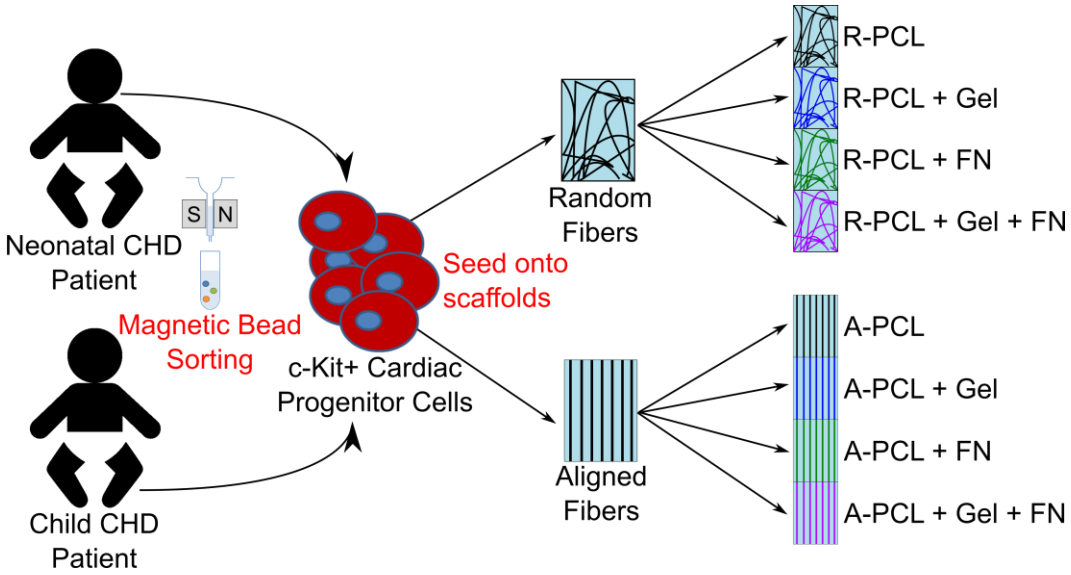

Figure 1. Experimental design for characterizing the cellular responses of neonatal and child CPCs to electrospun scaffolds composed of random or aligned nanofibers and including gelatin, fibronectin, or both. The 8 different scaffolds characterized are as follows: random PCL nanofibers (R-PCL), random PCL/gelatin nanofibers (R-PCL + Gel), random PCL nanofibers with fibronectin (R-PCL + FN), random PCL/gelatin nanofibers with fibronectin (R-PCL + Gel + FN), aligned PCL nanofibers (A-PCL), aligned PCL/gelatin nanofibers (A-PCL + Gel), aligned PCL nanofibers with fibronectin (A-PCL + FN), and aligned PCL/gelatin nanofibers with fibronectin (A-PCL + Gel + FN).

3.3 Materials and Methods

3.3.1 Chemical and materials

All materials were purchased from Thermo Fisher Scientific Life Sciences unless otherwise stated. PCL (Mn ≈ 80 kDa), 2,2,2-trifluroroethanol, and fluorescein-5-maleimide were obtained from Sigma-Aldrich. Ham's F12 medium and Matrigel® were obtained from Corning. Endothelial cell growth media and the Luminex® assays were purchased from R&D systems. Fetal bovine serum was obtained from GE Healthcare. L-glutamine was purchased from MP Biochemicals, and basic fibroblast growth factor (bFGF) was purchased from Stem Cell Technologies. TRIzol was purchased from Invitrogen.

3.3.2 Fabrication of electrospun nanofiber-based scaffolds

A PCL electrospinning solution with a concentration of 12 wt.% was prepared by dissolving PCL pellets in 2,2,2-trifluroroethanol under magnetic stirring for 24 h at room temperature. Scaffolds made of electrospun nanofibers were fabricated using the traditional electrospinning process. The PCL solution was fed at a rate of 1.0 mL/h through a blunt needle with a syringe pump. The needle was located at a distance of 20 cm from a ground mandrel, which was covered by aluminum foil. An optimized voltage (DC, 10–15 kV) was applied between the needle and the grounded mandrel to obtain a stable polymer jet. A rotating rate of 300 or 1000 rpm for the mandrel was used to generate random or uniaxially aligned nanofibers. The electrospinning process was carried out at room temperature and a relative humidity of 40%. After collection for 4 h, the as-obtained mats were peeled off and further dried at ambient temperature to remove the residual organic solvent. The mats were then punched into discs with a diameter of 1.2 cm. After sterilization for 1 h under UV light, the discs were fixed onto sterilized glass coverslips using a medical silicone adhesive, placed in the wells of a 24-well plate, and then treated with oxygen for 2 min in

a plasma cleaner. To coat fibronectin, the mats were incubated in a fibronectin solution (1 μg/mL) overnight at 4 °C, followed by washing with PBS buffer three times.

PCL and gelatin were separately dissolved in 2,2,2-trifluroroethanol to prepare solutions at a concentration of 6 wt.%. Then, the solutions were mixed at a mass ratio of 50:50, together with a small amount of acetic acid (0.2 v/v%), in 2,2,2-trifluroroethanol to obtain a transparent solution under magnetic stirring at room temperature prior to electrospinning. The random and uniaxially aligned nanofibers made of a blend of PCL and gelatin were separately fabricated using the same procedure used for the fabrication of PCL nanofibers.

3.3.3 Characterization of the nanofiber scaffolds

The morphology of the nanofibers was observed under a scanning electron microscope (SU8230). The average diameter and the diameter distribution of the nanofibers were measured and analyzed using the ImageJ software from 200 fibers in the scanning electron microscopy (SEM) images. Fast Fourier transform (FFT) analysis of the SEM images was performed by utilizing the FFT function of the ImageJ software to demonstrate the alignment of the nanofibers in the different scaffolds. A quantitative analysis of the alignment of the nanofibers was also performed by summation of pixel intensities at different degrees. The surface properties of the scaffolds were determined through measuring the static water contact angle using a SL200A-type contact angle analyzer at ambient temperature. Deionized water droplets (3.0 μL) were dropped carefully onto the surface of the scaffold, and the average water contact angle value was obtained by measuring ten water droplets at randomly distributed positions. The tensile properties of

the scaffolds in the dry state were evaluated using a BOSE ElectroForce 3200 test instrument with a 50-N load cell at a crosshead speed of 5 mm/min. All samples were cut into rectangles with dimensions of 25 mm × 4 mm. Five samples were tested for each typical type of membrane. The thickness of a sample was measured with a micrometer accurate to 1 μm.

3.3.4 CPC isolation and culture

This study was approved by the Institutional Review Board at Children's Healthcare of Atlanta and Emory University. CPCs were isolated from neonatal (0–1 month old) and child (1–5 years old) patients undergoing routine surgery for CHD. Approximately 70–100 mg of right atrial appendage tissue was obtained from patients. The tissue samples were transported in Krebs-Ringer solution containing 35 mM NaCl, 4.75 mM KCl, 1.2 mM KH_2PO_4, 16 mM Na_2HPO_4, 134 mM sucrose, 25 mM $NaHCO_3$, 10 mM glucose, 10 mM HEPES, and 30 mM 2,3-butanedione monoxime, at a pH of 7.4 with NaOH. CPCs were isolated within 4 h of acquiring the sample using magnetic bead sorting for the c-Kit protein as previously described.[38] Following isolation, CPCs were maintained in culture in Ham's F12 medium supplemented with 10% fetal bovine serum, 1% Pen-Strep, 1% L-glutamine, and 0.01 ng/mL bFGF.

3.3.5 CPC culture on the nanofiber scaffolds

Nanofiber-based scaffolds were adhered to a 12 mm-diameter circular coverslip using medical silicone adhesive. The coverslip and scaffold were then affixed to the bottom of the well of a 24-well plate, covering approximately 85.2% of the well's total area. A total of 125,000 cells were seeded onto each PCL nanofiber-based scaffold in each well of

the plate. CPCs were maintained in the treatment medium composed of 500 μL of Ham's F12 medium supplemented with Insulin-Transferrin-Selenium, 1% Pen-Strep, 1% L-glutamine, and 0.01 ng/mL bFGF. After 2, 3, 5, and 7 days, the culture media were collected, termed as the conditioned media of the patches, and stored at -80 °C until further analysis, and fresh treatment media were added to the wells at the corresponding time points.

3.3.6 CPC alignment and morphology on the nanofiber scaffolds

After culture for 7 days, the cells on the scaffolds were fixed with 4% paraformaldehyde for 30 min at room temperature. The cells were then washed with PBS for three times and permeabilized in 0.1% Triton X-100 for 30 min. Following three more washes in PBS, the cells were incubated with 10 μg/mL fluorescein-5-maleimide at 4 °C overnight and then incubated with 1 μg/mL 4′ ,6-diamidino-2-phenylindole (DAPI) for 10 min in the absence of light. Finally, the cells were mounted onto MatTek glass bottom dishes using ProLong® Gold Antifade Reagent. The samples were stored at 4 °C until imaging on a confocal microscope (Olympus IX81 FluoView FV1000). Quantifications of the alignment, area, and eccentricity (elongation) of the cells on the different types of nanofiber scaffolds were measured using the CellProfiler^{TM} software. The mean cell angle of all cells measured on a given patch was determined, and a cell was considered "aligned" if its angle fell within 10° of this mean (preferred) angle[244].

3.3.7 CPC metabolism on the nanofiber scaffolds

The metabolism of CPCs was measured using an alamarBlue® assay after culture for 1, 3, and 7 days on each scaffold according to the manufacturer's instructions. The

CPCs grown on tissue culture plastic (TCP) served as a blank control group. Briefly, 500 µL of alamarBlue reagent in the cell treatment medium was added to the well. The cells were incubated in the solution for 1, 2, or 4.5 h to discern differences in alamarBlue fluorescence. Following incubation, 100 µL of the alamarBlue solution was plated into the well of a 96-well plate in triplicate. Fluorescence readings were taken using a microplate reader (BioTek Synergy 2) with an excitation wavelength of 540 nm and an emission wavelength of 590 nm. Fluorescence readings for each patch were then normalized to the TCP control.

3.3.8 Rat cardiac fibroblast TGF-β stimulation assay

RCFs were cultured in the well of a 24-well plate and then quiesced for 12 h. Then, 500 µL of the conditioned medium collected at the 2-day and 5-day incubations of the CPCs on the nanofiber scaffolds was added to the well. The RCFs cultured in the full medium (Dulbecco's modified eagle medium supplemented with 10% fetal bovine serum) served as the control group. After culture for 12 h, the RCFs were stimulated with 10 ng/mL TGF-β. After culture for another 12 h, the RCFs were collected, and their RNA was extracted using the TRIzol reagent according to the manufacturer's protocol. First strand cDNA synthesis was performed with M-MLV reverse transcriptase primed by random hexamers and oligo(dT)18. Real-time polymerase chain reaction (PCR) was then performed using SYBR Green fluorescence detection of amplified PCR products by the StepOne System. Rat primers (sequences shown in Table S1) for connective tissue growth factor (CTGF), collagen type 1 pro-α1 chain (COL1A1), and vimentin (VIM) were used to evaluate their respective transcript expression levels.

3.3.9 HUVEC tube formation assay

HUVECs were maintained on 0.1% w/v gelatin-coated culture flasks until use in assays. HUVECs were dissociated by trypsinization, and 10,000 cells were plated into the Matrigel®-coated well of a 96-well plate. The conditioned media (200 µL) collected at the 2-day and 5-day incubations of the CPCs on the nanofiber scaffold were added to each well immediately following plating. After culture the cells for 6 h, calcein-AM dye at a concentration of 2 mg/mL was added, and the HUVECs were imaged under a fluorescence microscope. The Angiogenesis Analyzer plug-in for ImageJ software was used to quantify the total tube length and number of tubules for each image.

3.3.10 Characterization of patch conditioned media

Conditioned media collected at the 3- and 7-day incubation of CPCs on each nanofiber scaffold group was diluted 1:2 and processed using a Luminex® Assay according to manufacturers' instructions. Briefly, conditioned media samples were incubated with color-coded magnetic beads bound to capture antibodies specific to analytes of interest. Biotinylated detection antibodies were then added, sandwiching the analytes of interest between the detection antibodies and capture antibodies bound to the magnetic beads. Phycoerythrin-coated streptavidin was then added and bound to the detection antibodies. The analyte concentrations were measured using fluorescence readings taken from a Luminex® 100 analyzer and calculations based on readings from a standard curve. These concentrations were then normalized to the total protein content of each conditioned media sample, as measured by a NanoDrop™ One Spectrophotometer.

3.3.11 Statistical analysis

All statistical analysis was performed in GraphPad Prism 5, and all numerical data are represented as mean ± standard error of the mean, except for cell alignment data which are represented as the fraction of cells aligned (aligned cells/total cells measured). For all comparisons of random *vs.* aligned nanofiber scaffolds, a paired Student's t-test was employed. For all comparisons of the nanofiber scaffolds containing the adhesion factors and the TGF-β stimulation assay, a one-way ANOVA with Tukey's post-hoc test was used. For cell alignment data, a Fisher's exact test with Bonferroni's correction was applied to counts of aligned and unaligned cells. All experiments used sample sizes of n = 5‑6 except for cell alignment and morphology experiments which examined cells from at least three different fields of view on at least three different scaffolds, giving measurements for at least 300 individual cells per scaffold group.

3.4 Results

3.4.1 Mechanical properties of the nanofiber-based scaffolds

The growth of CPCs and their secretion of paracrine signals should be dependent on their viability and the configuration of their cytoskeletons, which are largely determined by the underlying fibers. To this end, we varied the alignment and composition of the electrospun nanofibers. Figure 2A shows the SEM image of a typical sample of random PCL nanofibers with an average diameter of 680±160 nm. The nanofibers show a smooth morphology with no beads formed. The FFT pattern of the image at the right corner confirms that the nanofibers were randomly oriented as the pixel intensities showed essentially no dependence on the direction. Figure 2B shows the SEM images of PCL

nanofibers with a uniaxial alignment, which was further confirmed by the corresponding FFT pattern.

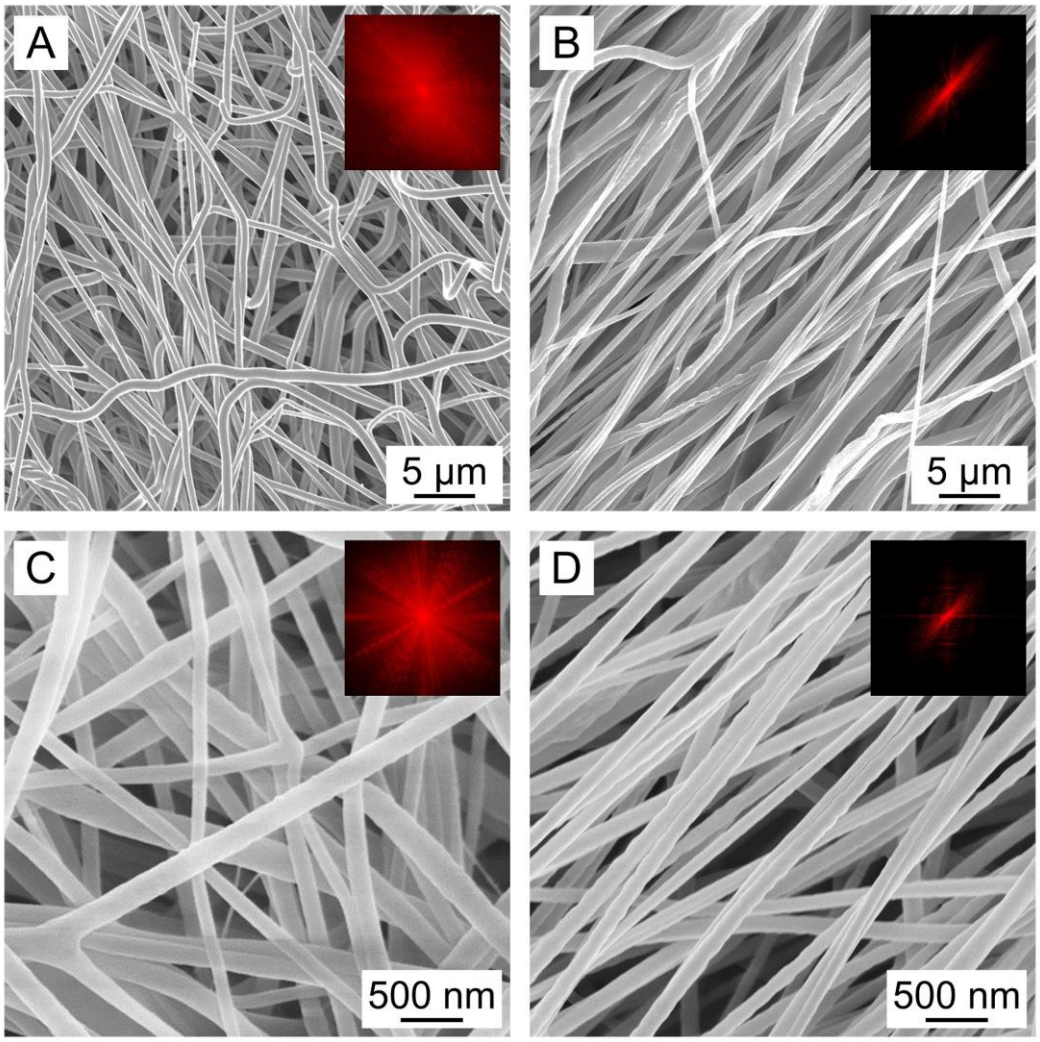

Figure 2. SEM images of the scaffolds comprised of (A, C) random and (B, D) aligned nanofibers made of PCL (A, B) before and (C, D) after coating with gelatin, respectively. The insets show the FFT analysis of the corresponding SEM image.

The uniaxially aligned PCL nanofibers had an average diameter of 610±190 nm, slightly thinner than that of the random nanofibers due to the further elongation of the nanofibers under mechanical stretching (Figure 3A and B). The morphologies of the random and uniaxially aligned nanofibers made of a mixture of PCL and gelatin are shown

in Figure 2C and D, respectively, with an average diameter of 160±60 nm and 120±50 nm (Figure 3C and D).

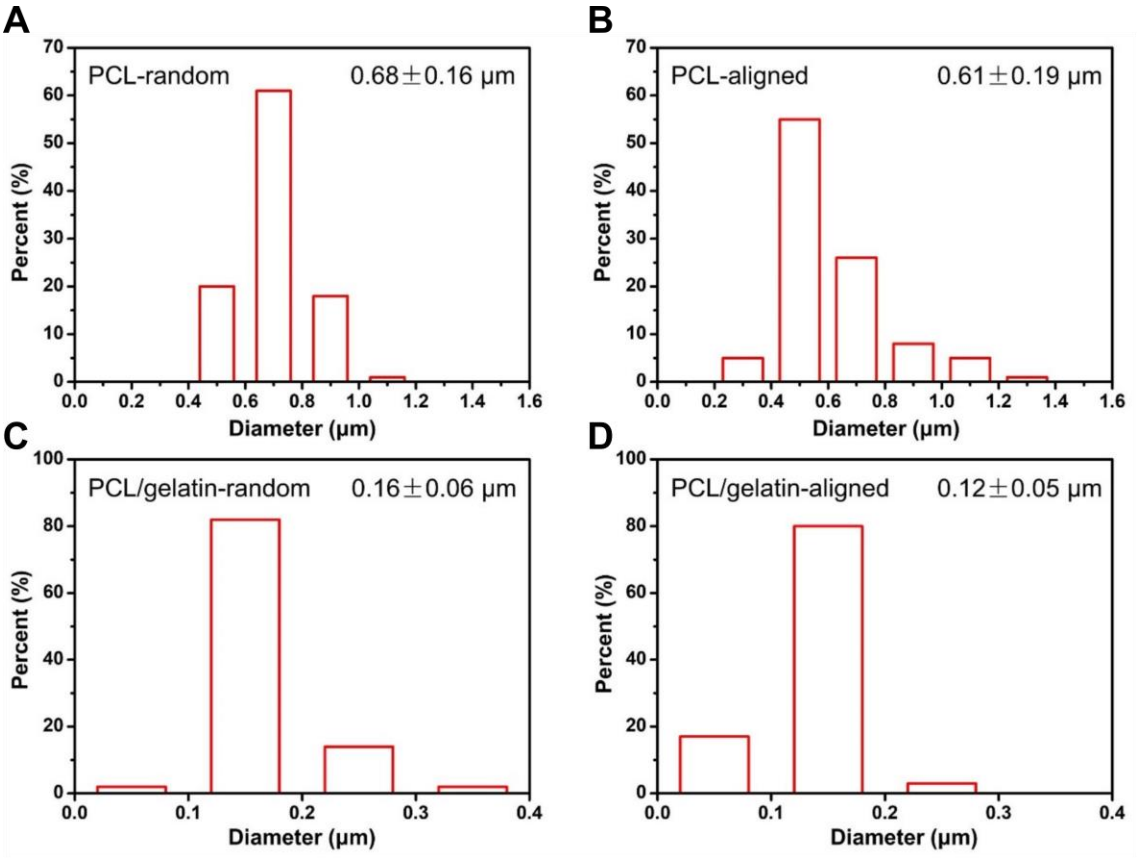

Figure 3. The distribution of fiber dimeter of the nanofibers in the different types of scaffolds composed of PCL nanofibers in (A) random and (B) aligned orientations, and blended PCL/gelatin nanofibers in (C) random and (D) aligned orientations, respectively.

The alignment of the nanofibers was also confirmed by the corresponding FFT patterns. With the introduction of gelatin, the diameter of the nanofibers was significantly reduced owing to the increase in conductivity of the electrospinning solution[245]. The alignment of the nanofibers in the different samples was further confirmed by measuring the directionalities of the images using ImageJ, as shown in Figure 4.

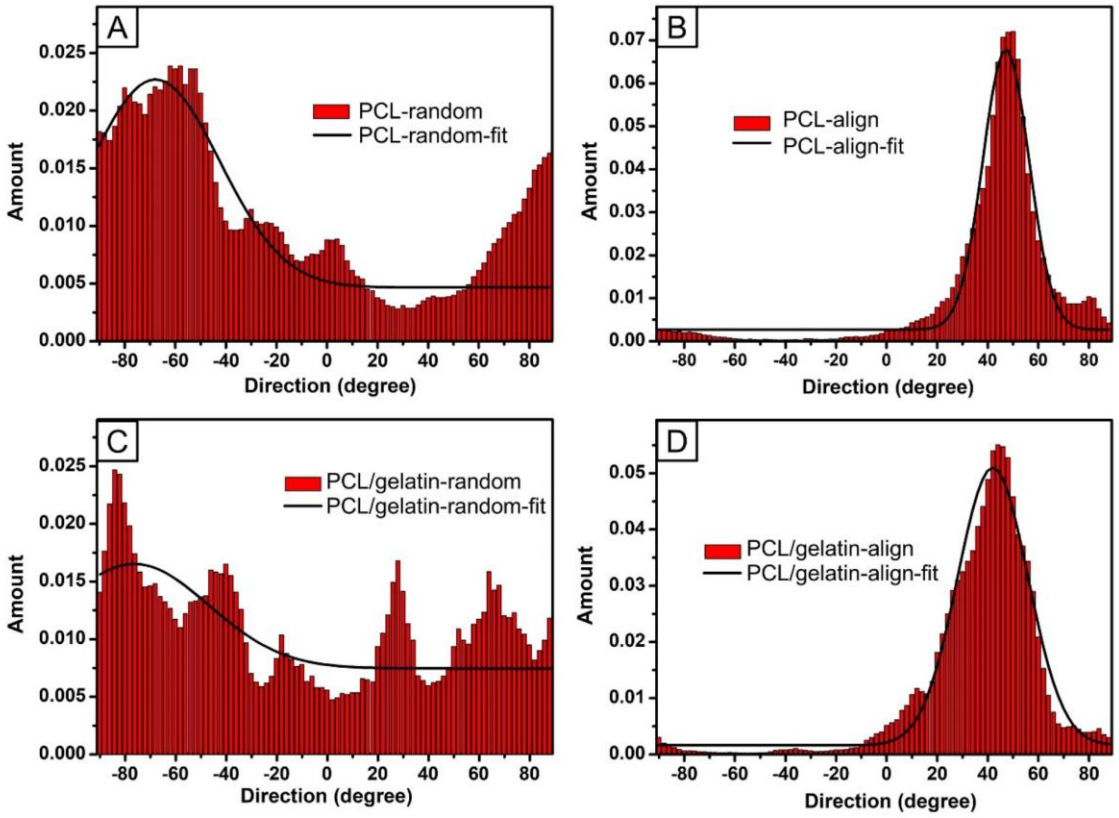

Figure 4. The plots indicating the directionalities of the nanofibers in the different types of scaffolds composed of PCL nanofibers in (A) random and (B) aligned orientations, and blended PCL/gelatin nanofibers in (C) random and (D) aligned orientations, respectively.

The surface wettability of a scaffold has great influence on the adhesion and proliferation of cells seeded on it. The electrospun PCL nanofibers, either in a random or uniaxially aligned orientation, were moderately hydrophobic with contact angels of 129.6° and 121.5°, respectively. After plasma treatment, the water contact angels of the random and uniaxially aligned PCL nanofibers were significantly reduced to 82.1° and 81.5°, respectively. For the nanofibers made of a mixture of PCL and gelatin, the random and uniaxially aligned nanofibers showed static water contact angles of 61.8° and 60.3°, respectively. The incorporation of gelatin significantly enhances the hydrophilicity of the nanofiber scaffolds because of the amine and carboxyl functional groups in the gelatin structure. Furthermore, by depositing fibronectin on the different types of nanofiber

scaffolds, the water droplets were almost completely absorbed by the samples because of their enhanced hydrophilicity. Such an improvement in hydrophilicity will be beneficial to both the cell adhesion and proliferation.

For cardiac repair, the nanofiber-based patch must be strong enough to withstand the forces exerted by physiological activities and/or by tissue growth. Furthermore, the modulus of the scaffold can also impact the behavior of the cells seeded on it and thus the reparative efficacy of the obtained cellular patch. Figure 5 shows the stress–strain curves of the different types of nanofiber scaffolds. The aligned nanofibers showed a higher tensile strength than the random nanofibers, while the incorporation of gelatin resulted in decreases for both the tensile strength and the elongation at break of the scaffolds. The Young's moduli of the scaffolds made of PCL nanofibers in a random or aligned orientations were 15.3±4.7, 24.2±6.4 MPa, while those scaffolds made of a mixture of PCL and gelatin in a random or aligned orientations were 50.72±9.34 and 71.9±8.3 MPa, respectively. Although the incorporation of gelatin led to increase in the moduli of the nanofiber scaffolds, all the nanofiber scaffolds can meet clinical suturing and transportation requirements.

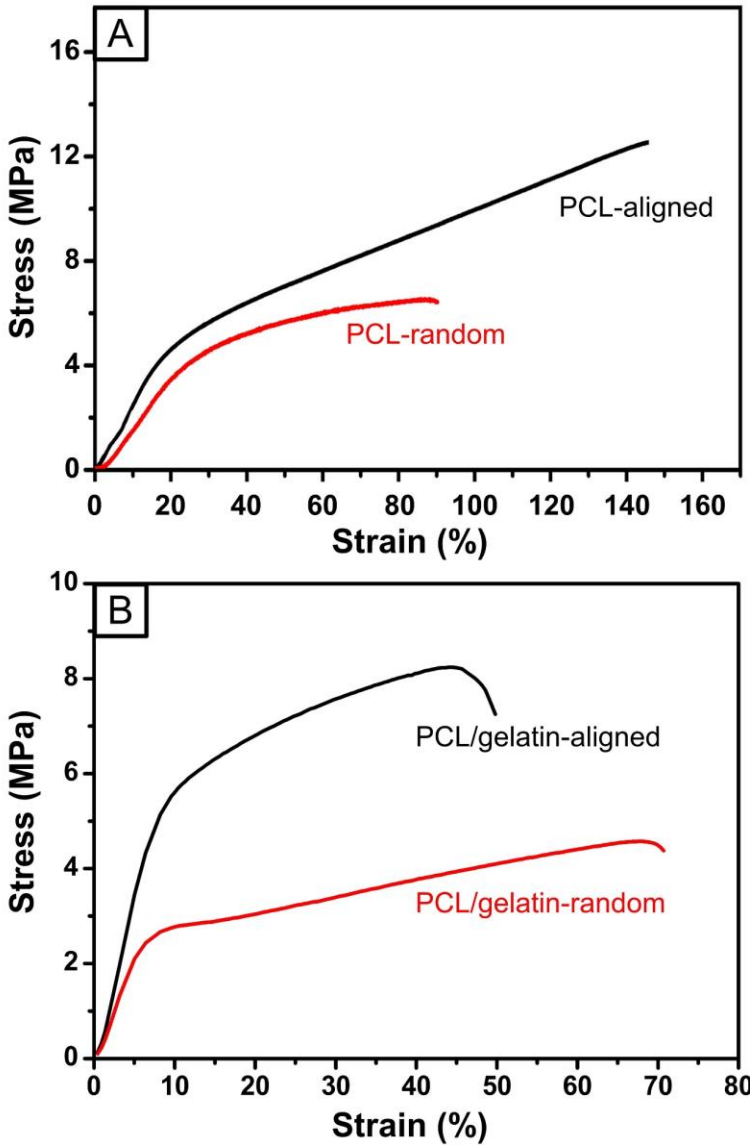

Figure 5. Curves for scaffolds comprised of random or uniaxially aligned electrospun nanofibers made of (A) PCL and (B) a mixture of PCL and gelatin.

3.4.2 CPC alignment and morphology on random and aligned nanofiber-based scaffolds

We firstly compared the behavior of the CPCs on the scaffolds made of only PCL nanofibers. Neonatal and child CPCs were separately seeded onto either random or aligned nanofiber scaffolds and maintained in culture for up to 7 days. Figure 6A and C shows the

morphologies of the cells on the nanofiber scaffolds, respectively. On the random fibers, the cells showed no preferred cytoskeletal orientation. On the aligned fibers, more cells extend their cytoskeletons along the fiber alignment. The quantified cell alignment, area, and elongation are shown in Figure 6B and D. Both neonatal and child CPCs showed increase in their alignment on aligned nanofiber scaffolds compared to that on random nanofiber scaffolds. Cell area and eccentricity (elongation), however, were not significantly affected by the alignment of the nanofibers.

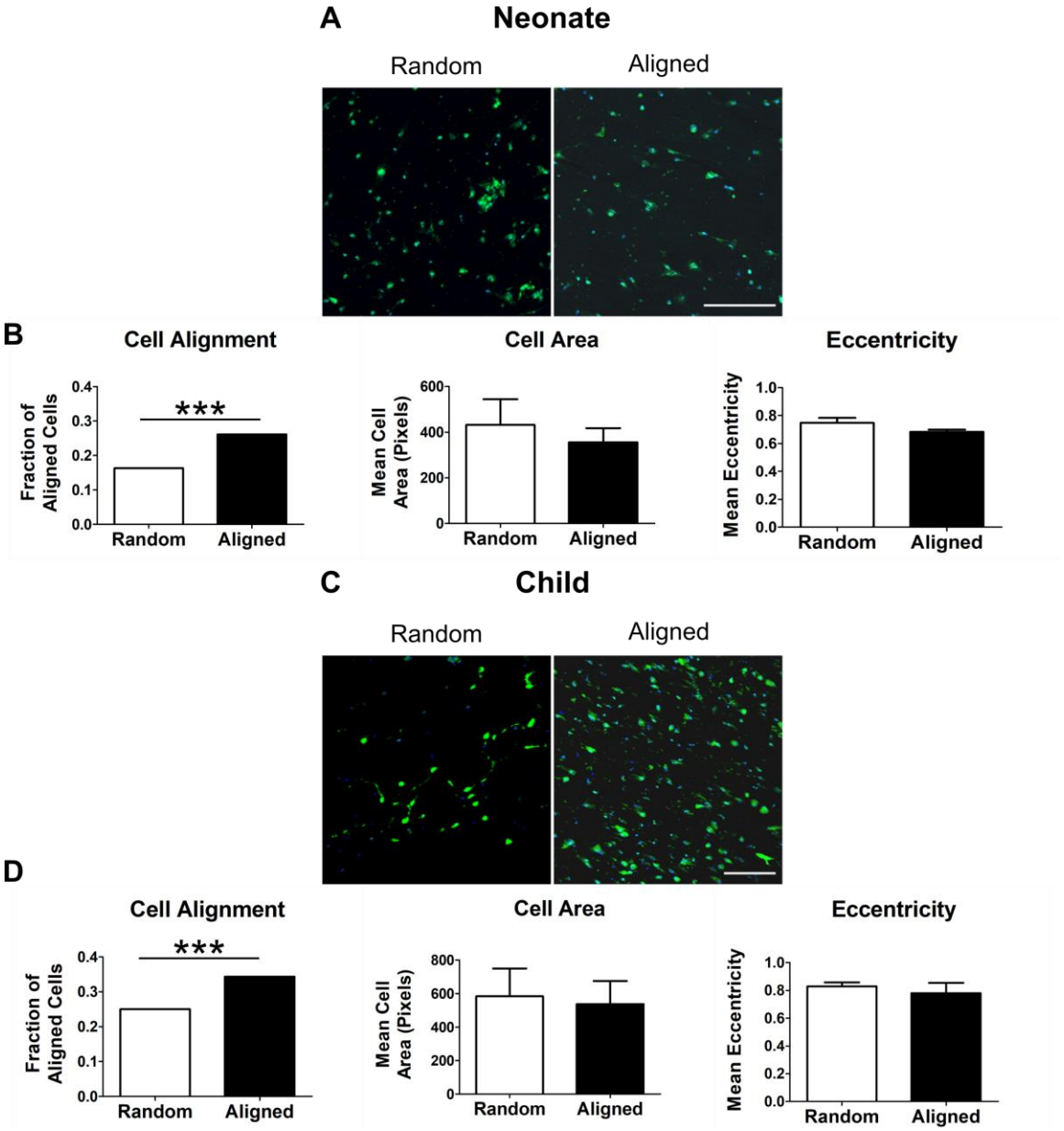

Figure 6. Fluorescence images of the (A) neonatal and (C) child CPCs on random or aligned PCL nanofiber scaffolds, respectively. Fluorocein-5-maleimide and DAPI staining are shown in green and blue, respectively. Scale bar = 200 μm. Alignment, area, and eccentricity of the (B) neonatal and (D) child CPCs on the different types of scaffolds are quantified. (n = 3 fields of view from at least 3 different patches, ***p <0.001 by Fisher's exact test with Bonferroni correction)

3.4.3 CPC metabolism on random and aligned nanofiber-based scaffolds

Cell retention and survival following injection into the myocardium is often low due to leakage at the injection site and subsequent washing away by circulating blood, reducing the effectiveness of cell therapy[240]. The use of a scaffold may help enhance cell retention at the site of implantation, and it is therefore important to assess the scaffold's ability to maintain cell viability and proliferation. We measured the relative CPC metabolic activity at 1, 3, and 7 days on random and aligned PCL nanofiber scaffolds. From Figure 7A, neonatal CPCs had significantly greater fluorescence readings at day 1 on scaffolds made of random nanofibers compared to those made of aligned nanofibers, and, although not statistically significant, also showed higher readings on the scaffolds made of random nanofibers at days 3 and 7. Child CPCs displayed similar metabolic activity regardless of the orientation of the nanofibers across all the different time points (Figure 7B).

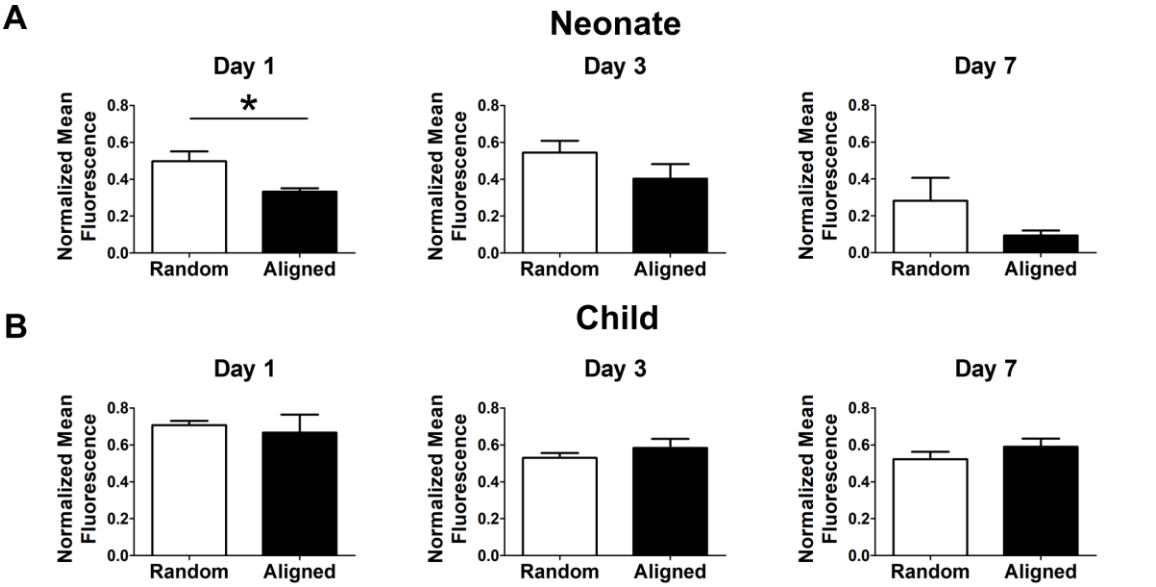

Figure 7. The Alamar Blue® normalized mean fluorescence of the (A) neonatal and (B) child CPCs quantified at 1, 3, and 7 days post-seeding on the random and aligned PCL nanofibers. (n = 5–6, *$p < 0.05$ by Student's t-test)

3.4.4 Functional anti-fibrotic paracrine release of CPCs on random and aligned nanofiber-based scaffolds

While cell retention is low following injection, many cardiac stem cell-based therapies still elicit modest improvements in cardiac function. Because of this, the main mode of action of the injected cells is thought to be through the secretion of reparative and cardioprotective paracrine factors[12]. To compare the functionality of paracrine factors secreted by the CPCs on random and aligned PCL nanofibers, we examined the influence of the different conditioned media on the fibrotic gene expression from rat cardiac fibroblasts (RCFs) by stimulating the cells with transforming growth factor beta (TGF-β) to induce fibrotic gene expression. We first treated RCFs with conditioned media collected from patches with neonatal CPCs at Day 2 and observed that the patch conditioned media collected at Day 2 was not able to decrease RCF fibrotic gene expression (Figure 8).

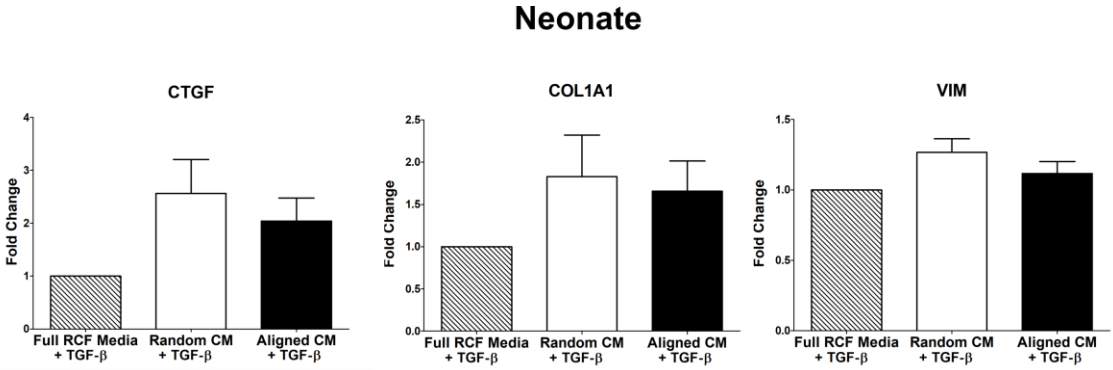

Figure 8. The expression of fibrotic genes from RCFs after incubation upon the TGF-β stimulation in conditioned media collected at day 2 from the random and aligned patches with neonatal. (n = 5)

We then treated RCFs with conditioned media collected from patches collected at Day 5. As shown in Figure 9A, the expression levels of VIM and COL1A1 in RCFs significantly decreased after treatment with the conditioned medium collected at day 5 from patches comprised of neonatal CPCs on PCL nanofibers relative to the case when RCFs were cultured in the full medium ($p < 0.01$). From Figure 9B, when RCFs were treated with conditioned media collected at day 5 from child CPCs cultured on random or aligned PCL nanofibers, the expression levels of COL1A1 and CTGF in RCFs were reduced relative to the case when the RCFs were treated with the full medium ($p < 0.01$).

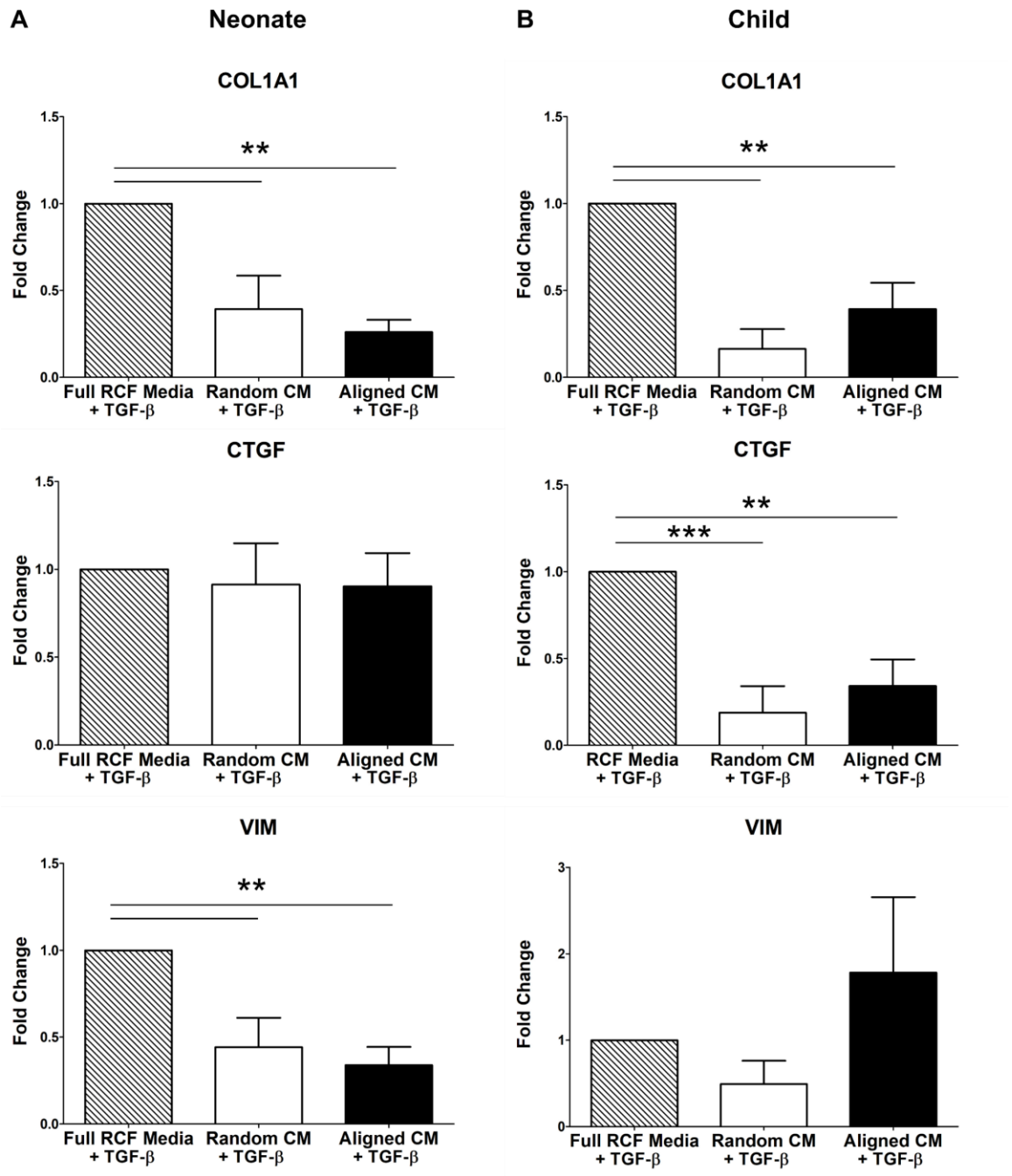

Figure 9. The expression of fibrotic genes from RCFs after incubation upon the TGF-β stimulation in conditioned media collected at day 5 from the random and aligned patches with (A) neonatal or (B) child CPCs. (n = 6, ***$p < 0.001$, **$p < 0.01$ by one-way ANOVA with Tukey's post-hoc test)

3.4.5 Functional pro-angiogenic paracrine release of CPCs on random and aligned nanofiber-based scaffolds

To examine the pro-angiogenic potential of the paracrine factors secreted by the CPCs on the patches, we performed a tube formation assay. Figure 10 shows the typical morphology of the HUVECs and the number and total length of the tubules after cultured in the different conditioned media for 6 h. As shown in Figure 10A, the conditioned medium collected at day 2 from the patches comprised of neonatal CPCs on random PCL nanofibers led to a significant increase in both the total tube length and the number of formed tubules than that collected from the patches comprised of neonatal CPCs on aligned PCL nanofibers ($p < 0.05$). A similar result was also observed from the patches containing the child CPCs (Figure 10B). The random nanofibers resulted in the formation of significantly more tubules ($p < 0.05$) with increased total tube length ($p < 0.01$) from the HUVECs. This effect was also observed with conditioned media collected at day 5 from patches with child CPCs (Figure 11B) but not with conditioned media collected at day 5 from patches with neonatal CPCs (Figure 11A). In total, CPCs cultured on random PCL nanofibers exhibited greater secretion of pro-angiogenic paracrine signals than those on the aligned PCL nanofibers.

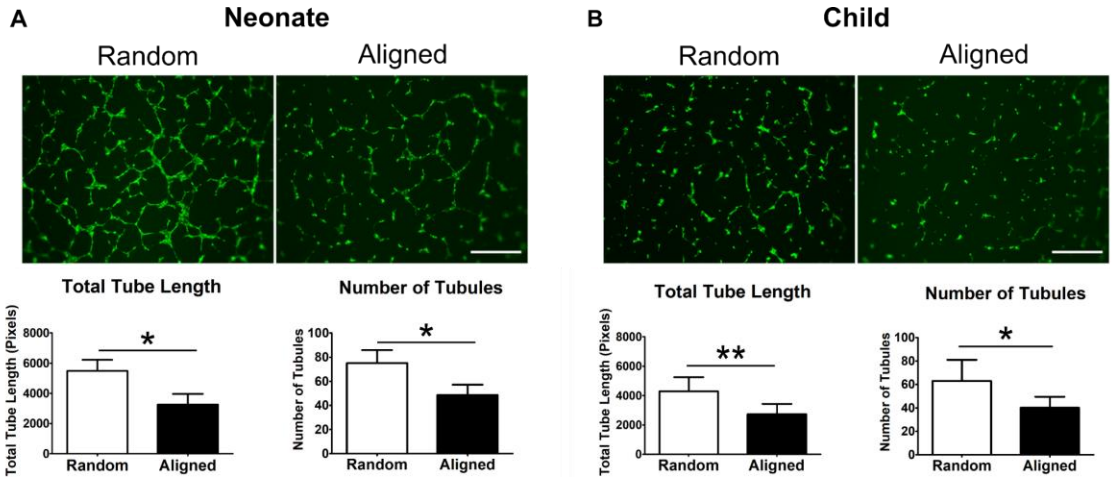

Figure 10. HUVEC tube formation on Matrigel following 6 h incubation in conditioned media collected at day 2 from random and aligned patches with (A) neonatal or (B) child CPCs, respectively. Calcein-AM staining is shown in green. Scale bar = 200 µm. Total tube length and number of tubules are quantified for HUVECs. (n = 6, $^{**}p < 0.01$, $^{*}p < 0.05$ by Student's t-test)

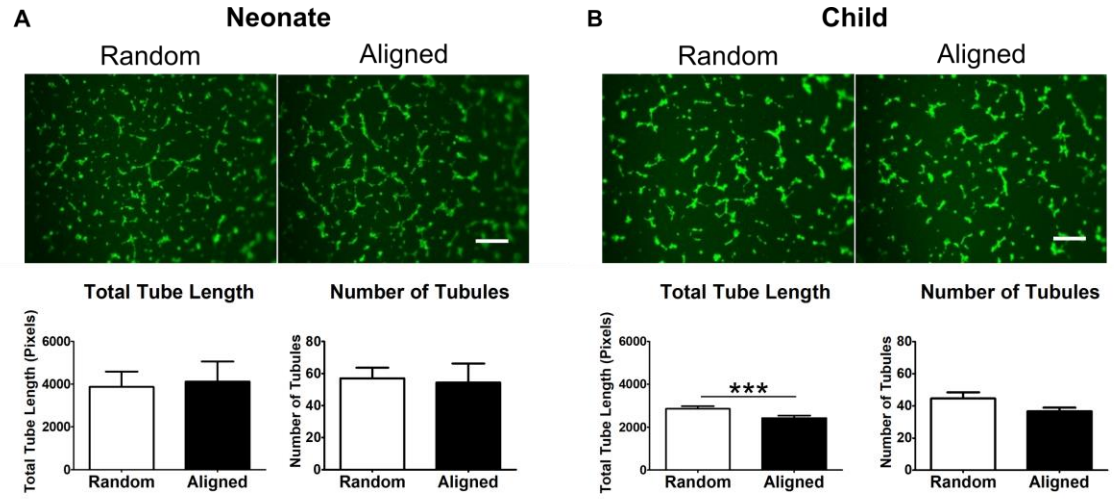

Figure 11. HUVEC tube formation on Matrigel following 6 h incubation in 5-day conditioned media collected from random or aligned electrospun nanofiber-based patches with (A) neonatal or (B) child CPCs, respectively. (n = 3, ***p < 0.001 by Student's t-test)

3.4.6 CPC alignment and morphology on the modified scaffolds including gelatin and fibronectin

Electrospun nanofibers can be easily functionalized with adhesion factors. To mimic the composition of the ECM more closely in the native CPC niche, we introduced gelatin (Gel) into the electrospun PCL nanofibers and/or coated the surface of the scaffolds with fibronectin (FN). We assessed the behaviors of cells on 8 different types of scaffolds: random PCL alone, random PCL + Gel, random PCL + FN, random PCL + Gel + FN, aligned PCL alone, aligned PCL + Gel, aligned PCL + FN, and aligned PCL + Gel + FN. The morphology and alignment of both neonatal and child CPCs were assessed on the different types of scaffolds, as was done for the scaffolds made of random and aligned PCL nanofibers.

As shown in Figure 12, A and B, both the neonatal and child CPCs extended their cytoskeletons along the fiber alignment on the uniaxially aligned fibers. Further, the alignment and cell area of the neonatal CPCs were increased on the PCL + Gel + FN scaffolds. In addition, the largest number of the neonatal cells were observed on PCL + Gel + FN scaffolds. For child CPCs, integration of adhesion factors with the scaffold did not significantly increase the alignment of the cells in the aligned fiber group, but scaffolds containing gelatin did show decreases in cell alignment (Figure 12C and D). The area of the child CPCs showed no significant changes upon addition of gelatin and fibronectin in the scaffold (Figure 12D).

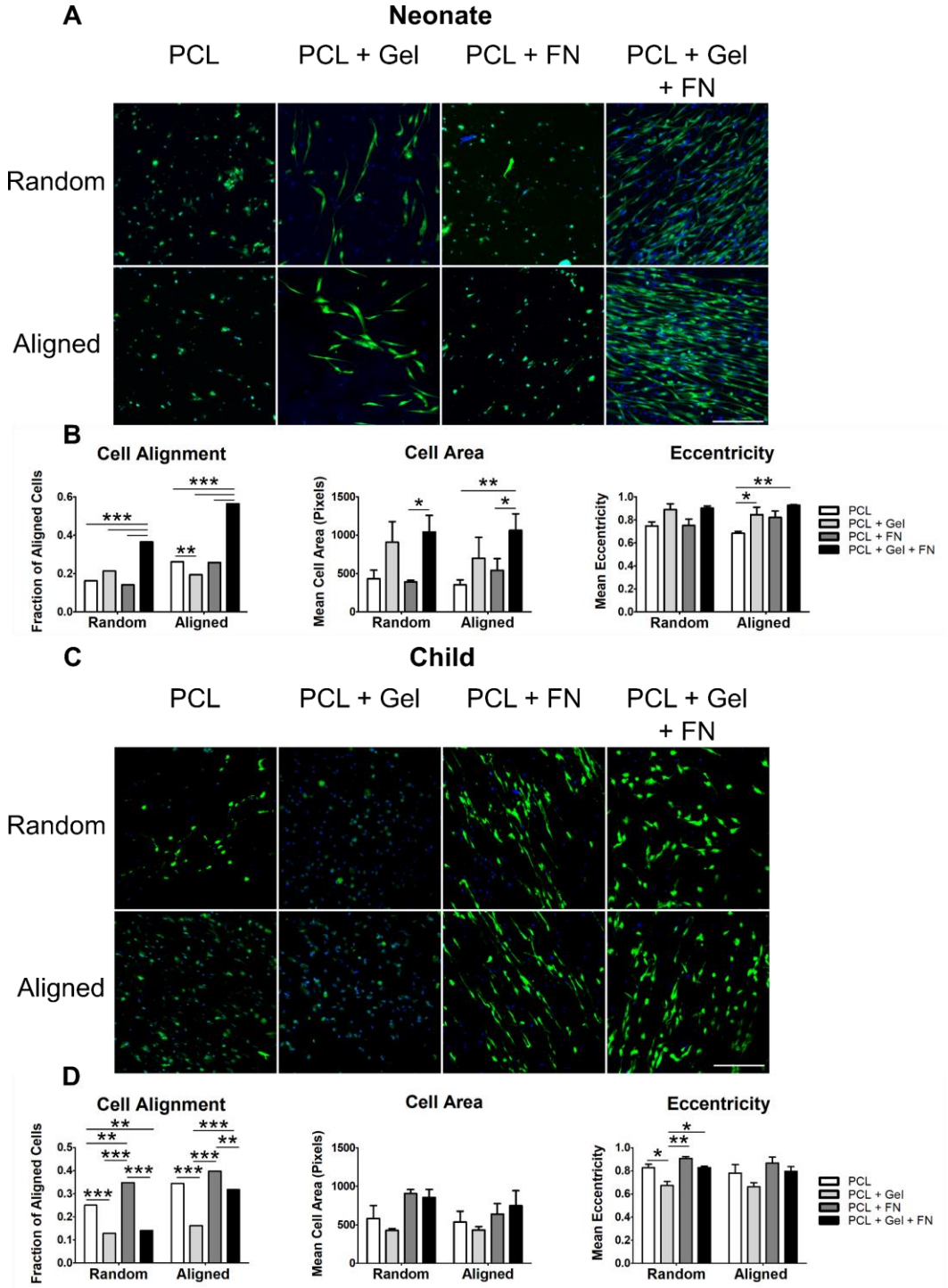

Figure 12. Cell morphology images for (A) neonatal and (C) child CPCs on random or aligned PCL, PCL + Gel, PCL + FN, and PCL + Gel + FN scaffolds. Fluorocein-5-maleimide and DAPI staining are shown in green and blue, respectively. Scale bar = 200 μm. Analysis of the alignment, area, and eccentricity is quantified for (B) neonatal and (D) child CPCs on the different types of scaffolds. (n = 3 fields of view from at least three different scaffolds, ***$p < 0.001$, **$p < 0.01$ by Fisher's exact test with Bonferroni correction)

3.4.7 CPC metabolism on the modified scaffolds including gelatin and fibronectin

Cell metabolism of neonatal and child CPCs was also measured on the 8 different types of nanofiber scaffolds at 1, 3 and 7 days. At day 1, neonatal CPCs showed increased metabolic activity on PCL + Gel + FN scaffolds within the random group and on all scaffolds with adhesion factors within the aligned groups. These increases were later only seen in the aligned group, with increased activity on PCL + FN scaffold at day 3 and on PCL + FN and PCL + Gel + FN scaffolds on day 7 (Figure 13A). Child CPCs showed no significant changes in metabolic activity on day 1 regardless of the type of the scaffolds. At day 3 and day 7, PCL + FN and PCL + Gel + FN scaffolds showed increased metabolism of the CPCs compared within the random group, while only PCL + Gel + FN scaffold showed increased cell metabolism within the aligned group (Figure 13B).

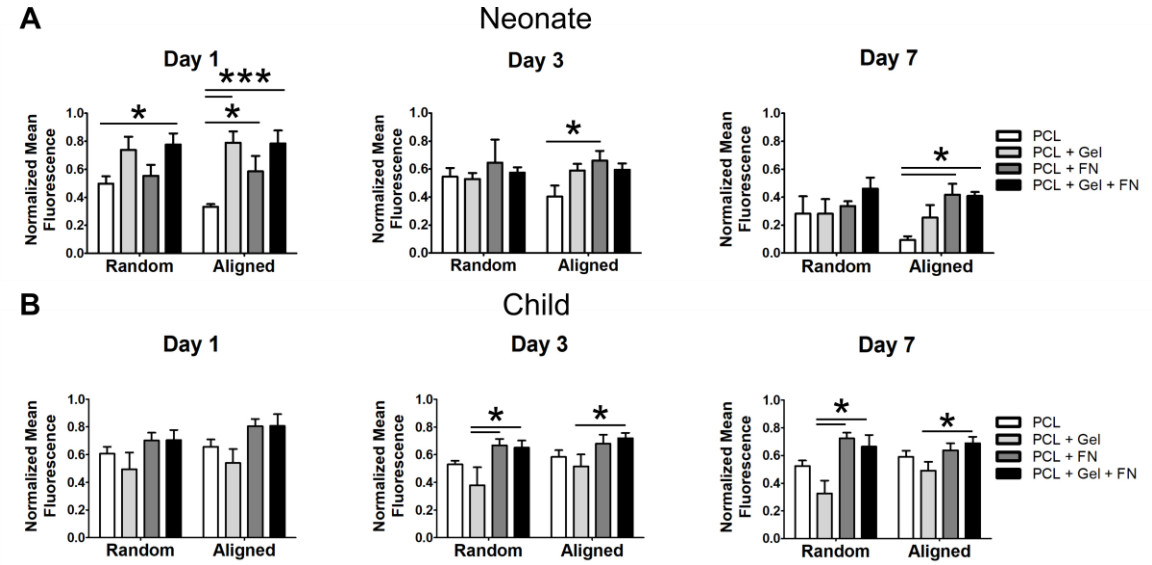

Figure 13. Cell metabolism of the (A) neonatal and (B) child CPCs quantified at 1, 3, and 7 days post-seeding on the different types of scaffolds. (n = 5–6, **p* < 0.05 by one-way ANOVA with Tukey's post-hoc test)

3.4.8 Reparative growth factor secretion of neonatal CPCs from patches including gelatin and fibronectin

Inclusion of adhesion factors in the nanofiber-based scaffolds was done not only to modulate CPC morphology and viability, but also to investigate their influence on the reparative paracrine secretion from the resultant cellular patches. Therefore, we performed a Luminex® assay on conditioned media collected at day 3 and day 7 from each patch seeded with neonatal CPCs to measure reparative growth factor secretion. Using this assay, we measured the growth factor concentration of the following 8 different reparative growth factors in patch conditioned media: Interleukin-2 (IL-2), basic fibroblast growth factor (FGFb), vascular endothelial growth factor A (VEGF-A), stromal cell-derived factor 1α (SDF-1a), matrix metalloproteinase-1 (MMP-1), angiogenin, hepatocyte growth factor (HGF), and matrix metalloproteinase-9 (MMP-9). In conditioned media at day 3, conditioned media from aligned PCL + Gel patches had a decreased MMP-9 concentration compared to conditioned media from PCL alone patches ($p < 0.05$). This was the only instance in which inclusion of gelatin and/or fibronectin changed the reparative growth factor secretion in day 3 conditioned media collected from each patch (Figure 14A). For day 7 conditioned media, there were no changes in the concentration of any growth factor measured (Figure 14B).

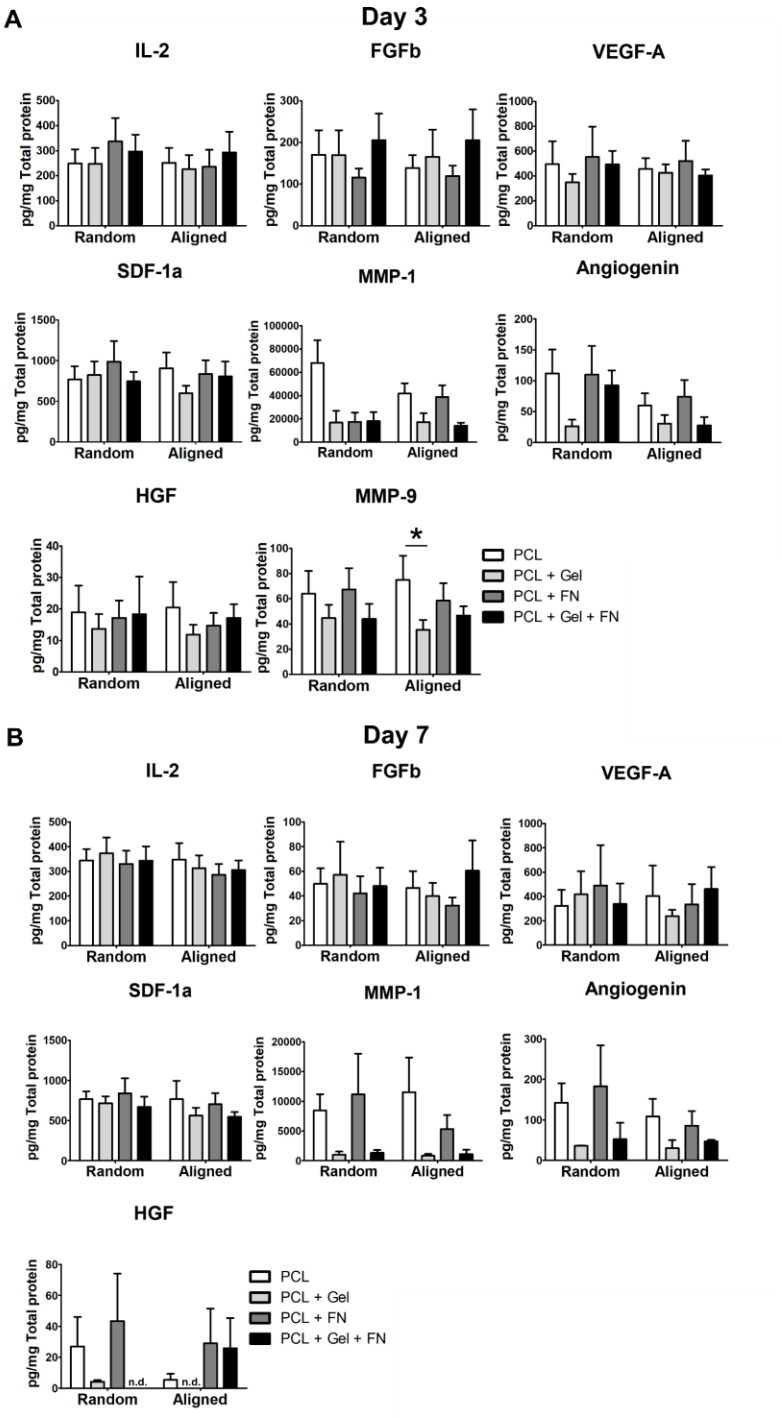

Figure 14. Normalized growth factor concentrations in (A) 3- and (B) 7-day conditioned media collected from each neonatal CPC patch group as measured by a Luminex® Assay. Concentrations for interleukin-2 (IL-2), basic fibroblast growth factor (FGFb), vascular endothelial growth factor A (VEGF-A), stromal cell-derived factor-1α (SDF-1a), matrix metalloproteinase-1 (MMP-1), angiogenin, hepatocyte growth factor (HGF), and matrix metalloproteinase-9 (MMP-9) are displayed (n = 2-6, *$p < 0.05$ by one-way ANOVA with Tukey's post-hoc test, n.d.= no data).

3.4.9 Functional angiogenic paracrine release of CPCs from patches including gelatin and fibronectin

We next performed a tube formation assay with the conditioned media collected from the different groups of patches containing either the neonatal or the child CPCs to measure functional angiogenic paracrine secretion. Figure 15 shows the morphologies of the HUVECs cultured in the conditioned media collected from the different types of patches at day 2. As shown in Figure 15, when the conditioned media were collected from the patches with neonatal CPCs, both total tube length and number of tubules formed in the media were unaffected by inclusion of gelatin and fibronectin in the random nanofibers and was not enhanced but rather diminished by inclusion of gelatin in the aligned nanofibers. For the conditioned media collected from patches with child CPCs, their angiogenic potential was the greatest in the aligned PCL + FN group (Figure 15B). No changes in the angiogenic potential of conditioned media collected at day 5 from patches with neonatal CPCs were observed (Figure 16A)., while conditioned media collected at day 5 from child CPCs cultured on random PCL + Gel + FN scaffolds had reduced angiogenic potential (Figure 16B). Although not statistically significant, conditioned media from aligned PCL + FN patches with child CPCs again increased HUVEC tube formation. Taken together, these data suggest that while inclusion of gelatin and fibronectin does not improve the pro-angiogenic paracrine secretion of neonatal CPCs, the angiogenic paracrine secretion of child CPCs may improve from inclusion of fibronectin in aligned-fiber patches.

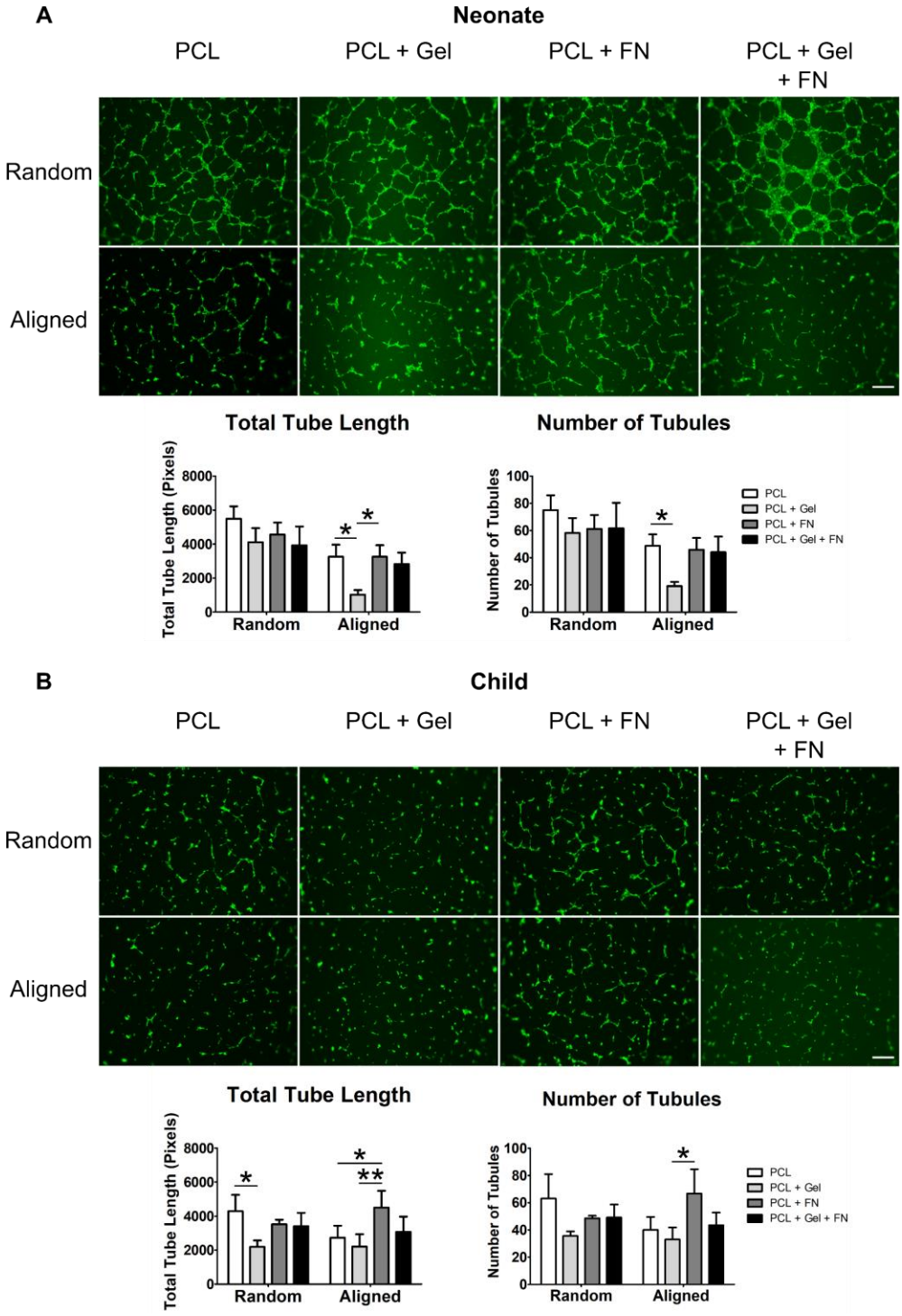

Figure 15. Fluorescence images showing the morphologies of HUVECs after incubation in conditioned media collected at day 2 from random or aligned PCL, PCL + Gel, PCL + FN, and PCL + Gel + FN patches with (A) neonatal or (B) child CPCs. Calcein-AM staining is shown in green. Scale bar = 200 μm. The total tube length and number of tubules are quantified from the corresponding images. (n = 6, $^{**}p < 0.01$, $^{*}p < 0.05$ one-way ANOVA with Tukey's post-hoc test)

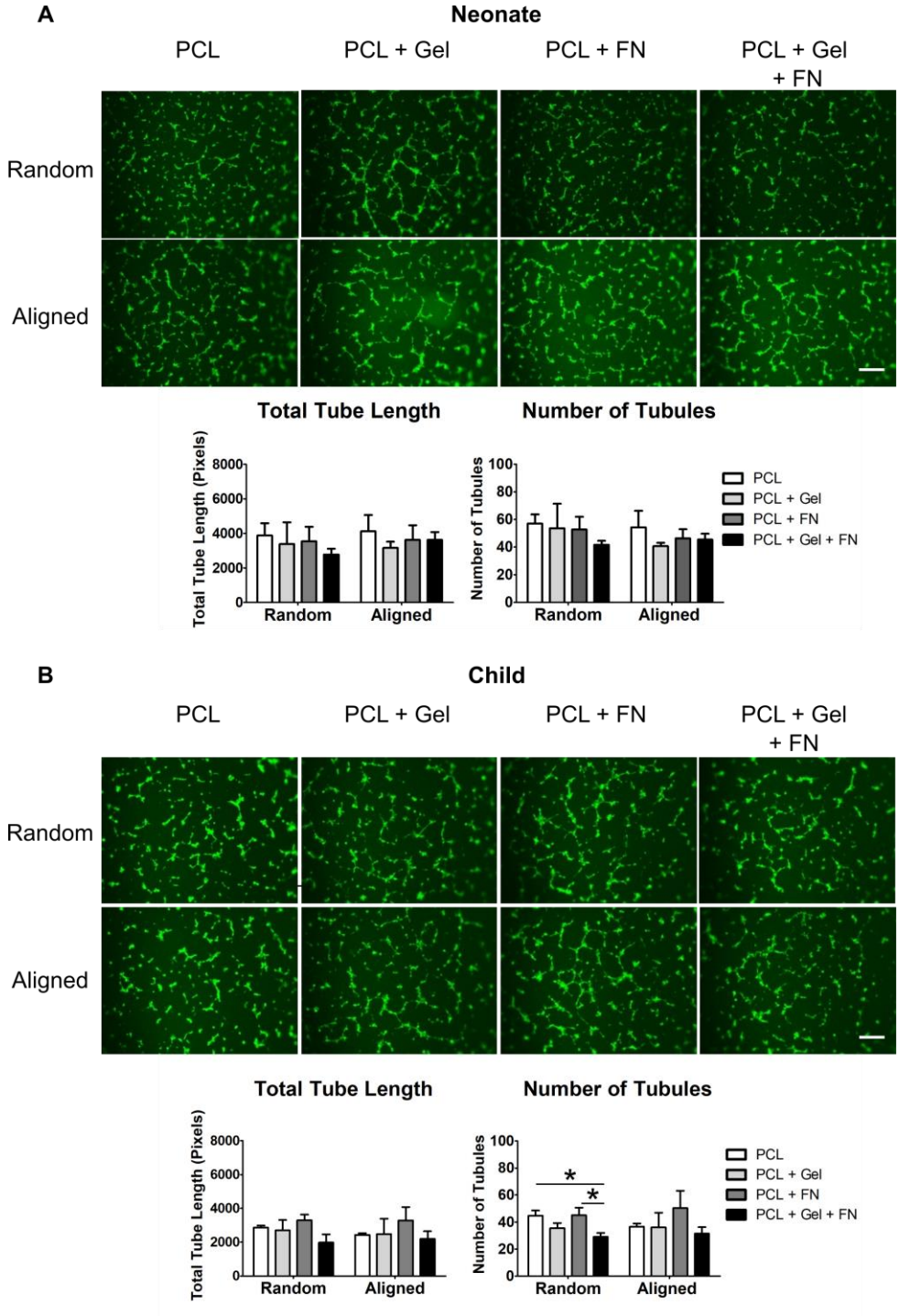

Figure 16. Fluorescence images showing the morphologies of HUVECs after incubation in conditioned media collected at day 5 from random or aligned PCL, PCL + Gel, PCL + FN, and PCL + Gel + FN patches with (A) neonatal or (B) child CPCs. Calcein-AM staining is shown in green. Scale bar = 200 μm. The total tube length and number of tubules are quantified from the corresponding images (n = 3, $*p < 0.05$ by one-way ANOVA with Tukey's post-hoc test)

3.5 Discussion

Stem cell therapies, including those using c-kit$^+$ CPCs, continue to show promise in preclinical studies to restore cardiac function that has been lost due to the deleterious effects of CHD and subsequent palliative surgery[147,225,230]. However, these therapies are still hampered by low cell retention at the site of injection and little-to-no replacement of the damaged native cardiomyocytes[15,16]. Because of this, it is widely thought that paracrine signals, such as reparative growth factors and exosomes, secreted by the implanted cells are the main source of cardiac improvement following cell injection[12–14]. Therefore, there is a need to both improve the cell retention following implantation and to maximize the reparative paracrine signal secretion of the implanted cells. Here, we present a method to accomplish these goals by combining electrospun nanofiber-based scaffolds and c-kit$^+$ CPCs to create reparative cardiac patches.

Electrospun nanofiber-based patches have been investigated extensively in pre-clinical studies for cardiac repair. Additionally, because of the ease in modification and functionalization of electrospun nanofiber-based scaffolds, many previous studies have combined different polymers with various modifications to make unique cardiac patches[181]. For example, plasma-treated PCL electrospun nanofiber patches could be used to effectively deliver bone marrow-derived mesenchymal stem cells (MSC) to repair the chronic myocardial infarction in a rat model[246]. The MSC-loaded patches improved cardiac functional parameters such as ejection fraction and fractional shortening four weeks after implantation and improved vessel formation in the patch-treated hearts. Other studies report functional benefit conferred through processes such as angiogenesis and reductions in fibrosis following patch implantation[186,247]. We were able to create electrospun nanofiber

scaffolds made of PCL or a mixture of PCL and gelatin with both random and aligned orientations and successfully modified each of these scaffolds by coating their surface with fibronectin. Following culturing of CPCs on each scaffold, we found that the resulting patches were able to produce paracrine signals that had anti-fibrotic and pro-angiogenic functionality. The nanofiber-based patches' paracrine effect on cardiomyocytes is also an important consideration for the patches' use as a treatment for ventricular failure. While not explored in this study, changes in cardiomyocyte phenotypic parameters, such as proliferation and hypertrophy, and functional parameters, such as contractility, are of great interest. We also detected the presence of pro-angiogenic growth factors vascular endothelial growth factor and angiogenin, immunomodulatory factors IL-2 and hepatocyte growth factor, ECM remodeling factors MMP-1 and MMP-9, and stem cell recruitment factors bFGF and SDF-1a in the conditioned media of the nanofiber-based patches (Figure S3), further suggesting the reparative potential of our patch's paracrine release.

CPCs begin to lose their reparative potential as early as one year old, showing the age-dependent difference in CPCs behavior[248]. Neonatal CPCs injected into a rat model of RVHF could increase RV ejection fraction, decrease RV wall thickness, and improve tricuspid annular plane systolic excursion, but child CPCs did not have this reparative capability[147]. Other studies have also shown age-dependent changes in c-kit$^+$ CPC paracrine release[12]. However, clinical trials using stem cell therapy to treat CHD often have patient pools with varying ages, meaning that the autologous therapies used in these trials may have varying degrees of success simply due to the age the of the patient. For example, the average age of patients enrolled in the recent Transcoronary Infusion of Cardiac Progenitor Cells in Patients With Single Ventricle Physiology (TICAP, NCT01273857)

trial was 1.8 ± 1.5 years-old,[230] meaning that the reparative capacity of stem cells from many of these patients may have already begun to decline. As such, it is important to use a scaffold that can successfully support CPCs with varying ages and reparative capabilities.

Our results showed marked age-dependent differences in CPC alignment and morphology in response to the inclusion of adhesion factors to the scaffolds. While addition of both gelatin and fibronectin into the nanofibers increased alignment in neonatal CPCs, inclusion of fibronectin into random nanofibers was the only instance that increased alignment of child CPCs on the patch. Additionally, inclusion of gelatin and fibronectin was not able to increase neonatal CPC patches' ability to induce angiogenesis, but addition of fibronectin into aligned nanofibers did increase this ability in child CPC patches. Taken together, our study shows how different parameters can affect CPCs from various donors, suggesting which nanofiber-based patch may be most suitable for a given patient's CPCs. These considerations are vitally important to the success of autologous, patient-specific cardiac therapies.

The causes of heart failure in different CHDs may differ from each other, so it is important to tailor a therapy according to the specific condition of a patient. For example, conditions such as hypoplastic left heart syndrome in which pressure and volume overloads are imposed on the RV can lead to myocyte hypertrophy. In this case, there will be increased metabolic demand in the myocardium, and increased nutrient delivery through angiogenesis would be beneficial[214]. To this end, our data suggests that random nanofiber-based patches would be most beneficial upon implantation in these patients, as the conditioned media collected from the random nanofiber-based patches induced higher degrees of angiogenesis. Other diseases caused by ischemic events may lead to myocyte

death and subsequent replacement fibrosis[249]. Because both aligned and random nanofibers-based patches were shown to decrease fibrotic gene expression in RCFs, both patches may be suitable for treating such a condition. The differences in the mechanical properties of each scaffold may also confer differing mechanical supports to the failing heart. We found that random fiber-based scaffolds had a lower Young's modulus compared to aligned fiber-based scaffolds, and that addition of gelatin decreased the Young's modulus of scaffolds with either fiber orientation. The anisotropic properties of aligned fiber-based scaffolds may enhance their mechanical support to the anisotropic myocardium. Hydrophobicity has also been shown to affect the effectiveness of implanted biomaterials, with hydrophilic biomaterials being more easily accepted[250]. Our data showed that patches with either gelatin or fibronectin were much more hydrophilic than patches based on PCL alone. Although not specifically investigated here, PCL patches with adhesion factors may be better tolerated upon implantation.

3.6 Conclusion

We have demonstrated that the scaffolds based on electrospun nanofibers could successfully maintain viable neonatal and child CPCs and that the cell-loaded patches were easily adaptable to mimic the native myocardial microenvironment more closely. Various modifications could be used to optimize the morphology and reparative capacity of CPCs. However, the impacts of all these modifications on the CPC behavior were found to be dependent on the age of the cells. This study sets the stage for the use of electrospun nanofibers as appropriate scaffolds to generate cellular patches. The patches may be suitable for autologous pediatric cardiac cell-based therapies for *in vivo* treatment of RVHF.

CHAPTER 4. PATIENT-SPECIFIC DESIGN AND IMPLANTATION OF CARDIAC PATCHES FOR RIGHT VENTRICULAR HEART FAILURE

4.1 Abstract

Autologous cardiac cell therapy is a promising treatment for combating the right ventricular heart failure (RVHF) that can occur in patients with congenital heart disease (CHD). However, autologous cell therapies suffer from low cell retention following injection and patient-to-patient variability in cell quality. Here, we demonstrate how computational methods can be used to identify mechanisms of cardiac-derived c-Kit^{+} cell (CPC) reparative capacity and how biomaterials can be designed to improve cardiac patch performance by engaging these mechanisms. Computational modeling revealed the integrin subunit α_V (ITGAV) as an important mediator of repair in CPCs with inherently low reparative capacity (CPCs^{low}). We could engage ITGAV on the cell surface and improve reparative capacity by culturing CPCs on electrospun polycaprolactone (PCL) patches coated with fibronectin (PCL + FN). We tested CPCs from 4 different donors and found that only CPCs^{low} with high ITGAV expression (patient 956) had improved anti-fibrotic and pro-angiogenic paracrine secretion on PCL + FN patches. Further, knockdown of ITGAV via siRNA led to loss of this improved paracrine secretion in patient 956 on PCL + FN patches. When implanted in rat model of RVHF, only PCL + FN + 956 patches were able to improve RV function, while PCL + 956 patches did not. In total, we demonstrate how cardiac patches can be designed in a patient-specific manner to improve *in vitro* and *in vivo* outcomes.

4.2 Introduction

Congenital heart disease (CHD), occurring in about 8 out of every 1000 newborns, is the most prevalent congenital disorder in the world and the leading cause of birth-defect related death[21,251]. Survival of CHD patients has greatly increased in the past two decades due in large part to improvements in palliative surgical techniques[23]. However, in more complex forms of CHD such as hypoplastic left heart syndrome (HLHS), right ventricular heart failure (RVHF) can occur following surgical palliation. For these reasons, HLHS is the leading cause of cardiac death from CHD despite only occurring in 0.016% to 0.036% of all births[41]. To address this issue, cell therapy has emerged as a potential supplemental therapy to rescue right ventricular function in HLHS patients[236,252]. Several therapeutic cell sources, including autologous cardiac-derived c-Kit$^+$ cells (CPCs), have been explored for use in cardiac cell therapy to combat RVHF (CHILD Trial, NCT03406884)[6,214,232]. Cardiac cell therapy, though, has its own issues that hamper its ability to improve right ventricular function, including low cell retention following injection and age-dependent decline in reparative function[70,147]. Further, because of the cells' low engraftment rate, it is thought that the injected cells cause functional improvements in the RV through paracrine mechanisms rather than by differentiating and replacing an endogenous cell population[12].

Recently, cardiac patches have been investigated as means to overcome the challenges associated with cell therapy [12,253]. Cardiac patches can improve cell function by providing biochemical and mechanical cues to induce the release of reparative paracrine factors as well as by prolonging retention *in vivo* to sustain this paracrine secretion for longer periods of time[166,254,255]. The design of a cardiac patch's biomaterial should be tailored to the cell of choice to increase cell survival and reparative paracrine factor

secretion. For cardiac patch therapies using autologous cell sources, cells from different patients may have differential expression of several genes including those encoding cell surface proteins (*i.e.*, integrins), and, therefore, may respond differently to the biomaterials in which they are delivered[12,218,256]. Thus, a "one-size-fits-all" approach to biomaterial design for a given primary cell type may work for cells from some donors but fail for cells from others.

Statistical modeling approaches have been employed for patient-specific biomaterial therapies. These approaches span tailoring the mechanics and geometries of cardiac biomaterial implants at the gross anatomical level to optimizing extracellular matrix (ECM) cues from a biomaterial's microenvironment to a given cell population[257,258]. Previously, our laboratory has used statistical modeling to identify mechanistic mRNA signals that are important for improving CPC reparative capacity and to predict the ability of CPCs from different donors to improve right ventricular function *in vivo*[218]. We have also investigated the influence of cardiac patches made of electrospun polycaprolactone (PCL) nanofibers on the reparative paracrine secretion of pooled lines of younger, more reparative CPCs and pooled lines of older, less reparative CPCs. Importantly, PCL patches whose surface was functionalized with the ECM protein fibronectin (PCL + FN) improved the less reparative CPCs' survival and angiogenic paracrine secretion[10]. Here, we seek to design a cardiac patch to improve the reparative capacity of inherently poor-performing CPCs in a patient-specific manner. Using a partial least squares regression model (PLSR), we show that expression of the α_v integrin subunit (ITGAV) in CPCs with low reparative capacity ($CPCs^{low}$) is highly correlated with improvements in predicted functional outcomes. We investigate how CPCs from four different donors with differing

characteristics (high/low reparative capacity and high/low ITGAV signaling) respond to culture on PCL or PCL + FN scaffolds and how knockdown of ITGAV affects these responses. Finally, we implant PCL + FN patches seeded with $CPCs^{low}$ that have high ITGAV expression into a rodent model of RVHF. We find that these PCL + FN + CPC^{low} patches improve function, increase angiogenesis, and decrease myocyte hypertrophy in the right ventricle compared to their PCL + CPC^{low} patch counterparts. Taken together, this work demonstrates how statistical modeling can be used to identify mechanisms of cellular responses to cardiac patch biomaterials and how these mechanisms can be exploited to improve cardiac patch design.

4.3 Materials and Methods

4.3.1 Chemicals and materials

All materials were purchased from Thermo Fisher Scientific Life Sciences unless otherwise stated. PCL (Mn ≈ 80 kDa), 2,2,2-trifluroroethanol, and Bouin's solution were obtained from Sigma-Aldrich. Ham's F12 medium and Matrigel® were obtained from Corning. Fetal bovine serum was obtained from GE Healthcare. L-glutamine was purchased from MP Biochemicals, and basic fibroblast growth factor (bFGF) was purchased from Stem Cell Technologies. TRIzol was purchased from Invitrogen. Endothelial cell media (EGM^{TM}-2 BulletKit) was purchased from Lonza. ITGAV siRNA, control siRNA, siRNA Transfection Reagent, and siRNA Transfection Medium were purchased from Santa Cruz Biotechnology. Isoflurane, USP was purchased from Piramal Healthcare. Histo-Clear was purchased from VWR.

4.3.2 Computational analysis of CPC patients and integrin expression

RV functional benefit following CPC injection for CPCs from 32 different patients was predicted using a PLSR model previously published by Shoja-Taheri et al[218]. Briefly, the PLSR model created using SIMCA-P software was based on the top 300 genes that were the most important signals for influencing functional outcomes and trained on previously acquired functional outcomes in rat pulmonary artery band (PAB) models. Gene expression values as measured by RNA-seq in a previously described process[218] were then used to train a model to predict the functional responses (tricuspid annular plane systolic excursion (TAPSE), angiogenesis, fibrosis, and RV wall thickness). Based on these functional responses, CPCs were sorted into a high reparative capacity (CPC^{high}) or low reparative capacity group (CPC^{low}). High reparative CPCs had predicted functional outcomes that were at least within 10% of healthy values in all categories. Each of the predicted functional responses was regressed against expression of 11 different integrin subunits (ITGA1, ITGA2, ITGA3, ITGA4, ITGA5, ITGAV, ITGB1, ITGB2, ITGB3, ITGB4, and ITGB5) for both the CPC^{high} and CPC^{low} subsets. A given integrin was said to significantly correlate with improvements in each outcome if the correlation was positive and the p-value of the regression was less than 0.05. CPC patients for further use were then chosen based on their ITGAV expression and reparative capacity. Four different patients (896, 903, 924, and 956) were chosen to give every possible combination of high or low reparative capacity and high or low ITGAV expression.

4.3.3 Fabrication of electrospun PCL and PCL + FN scaffolds

Scaffolds made of PCL electrospun nanofibers were fabricated using the traditional electrospinning process. Typically, a PCL solution with a concentration of 12 wt.% was prepared by dissolving PCL pellets in 2,2,2-trifluroroethanol under magnetic stirring for

12 h at room temperature. The PCL solution was injected at a rate of 1.0 mL/h through a blunt needle with a syringe pump. The needle was located at a distance of 20 cm from a ground mandrel, which was covered by aluminum foil. An optimized voltage (DC, 15 kV) was applied between the needle and the grounded mandrel to obtain a stable polymer jet. A rotating rate of 1000 rpm for the mandrel was used to collect the aligned nanofibers. The electrospinning process was carried out at room temperature and a relative humidity of 40%. After collection for 4 h, the as-obtained mats were peeled off from the aluminum foil and further dried at ambient temperature to remove the residual organic solvent. Afterwards, the PCL mats were treated with oxygen for 2 min in a plasma cleaner (Plasma Etch PE50). The mats were cut into 15 mm disks and sterilized under UV light for 30 min for both sides. To coat fibronectin, the mats were incubated in a fibronectin solution (1 μg/mL) overnight at 4 °C, followed by washing with PBS buffer and CPC media.

4.3.4 CPC isolation and culture

This study was approved by the Institutional Review Board at Children's Healthcare of Atlanta and Emory University. CPCs were isolated from patients undergoing routine surgery for various forms of CHD. A biopsy from the right atrial appendage (~70-100 mg) was obtained and transported in Krebs-Ringer solution with 35 mM NaCl, 4.75 mM KCl, 1.2 mM KH_2PO_4, 16 mM Na_2HPO_4, 134 mM sucrose, 25 mM $NaHCO_3$, 10 mM glucose, 10 mM HEPES, and 30 mM 2,3-butanedione monoxime, at a pH of 7.4 with NaOH. CPCs were isolated within 4 hours of acquiring the biopsy via magnetic bead sorting against the c-Kit protein using a process previously described[216]. Following isolation, CPCs were cultured in Ham's F12 media with 10% fetal bovine serum, 1% Pen-Strep, 1% L-glutamine, and 0.01 ng/mL bFGF (growth media).

4.3.5 Integrin adhesion array

The protein expression of α and β integrin subunits of each CPC patient (896, 903, 924, 956) was quantified using an Alpha/Beta Integrin-Mediated Cell Adhesion Array Combo Kit (Millipore Sigma) according to the manufacturer's instructions. Briefly, a total suspension of 1 million cells was dissociated form culture plates using 5 mM EDTA. A total of 10,000 cells of each CPC patient were seeded into each well of two columns (in other words, run in duplicate) of the Alpha Integrin mAb Array and Beta Integrin mAb Array plates and incubated at 37°C for 1 hour. Following incubation, cells were washed with Assay Buffer, stained with Cell Stain Solution, and treated with Extraction Buffer to produce solubilized stain in each well. The absorbance of each well was then read on a microplate reader (BioTek Synergy 2) at 550 nm.

4.3.6 CPC culture on PCL and PCL + FN patches for in vitro experiments

PCL or PCL + FN patches with a diameter of 15 mm were placed in the wells of a 24-well plate using Sigma-Aldrich Cellcrown^{TM} 24-well plate inserts. A total of 350,000 CPCs were seeded on each patch. CPCs were maintained in 2 mL of growth media for 2 days before being quiesced in Ham's F12 medium supplemented with Insulin-Transferrin-Selenium, 1% Pen-Strep, 1% L-glutamine, and 0.01 ng/mL bFGF for 1 day (treatment media). Following quiescence, the culture media was collected and termed the conditioned media of each patch. The conditioned media was then stored at -80°C until further experimentation.

4.3.7 CPC mRNA expression measured by RT-PCR

Total RNA was extracted from CPCs cultured on each patch using TRIzol reagent following the one-day quiescence in treatment media. First strand cDNA synthesis was performed with M-MLV reverse transcriptase primed by random hexamers and oligo(dT)18. Real-time PCR was performed using the StepOne system and SYBR Green fluorescence. Primer sequences are shown in Table S1.

4.3.8 Rat cardiac fibroblast TGF-β stimulation assay

Rat cardiac fibroblasts (RCFs) were cultured in 24-well plates before being quiesced for 12 hours. Following quiescence, RCFs were cultured in conditioned media from the different patches for another 12 hours. Finally, RCFs were stimulated with 10 ng/mL transforming growth factor beta (TGF-β) added directly to the conditioned media for another 12 hours. Following TGF-β stimulation, RNA was collected, and RT-PCR was run using the same protocol described above in section 2.6. Primer sequences for RCF fibrotic gene expression are shown in Table S1.

4.3.9 CEC tube formation assay

A total of 10 µl of Matrigel was pipetted into each well of an Ibidi µ-Slide. The Matrigel-coated slide was then centrifuged at 1000 rpm for 2 minutes and incubated at 37°C for 30 minutes. During this incubation, cardiac endothelial cells (CECs) were trypsinized, and 10,000 cells were seeded in each Matrigel-coated well of the slide. CECs were then incubated in 25 µl of endothelial cell basal media and 25 µl of each patch's conditioned media for 20 hours. Following incubation, CECs were stained in calcein-AM dye at a concentration of 2 mg/mL and imaged on a fluorescence microscope. The

Angiogenesis Analyzer plug-in for ImageJ was used to quantify the total tube length of the CECs.

4.3.10 Knockdown of ITGAV

ITGAV was knocked down using an ITGAV siRNA (Santa Cruz Biotechnology, sc-29373) according to the manufacturer's instructions. Briefly, cells were seeded in a 6-well plate in antibiotic-free growth media for 24 hours. For each well, 8 µl of the ITGAV siRNA duplex and 6 µl of siRNA Transfection Agent were each diluted in 100 µl of siRNA Transfection Medium. The two solutions containing the siRNA duplex and siRNA Transfection Agent were combined and incubated at room temperature for 45 minutes. Each well was washed with 2 mL of Transfection Medium and 0.8 mL of the duplex/Transfection Agent solution was added to each well. Following a 7-hour incubation, 1 mL of growth media with 2x fetal bovine serum and 2x antibiotic concentrations was added on to each well. The cells were incubated another 24 hours, and the media was changed to full growth media. Following one final 24-hour incubation, cells were either seeded onto patches for experimentation or cultured in 24-well plates for the same time course as the patch experiments. RT-PCR was performed on the cells in 24-well plates at the end of the time course to confirm ITGAV knockdown. ITGAV expression was compared to control cells that underwent the same procedures described here but with a control siRNA duplex.

4.3.11 Rat pulmonary artery banding model

All studies were approved by the Emory Institutional Animal Care and Use Committee. Adolescent athymic rats (Crl:NIH-*Foxn1*^{rnu}) (~150 g) were obtained from

Charles River Laboratories. Rats were anesthetized with 2% isoflurane, USP, orally intubated, and ventilated. A left thoracotomy was performed to expose the pulmonary trunk. The pulmonary artery (PA) was then partially ligated over an 18-guage angiocatheter with a silk thread under the PA. The catheter was removed rapidly to allow for antegrade flow through the band. Sham rats were given the same procedure minus the PA banding. Two weeks following PAB, rats were randomized, and patches were implanted in a blinded manner.

4.3.12 Patch implantation

For patch implantation, 1.5 million pooled neonatal CPCs, pooled child CPCs, or CPCs from patient 956 were seeded onto 15-mm-diameter circular random- or aligned-fiber PCL or PCL + FN patches seeded in 24-well plates. Patches were anchored to the bottom of the well using sterilized metal rings with an inner diameter of 13 mm and an outer diameter of 15 mm. Control, cell-free patches were anchored to the well like those seeded with cells and incubated in media. The day following cell seeding, a thoracotomy was performed using the same procedure described above to expose the heart. Patches were removed from the well plate and cut to an area of ~10 mm. The pericardial sac was exposed and pulled back, and the patch was carefully placed onto the RV of the heart, tucked under the pericardium. Patches remained attached to the RV via surface tension.

4.3.13 Cell injection

A total of 500,000 CPCs from patient 956-labeled cells, were resuspended in 75 µl saline and injected under echocardiographic guidance into the RV free wall using a 28-gauge BD Insulin Syringe with 12.7 mm BD Micro-Fine short bevel needle mounted on a

stereotactic frame (BD Medical Technology). A recording of the echocardiographic video of injection was taken to ensure no leakage out the RV occurred during injection.

4.3.14 Echocardiography

Transthoracic echocardiography was performed longitudinally at Weeks -2, 0, 2 and 4 using a Vevo 2100 digital high-frequency ultrasound system (FujiFilm Visualsonics). Tricuspid annular plane systolic excursion (TAPSE) was performed in the apical four-chamber M-mode. Right atrial (RA) diameter was measured perpendicular from the tricuspid valve to the opposing wall in the apical four-chamber view in B-mode at the end of systole. RV wall thickness was measured in the two-dimensional short-axis view in M-mode. RV end diastolic and end systolic two-dimensional areas were measured in the four-chamber view in B-mode. RV fractional area change was then calculated as $\frac{end\ diastolic\ area - end\ systolic\ area}{end\ diastolic\ area}$.

4.3.15 Histological tissue section staining

Rats were sacrificed at 4 weeks post-patch implantation and hearts were explanted for histological staining. The hearts were fixed in 10% formalin for 4 hours, cryoprotected in 30% sucrose overnight, and embedded in OCT medium. Hearts were then flash frozen in liquid nitrogen and stored at -80°C before further analysis. Hearts were cut into 8 μm sections using a Leica CM1520 Cryostat. Sections were stained in Isolectin B4 (IB4), wheat germ agglutinin (WGA), or Picrosirius red solutions. For IB4 and WGA staining, antigen retrieval was performed using sodium citrate solution, and sections were the blocked in 4% goat serum. The sections were then incubated overnight with IB4 (1:25

dilution) (Vector Laboratories, FL-1201) and WGA (1:200 dilution) (Vector Laboratories, RL10225) antibodies in blocking solution at 4°C. The following day, the sections were mounted using VECTASHIELD HardSet Antifade Mounting Medium with DAPI (Vector Laboratories, H-1500) and imaged using fluorescent microscopy. IB4 staining of vessels was quantified using CellProfiler™ software. WGA staining of myocyte area was quantified using ImageJ.

For Picrosirius red staining, sections were fixed in 10% formalin, incubated in Bouin's solution, and stained in Picrosirius red for 1 hour. The sections were then washed in acidified water, cleared in Histo-Clear, and dehydrated in ethanol. The slides were then mounted in Cytoseal and imaged using a Hamamatsu Nanozoomer 2.0HT slide scanner. Fibrosis in these sections was quantified using the Threshold Colour ImageJ plugin (G. Landini software, https://blog.bham.ac.uk/intellimic/g-landini-software/).

4.3.16 Statistical analysis

All statistical analysis was performed in GraphPad Prism 8, and all numerical data is represented as mean ± standard deviation. All comparisons of PCL versus PCL + FN patches use a paired Student's t-test to test significance. A two-way ANOVA with Tukey's post-hoc analysis was used to test significance in longitudinal echocardiography data and to confirm differences in pressure gradients following PAB surgery. An unpaired Student's t-test was used to analyze echocardiographic changes between two groups at specific time points. A one-way ANOVA with Tukey's post-hoc test was used to analyze histological staining data. All sample sizes are noted in the captions for each figure.

4.4 Results

4.4.1 Identification of ITGAV as a mediator of decreased CPC^{low} reparative capacity

Integrins are cell surface proteins that bind to the surrounding ECM to mediate cell adhesion[259]. Binding of integrins to the ECM protein FN has been shown to activate downstream signaling pathways that facilitate cardiac progenitor cell reparative function[243]. Therefore, we used statistical modeling methods to identify key integrins whose binding to FN may lead to improvement in CPC^{low} reparative capacity we have previously observed[10]. We used a previously published PLSR model based on RNA-seq data to predict functional outcomes for CPCs isolated from 32 different pediatric donors (Figure 17A). Using these predictions, CPCs were designated as either CPC^{low} (low in reparative capacity) or CPC^{high} (high in reparative capacity) (Table 2).

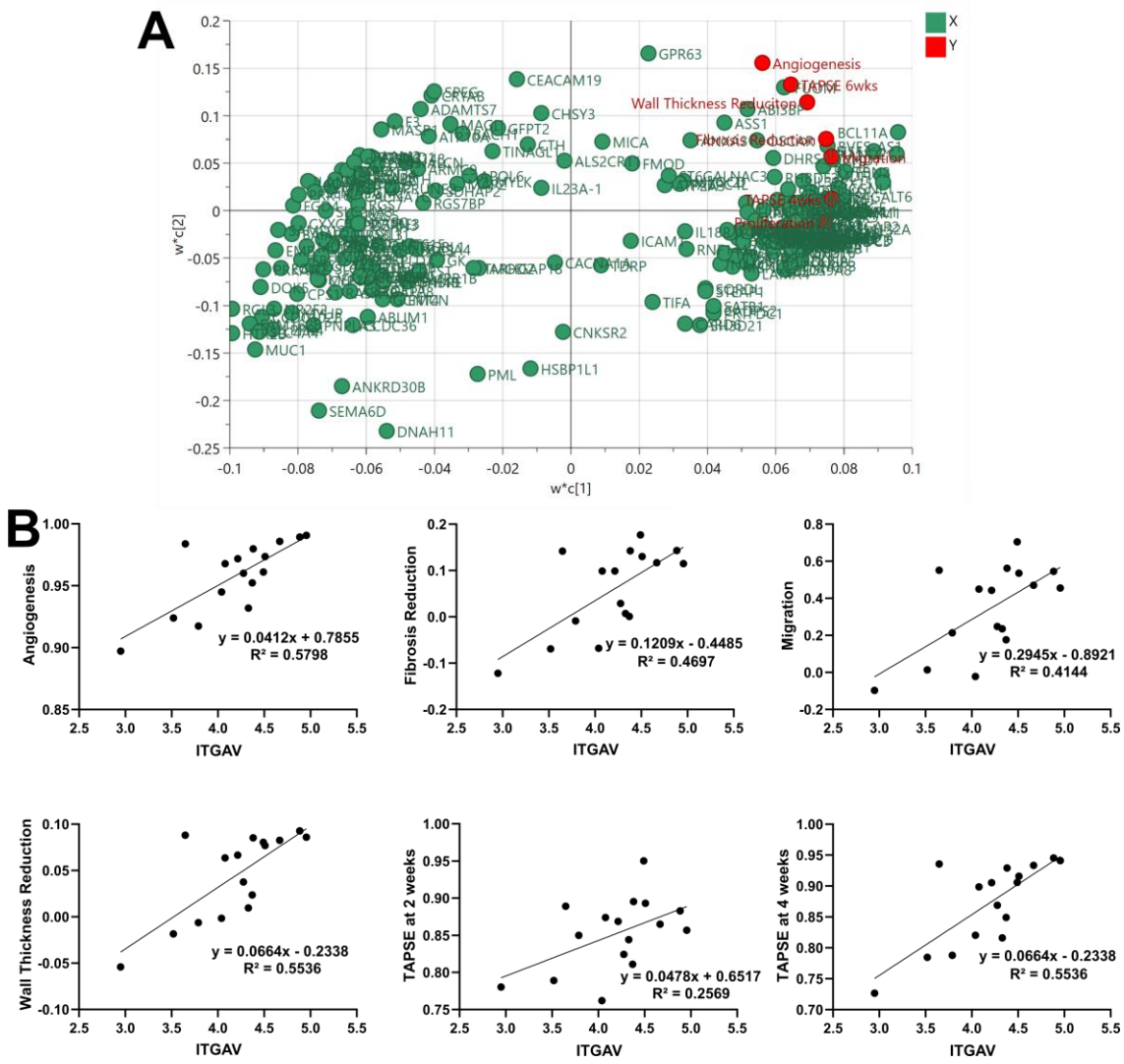

Figure 17. Computational modeling of CPC predicted outcomes and integrin expression. (A) PLSR analysis of CPC gene expression and functional outcomes plotted in principal component space. (B) Linear regressions of ITGAV expression and predicted functional outcomes from the PLSR model in a subset of CPCs that are low in reparative capacity.

Table 1. List of CPC patients and their designation as "High" or "Low" reparative capacity based on predicted functional outcomes.

Patient Number	Reparative Capacity
896	Low
902	Low
903	High
924	High
925	High
926	Low
930	High
938	Low
940	Low
956	Low
957	Low
975	Low
985	High
998	High
1045	High
1048	Low
1050	High
1057	High
1059	High
1063	High
1065	High
1066	High
1075	High
1082	High
1083	High
1089	Low
1092	Low
1094	Low
1096	Low
1097	Low
1099	Low

A given donor's cells were considered CPC^{high} if they were predicted to significantly increase tricuspid annular plane systolic excursion (TAPSE), increase angiogenesis, decrease fibrosis, and decrease RV wall thickness[218]. We performed individual linear regressions to examine correlations between 7 predicted functional outcomes

(angiogenesis, fibrosis reduction, migration, proliferation, TAPSE at 2 weeks post-cell injection, TAPSE at 4 weeks post-cell injection, and wall thickness reduction) and RNA levels of 11 different integrin subunits (ITGA1, ITGA2, ITGA3, ITGA4, ITGA5, ITGAV, ITGB1, ITGB2, ITGB3, ITGB4, and ITGB5) as measured by RNA-seq. The regressions were run for separately on both $CPCs^{low}$ and $CPCs^{high}$. Because in our previous study only $CPCs^{low}$ had increased reparative capacity on PCL + FN patches, we specifically looked for integrins that fit two criteria: 1) are a known FN receptor and 2) were significantly correlated with improvements in predicted outcomes of $CPCs^{low10}$. Expression of ITGAV was significantly correlated with improvements in all but one predicted outcome (proliferation) (Table 3 and Figure 17B). No other integrins that bind FN were significantly correlated with improvements in predicted outcomes. Therefore, we sought to confirm experimentally that ITGAV is a key mediator of improved CPC^{low} function on PCL + FN patches.

Table 2. Significance values for linear regressions of outcomes and expressions of integrins as measured by RNA-seq for High Reparative Capacity CPCs (top) and Low Reparative Capacity CPCs (bottom). The expression of 11 integrin subunits (ITGA1, ITGA2, ITGA3, ITGA4, ITGA5, ITGAV, ITGB1, ITGB2, ITGB3, ITGB4, and ITGB5) were correlated with the 7 outcomes listed in the tables.

High Reparative Capacity			
Outcome	*p<0.05	**p<0.01	***p<0.001
Angiogenesis		ITGAV	
Fibrosis Reduction	ITGA3	ITGA1	
Migration	ITGA3	ITGA1	
Proliferation		ITGA1	
TAPSE at 2 weeks		ITGA1, ITGA3	
TAPSE 4 weeks	ITGA1, ITGAV		
Wall Thickness Reduction	ITGA1		

Low Reparative Capacity			
Outcome	*p<0.05	**p<0.01	***p<0.001
Angiogenesis	ITGA4		ITGAV
Fibrosis Reduction		ITGAV	
Migration		ITGAV	
Proliferation	ITGA2		
TAPSE at 2 weeks	ITGAV, ITGA2		
TAPSE 4 weeks			ITGAV
Wall Thickness Reduction		ITGAV	

4.4.2 Selection of CPC donors

To improve the success rate of cardiac patches using autologous cells for CHD, the variability of patient donors must be considered when picking an appropriate biomaterial. We have obtained tissue biopsies from 32 different patients undergoing surgery for CHD and isolated CPCs from these biopsies using a previously described method[216]. From these 32 different patient-derived CPCs, we chose CPCs from 4 different donors based on ITGAV expression and CPC reparative capacity (Figure 18A). These 4 different donors (896, 956, 924, 903) gave every possible combination of high or low ITGAV expression and high or low reparative capacity (Figure 18B). We confirmed these patterns of ITGAV expression in each patient by measuring the protein expression of two integrins in the α_V family ($\alpha_V\beta_3$ and $\alpha_V\beta_5$) using an integrin-mediated assay (Figure 18C). Based on our computational results, we then expected that only patient 956 (CPC^{low} with high ITGAV expression) would show improved function on PCL + FN patches.

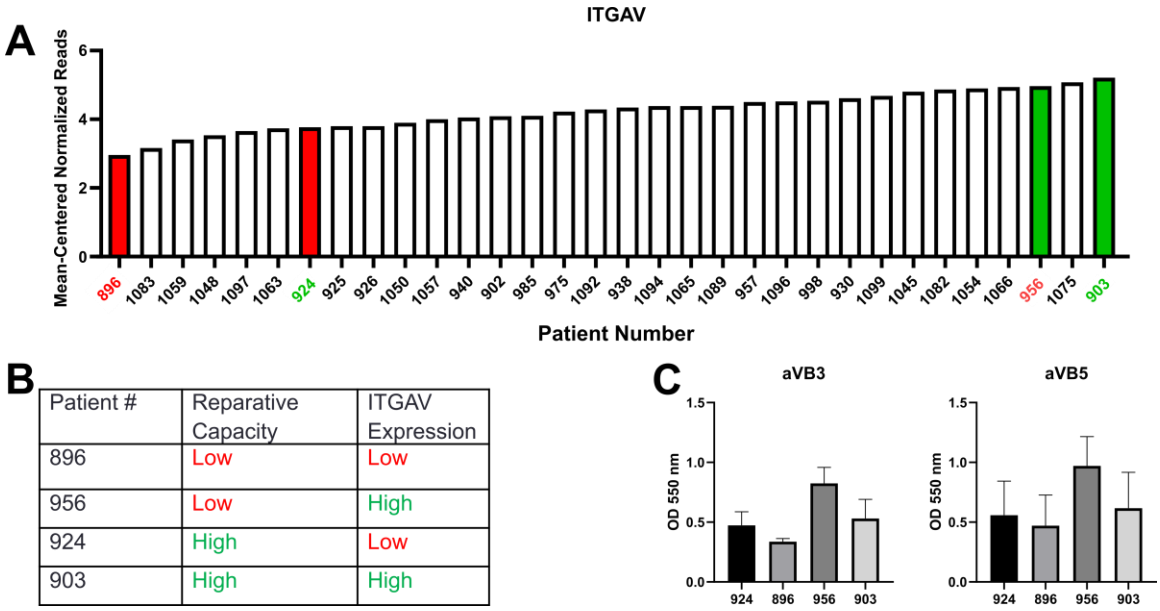

Patient #	Reparative Capacity	ITGAV Expression
896	Low	Low
956	Low	High
924	High	Low
903	High	High

Figure 18. Selection of 4 CPC donors (896, 903, 924, 956) and integrin expression measured by an integrin-mediated adhesion assay. (A) ITGAV expression for 32 different patients as measured by RNA-seq is shown. (B) The 4 patients selected give every possible combination of high or low ITGAV expression and high or low reparative capacity. (C) Protein expression of $\alpha_V\beta_3$ and $\alpha_V\beta_5$ integrins in each of 4 CPC patients as measured by integrin-mediated adhesion assay. (n = 3-5)

4.4.3 Reparative paracrine secretion of individual patient CPCs on PCL versus PCL + FN patches

Cell engraftment following injection into the myocardium is estimated to be 0.1 to 10%, but many cell therapies still elicit modest functional improvements[147,224,225,240]. Therefore, injected cells most likely improve cardiac function by secreting reparative paracrine factors rather than differentiating to a functioning cell population. We measured the gene expression of several cardiac transcription factors and endothelial lineage markers in the 4 different CPCs (896, 956, 924, and 903) cultured on PCL and PCL + FN patches

and found no differences in expression for any CPC on PCL compared to PCL + FN patches (Figure 19).

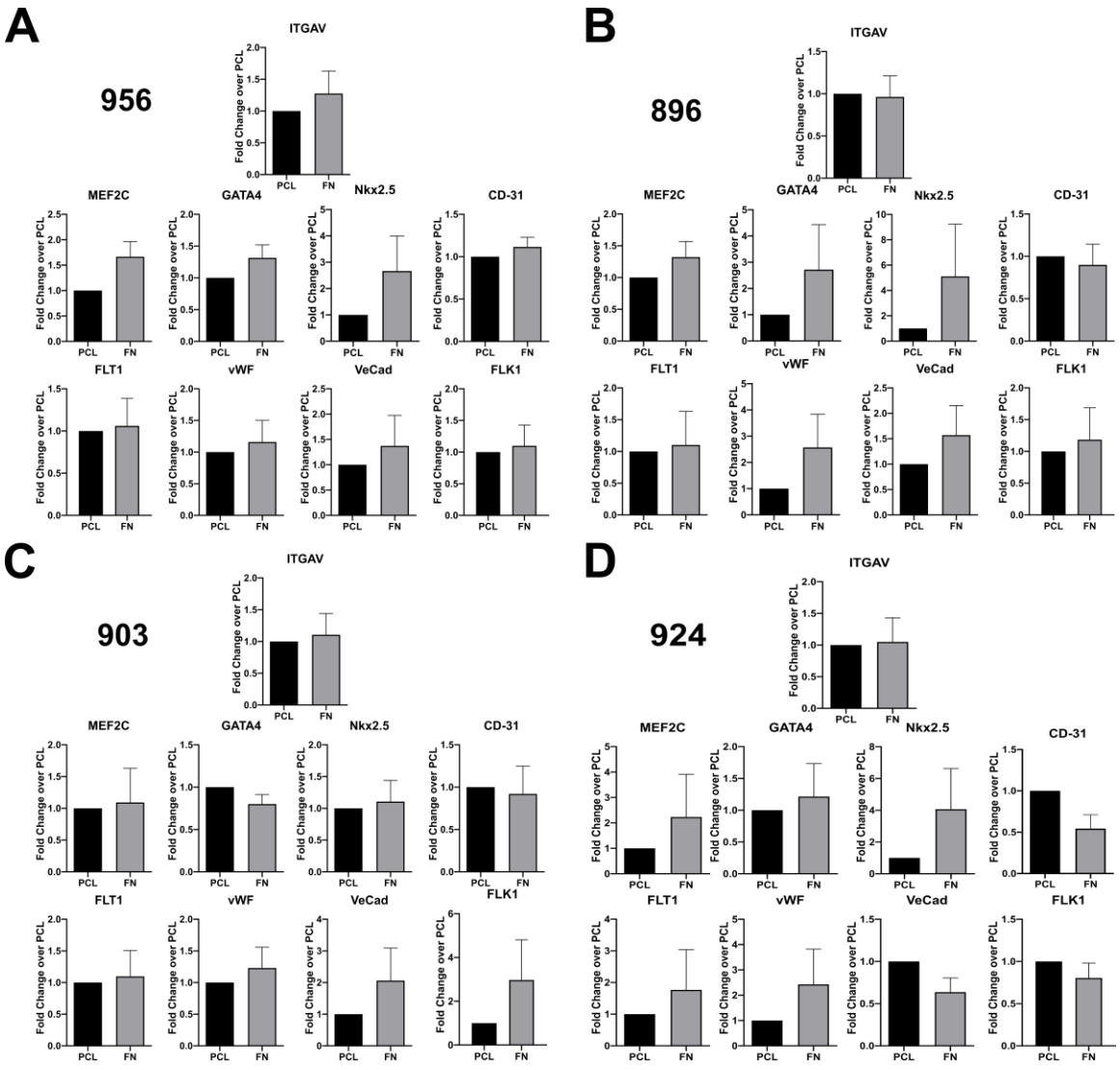

Figure 19. Transcript expression of ITGAV, cardiac transcription factors (MEF2C, GATA4, Nkx2.5), and endothelial lineage markers (CD-31, FLT1, vWF, VeCad, and FLK1) measured by RT-PCR in (A) 956s, (B) 896s, (C) 903s, and (D) 924s on PCL and PCL + FN patches. (n = 5-6)

Our expectation was that most functional benefits conferred by our patches would likely be due to paracrine signaling and not cellular differentiation. To this end, we investigated the anti-fibrotic and pro-angiogenic paracrine secretion of PCL versus PCL +

FN patches seeded with each of the 4 different patient-derived CPCs. To measure the ability of patch conditioned media (CM) to decrease fibrotic gene expression, we cultured rat cardiac fibroblasts (RCFs) in each patch's CM and stimulated the RCFs with TGF-β to induce fibrotic gene expression. As shown in Figure 20A, CM from PCL + FN patches with patient 956 (CPC^{low} with high ITGAV expression) significantly decreased vimentin (VIM) ($p < 0.05$) and decreased connective tissue growth factor (CTGF) expression, though not statistically significant ($p = 0.068$) compared to PCL patches with the same cells. Notably, in the 896 group PCL + FN patch CM decreased VIM expression compared to PCL patch CM, although not in a statistically significant manner (p = 0.057) (Figure 20B). For patches seeded with patient 903 or patient 924, CM from PCL + FN did not significantly decrease the expression of any fibrotic gene measured (Figure 20C and D).

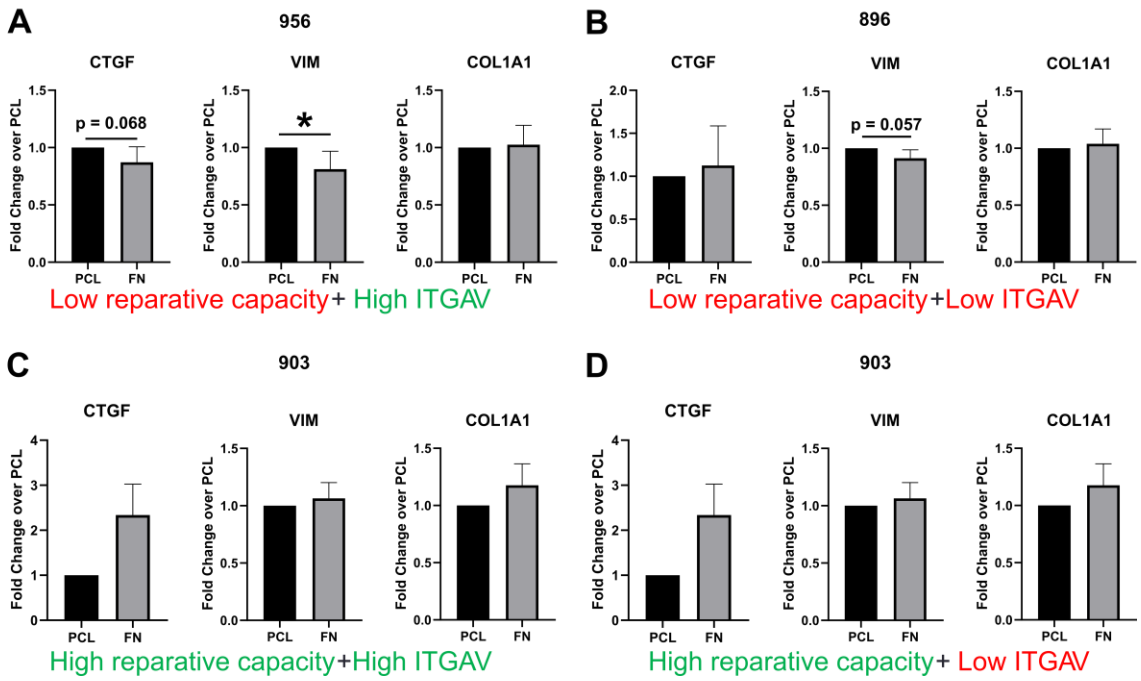

Figure 20. Fibrotic gene expression in RCFs following culture in patch CM. Differences in the fibrotic gene expression of RCFs cultured in CM collected from either PCL or PCL + FN patches with A) 956s, B) 896s, C) 903s, or D) 924s. (n = 4-6, *$p < 0.05$ by Student's t-test)

To examine the differences in angiogenic paracrine secretion of each patch, we measured tube formation of rat primary cardiac endothelial cells (CECs) cultured in patch CM. Figure 21A shows representative fluorescence images of CECs following culture in the different patch CMs. In Figure 21B, quantification of tube formation shows that PCL + FN patch CM led to more tube formation than PCL patch CM only in the patient 956 group ($p < 0.05$). For patches seeded with patients 896, 924, and 903, there were no differences in tube formation when using PCL + FN patch CM versus PCL patch CM. These results demonstrate that, like anti-fibrotic paracrine secretion, only the CPC^{low}, high-ITGAV-expressing cell line improved angiogenic paracrine secretion on PCL + FN patches.

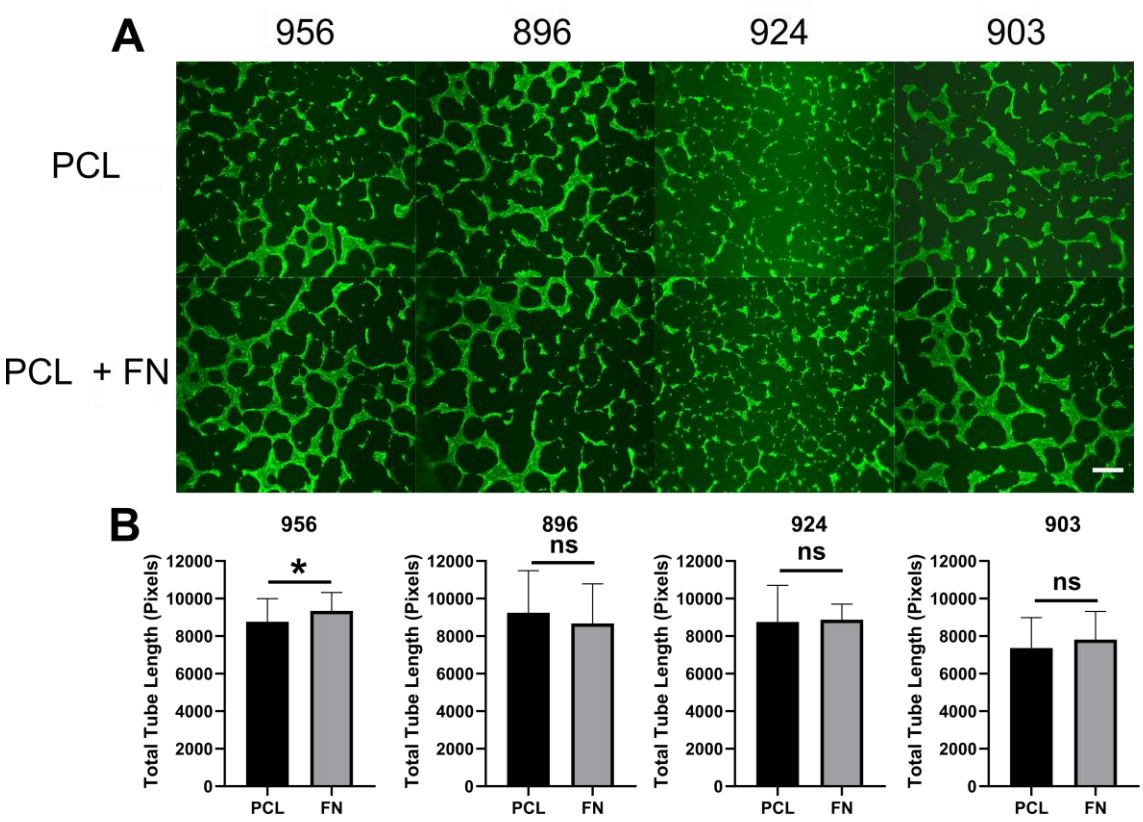

Figure 21. CEC tube formation in patch CM. (A) Representative fluorescence images of CEC tube formation on Matrigel following incubation in CM collected from PCL and PCL + FN patches with 956s, 896s, 924s, or 903s. Calcein-AM staining is shown in green. Scale bar = 300 μm (B) Quantification of total tube length of CECs in each patch's CM. (n=5-6, *$p < 0.05$ by Student's t-test)

4.4.4 Knockdown of ITGAV in patient 956 leads to loss of improved paracrine secretion on PCL + FN patches

We hypothesized that the improved paracrine secretion of patient 956 on PCL + FN patches was due to the binding of the α_v integrin to FN on the patch surface. Therefore, we knocked down the expression of α_v integrin (ITGAV) in this cell line using siRNA transfection. Figure 22A shows that transfection of patient 956 CPCs with an siRNA targeted to ITGAV significantly decreased ITGAV expression. We then ran both

conditioned media experiments (RCF fibrotic gene expression assay and tube formation assay) with PCL and PCL + FN patches seeded with the ITGAV knockout (KO) cells. After ITGAV KO in patient 956, CM from PCL + FN patches failed to decrease RCF fibrotic gene expression (Figure 22B) or increase CEC tube formation (Figure 22C) compared to CM from PCL patches, in contrast to Figure 20 and Figure 21. Based on this data, expression of ITGAV in 956s is necessary for 956s to develop improved reparative secretion on PCL + FN patches.

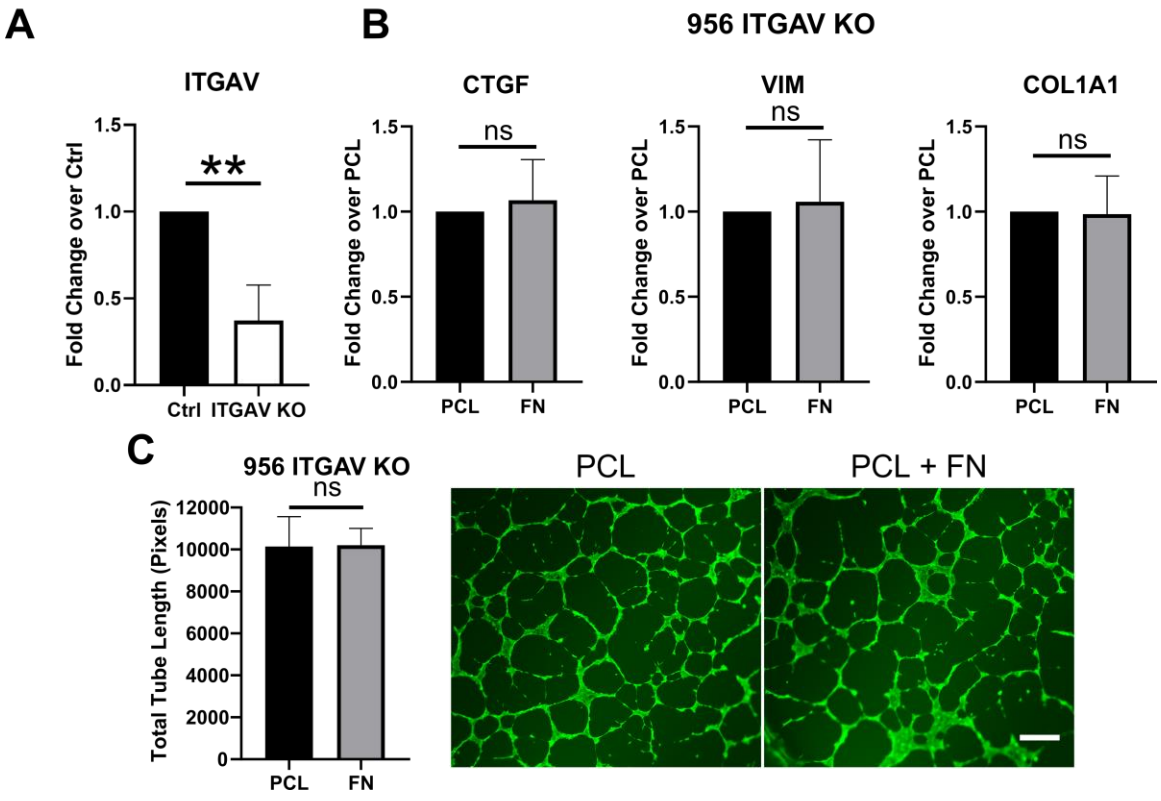

Figure 22. Knockdown of ITGAV in 956s. (A) ITGAV expression as measured by RT-PCR in control 956s versus 956s transfected with ITGAV siRNA. (n = 3, $^{**}p < 0.01$) (B) RCF fibrotic gene expression in PCL and PCL + FN patch CM seeded with 956 ITGAV KO cells (n = 3). (C) CEC tube formation expression in PCL and PCL + FN patch CM seeded with 956 ITGAV KO cells. Representative images show Calcein-AM staining in green. Scale bar = 300 μm. (n = 3)

4.4.5 Knock-in of ITGAV in patient 896 does not lead to improved paracrine secretion on PCL + FN patches

We showed that culturing the CPC^{low}, low-ITGAV-expressing patient 896 on PCL + FN patches did not improve paracrine secretion and that sufficiently high ITGAV expression is necessary for this improvement to occur. To examine if increased ITGAV expression would lead to improved paracrine secretion of patient 896 CPCs on PCL + FN patches, we knocked in ITGAV expression in 896s using an ITGAV overexpression (ITAV KI) plasmid. Shown in Figure 23A, transfection with the ITGAV KI plasmid significantly increased ITGAV expression in 896s compared to the control 896s ($p < 0.05$). However, after using CM from patches seeded with ITGAV KI 896s in a RCF fibrotic gene expression assay and a tube formation assay, we found no increases in anti-fibrotic and pro-angiogenic paracrine secretion from PCL + FN patches compared to their PCL patch counterparts (Figure 23B and C). When combined with the ITGAV knockout experiments, these data suggest that expression of ITGAV is necessary but not sufficient to improve reparative paracrine secretion of $CPCs^{low}$ on PCL + FN patches.

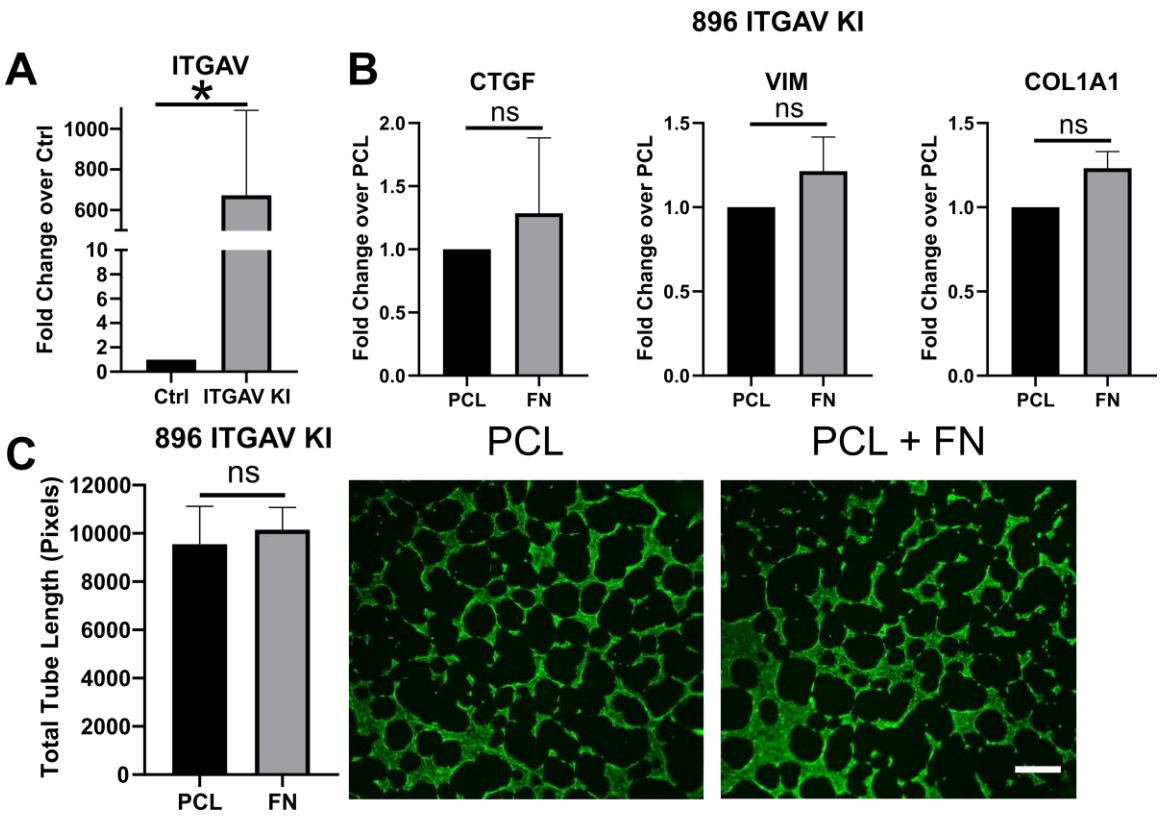

Figure 23. Knock-in of ITGAV in 896s. (A) ITGAV expression as measured by RT-PCR in control 896s versus 896ss transfected with a ITGAV over-expression plasmid. (n = 4, *$p < 0.05$) (B) RCF fibrotic gene expression in PCL and PCL + FN patch CM seeded with 896 ITGAV KI cells (n = 3). (C) CEC tube formation expression in PCL and PCL + FN patch CM seeded with 896 ITGAV KI cells. Representative images show Calcein-AM staining in green. Scale bar = 300 µm. (n = 3).

4.4.6 In vivo approach to assess cardiac patch therapy in a rat model of RVHF

Cardiac cell therapy has shown promise in treating RVHF, but cell injection is often hampered by low retention at the injection site[233]. Therefore, a cardiac patch may improve right ventricular function by enhancing cell retention and sustaining reparative paracrine secretion at the implantation site. To this end, we tested several different types of PCL nanofibrous patches in a pulmonary artery banding (PAB) rat model of RVHF. To

accomplish this, we first measured how efficiently CPCs were retained following seeding onto PCL patches anchored to the bottom of a 24-well plate by a metal ring with an inner diameter of 13 mm (Figure 24A). We tested two different seeding densities, 1 million cells and 5 million cells, and counted the cells following seeding to measure the true number of cells retained on each patch. Figure 24B shows representative images of DAPI staining of CPCs retained on random- and aligned-fiber patches at an initial seeding density of 1 million or 5 million cells per patch. As expected, the initial seeding density of 5 million cells yielded a higher a total of cells retained on the patches. However, a higher fraction of the initial density (~33%) was retained on the patches when an initial seeding density of 1 million cells was used (Figure 24C). We therefore estimate that seeding 1.5 million cells with will be sufficient to retain ~500,000 cell on the patch. This amount of cells is the same amount that has been used in previous studies of cell therapy in a rat PAB model[225].

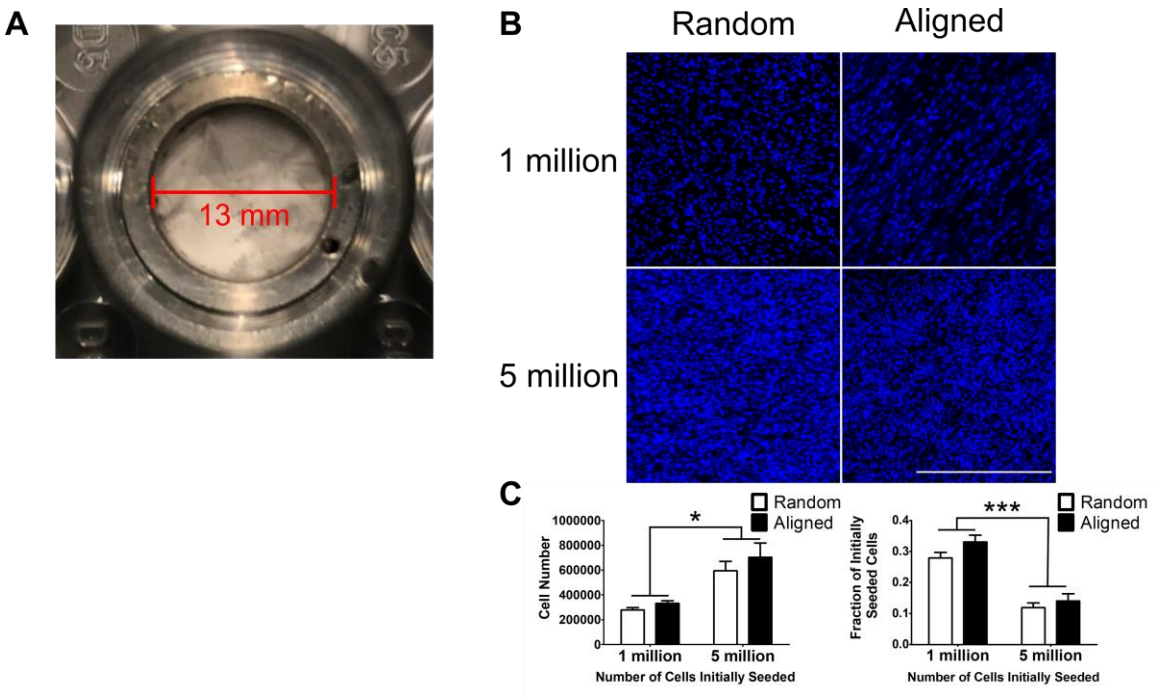

Figure 24. Setup for seeding cells on patches. (A) Representative image of a 15 mm-diameter patch seeded in the well of a 24-well plate anchored by a metal ring with an inner diameter of 13 mm. (B) Representative images of nuclei stained with DAPI (blue) and (C) quantification of total cell number and fraction of initial density seeded on random- or aligned-fiber patches after an initial seeding density of 1 million or 5 million cells was used. (n=5-6, ***$p < 0.001$, *$p < 0.05$ by two-way ANOVA with Tukey's post-hoc test)

Following cell seeding, patches were then implanted onto the RV 2 weeks following PAB surgery (Figure 25A). At 4 weeks post-patch implantation, rats were sacrificed to examine histological changes and to confirm retention of the patch on the RV. Figure 25B shows a whole-heart view with the implanted patch still intact on the epicardium of the RV 4 weeks post-patch implantation. We also were able to observe that the patches remained attached to the RV and remained cellularized 4 weeks post-implantation through isolectin B4 (IB4) staining DAPI, respectively (Figure 25C).

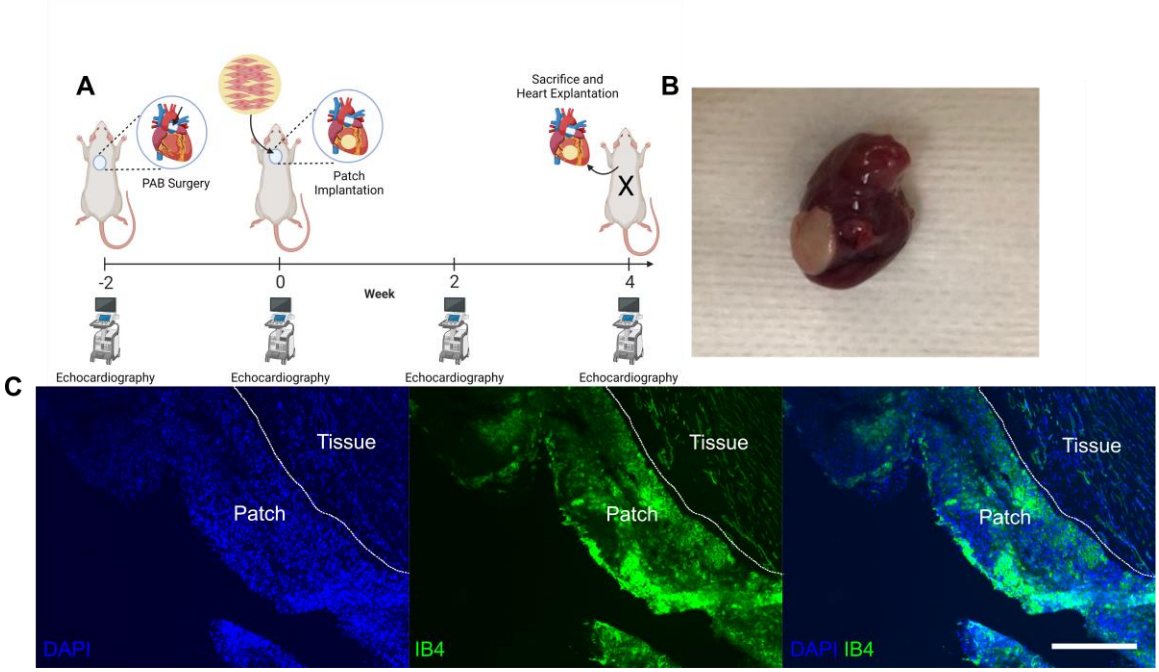

Figure 25. *In vivo* experimental design and patch retention. (A) Experimental timeline of PAB injury and patch implantation. (B) Patch retention on the RV 4 weeks following implantation. (C) Representative images of patches attached to the RV in tissue sections collected 4 weeks following implantation. DAPI (nuclei) staining is shown in blue and isolectin B4 (IB4) staining (total patch area) is shown in green. Scale bar = 200 μm.

We measured RV function of the PAB rats longitudinally using echocardiography (Figure 25A). To ensure that the PAB surgery induced pressure overload in the RV, we measured the PA mean pressure gradient at baseline (Week -2) and at two weeks post-PAB surgery (Week 0). The mean pressure gradient across the PA was significantly increased in all treatment groups other than the Sham group 2 weeks post-PAB surgery, confirming that the banding had induced a pressure overload in the RV (Figure 26).

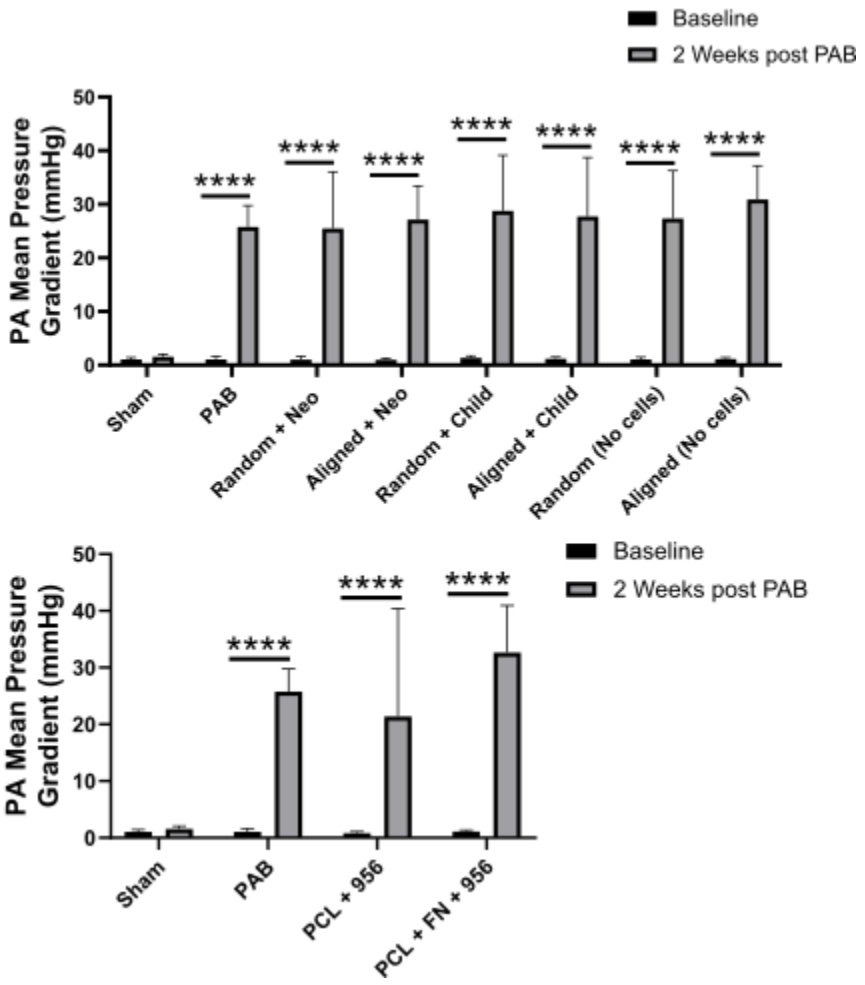

Figure 26. Mean pressure gradient across the pulmonary artery (PA) for pooled cell line (top) and patient-specific cell (bottom) studies at baseline and 2 weeks after PAB surgery. (n=6 Sham, n=5 PAB, n=7-8 PCL, n=6 PCL + FN, n = 8 for Random + Neo, n = 7-8 for Aligned + Neo, n = 7-8 Random + Child, n = 6-8 Aligned + Child, n = 8 Random (No cells), n = 7-8 Aligned (No cells), ***p<0.001 by two-way ANOVA with Tukey's post-hoc test).

4.4.7 Implantation of non-specific PCL patches

We first attempted to create an allogeneic "off-the-shelf" cardiac patch without considering the characteristics of the donors of the CPCs used in the patches. We implanted the six following patch groups in our rat model of PAB: random-fiber PCL + neonatal

CPC patches (Random + Neo), aligned-fiber PCL + neonatal CPC patches (Aligned + Neo), random-fiber PCL + child CPC patches (Random + Child), aligned-fiber PCL + child CPC patches (Aligned + Child), cell-free random-fiber PCL patches (Random (No cells)), cell-free aligned-fiber PCL patches (Aligned (No cells)). These patches used pooled cell lines and PCL scaffolds not specifically designed to any CPC patient.

Raw echocardiographic values of RV function in rats in each of the treatment and control groups are shown in Figure 27. PAB group rats received only the PAB surgery and Sham group rats received a sham PAB surgery. There were no statistically significant changes in the four echocardiographic parameters measured in the RV: tricuspid annular plane systolic excursion (TAPSE), right atrial (RA) Area, right ventricular wall thickness (RVWT), and right ventricular fractional area change (RVFAC). We also reported differences in echocardiographic parameters as a change to the Week 0 values (just before patch implantation) to account for varying degrees of injury observed in the raw data (Figure 28). The only instance in which patch implantation improved RV function was in the Random + Neo group where RVWT was decreased compared to the PAB group at Week 4 (Figure 28D). These results demonstrate that, even when the more reparative neonatal CPCs are used, non-specific PCL patches are not able to improve RV function.

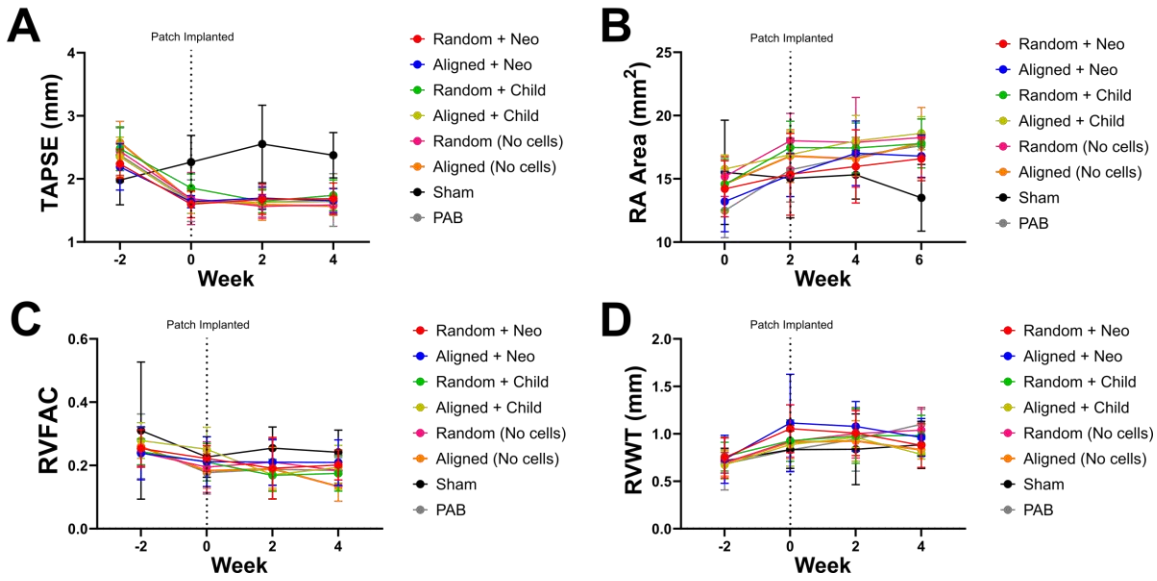

Figure 27. Raw values for A) tricuspid annular plane systolic excursion (TAPSE), B) right atrial (RA) Area, C) right ventricular wall thickness (RVWT), and D) right ventricular fractional area change (RVFAC) in rats treated with random-fiber PCL + neonatal CPC patches (Random + Neo), aligned-fiber PCL + neonatal CPC patches (Aligned + Neo), random-fiber PCL + child CPC patches (Random + Child), aligned-fiber PCL + child CPC patches (Aligned + Child), cell-free random-fiber PCL patches (Random (No cells)), cell-free aligned-fiber PCL patches (Aligned (No cells)), and PAB only or Sham rats over time. (n = 6 for Sham, n = 5 for PAB, n = 8 for Random + Neo, n = 7-8 for Aligned + Neo, n = 7-8 Random + Child, n = 6-8 Aligned + Child, n = 8 Random (No cells), n = 7-8 Aligned (No cells))

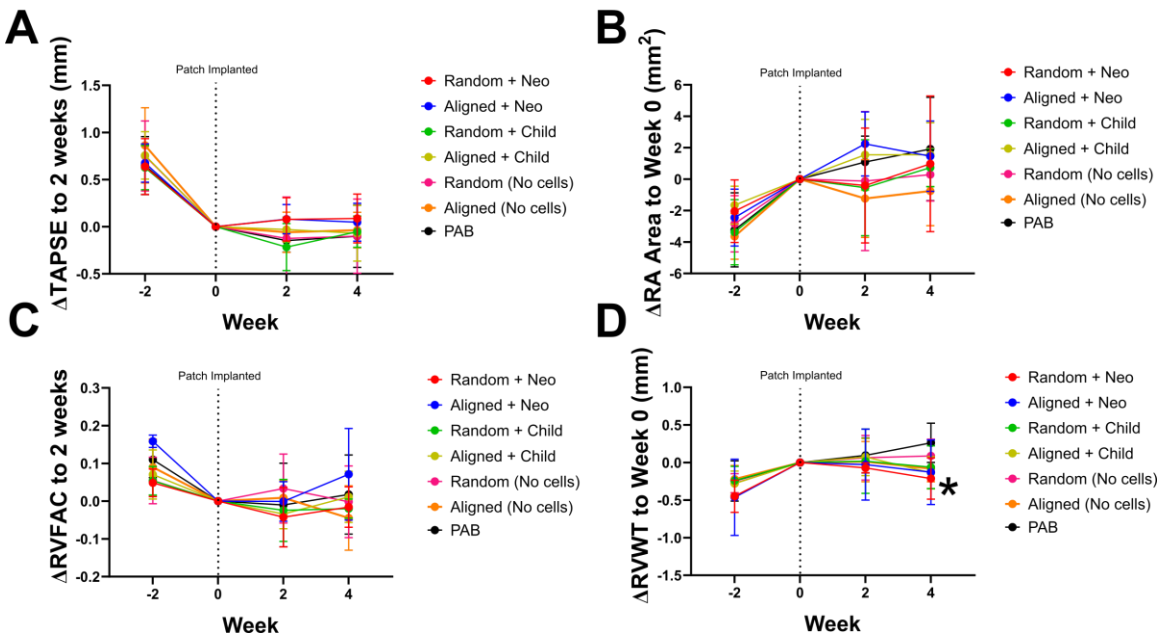

Figure 28. Normalized values for (A) TAPSE, (B) RA Area, (C) RVWT and (D) RVFAC over time in rats treated with Random + Neo, Aligned + Neo, Random + Child, Aligned + Child, Random (No cells), and Aligned (No cells) patches. Animals receiving PAB only are also reported. All values are reported as a change (Δ) to Week 0 values. (n = 5 for PAB, n = 8 for Random + Neo, n = 7-8 for Aligned + Neo, n = 7-8 Random + Child, n = 6-8 Aligned + Child, n = 8 Random (No cells), n = 7-8 Aligned (No cells), *$p < 0.05$ vs. PAB by two-way ANOVA with Tukey's post-hoc test) All values are reported as a change (Δ) to Week 0 values.

4.4.8 Implantation of patient-specific PCL + FN + patient 956 patches

Autologous cell therapy for RVHF in CHD patients has shown promise but may suffer from the patient-to-patient variance in cell quality[218,232]. Further, non-specific PCL patches loaded with pooled lines of CPCs were not able to improve RV function (Figure 27 and 28) Therefore, designing cardiac patches to improve a specific patient's cells may prove a superior treatment compared to cell injection. To this end, we tested PCL and PCL + FN patches loaded with CPCs from patient 956 in a PAB rat model of RVHF. Based on

our computational modeling and *in vitro* data, we expect that the specifically designed PCL + FN patches with patient 956 CPCs will improve RV function.

We first attempted to test the efficacy of PCL patches loaded with CPCs from patient 956 (PCL + 956) and PCL + FN patches loaded with CPCs from patient 956 (PCL + FN + 956) against the efficacy of an injection of CPCs from patient 956. Echocardiographic values of RV function from Week 0 to Week 4 for these groups and the control groups are shown in Figure 29. Unfortunately, the files containing the baseline (Week -2) values for the cell injection only group were corrupted during file transfer. Because PAB injury could therefore not be confirmed following surgery, the cell injection only group was omitted from further analysis.

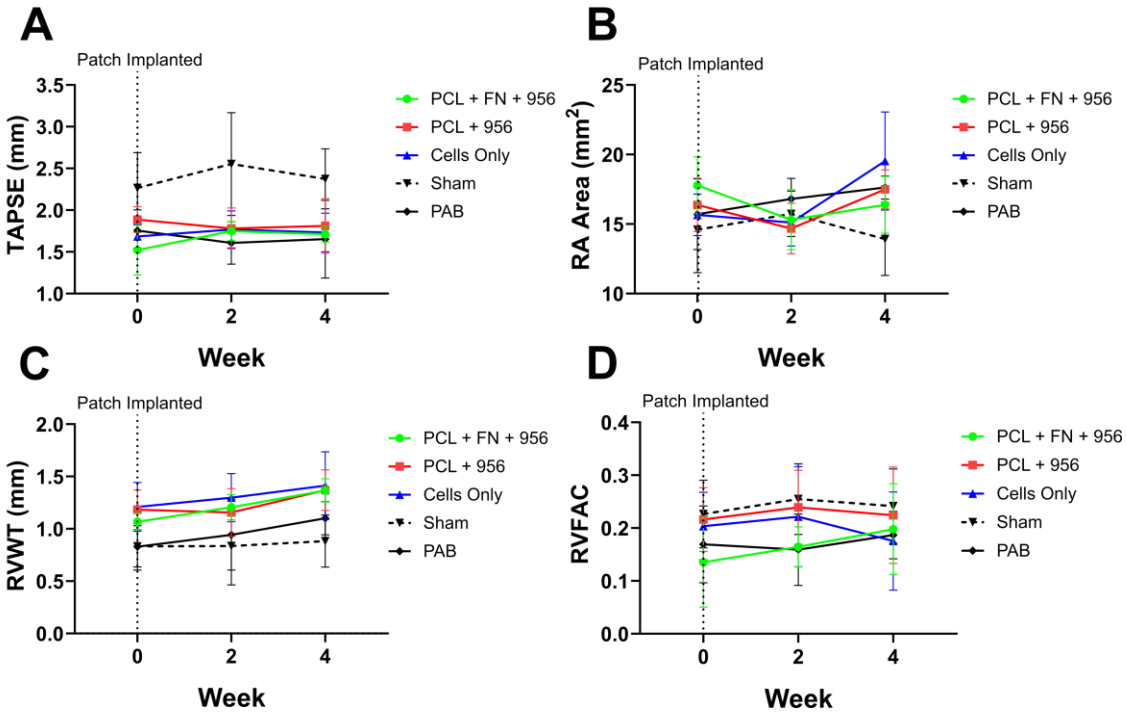

Figure 29. Raw values for (A) TAPSE, (B) RA Area, (C) RVWT and (D) RVFAC in rats treated with PCL + 956 patches, PCL + FN + 956 patches, cell injection only and PAB only rats. Baseline (Week -2) values are omitted. (n = 5 for PAB, n = 5-8 for PCL, n = 5-6 for PCL + FN, n = 7 Cells only)

As was done for the non-specific patch study, we reported differences in echocardiographic parameters as a change to the Week 0 values to account for varying degrees of injury observed in the raw data (Figure 30). Figure 31A and B show the changes in TAPSE and RA area over time, respectively. We found that at 2 weeks post-patch implantation, PCL + FN + 956 patches significantly improved TAPSE compared to the PAB alone ($p < 0.05$) and improved over PCL + 956 patch groups, though this was not considered statistically significant ($p = 0.0829$) (Figure 31C). RA area was significantly decreased by both the PCL + FN + 956 ($p < 0.001$) and PCL + 956 ($p < 0.05$) patch groups compared to the PAB alone group (Figure 31D). At 4 weeks post-patch implantation, TAPSE was increased in the PCL + FN + 956 group compared to the PCL + 956 and PAB groups, although this time not in a statistically significant manner (Figure 31E). However, RA area was significantly decreased at 4 weeks in the PCL + FN + 956 group compared to both PCL + 956 ($p < 0.05$) and ($p < 0.001$) PAB groups (Figure 31F). There were no statistically significant changes in RVFAC or RVWT observed (Figure 32).

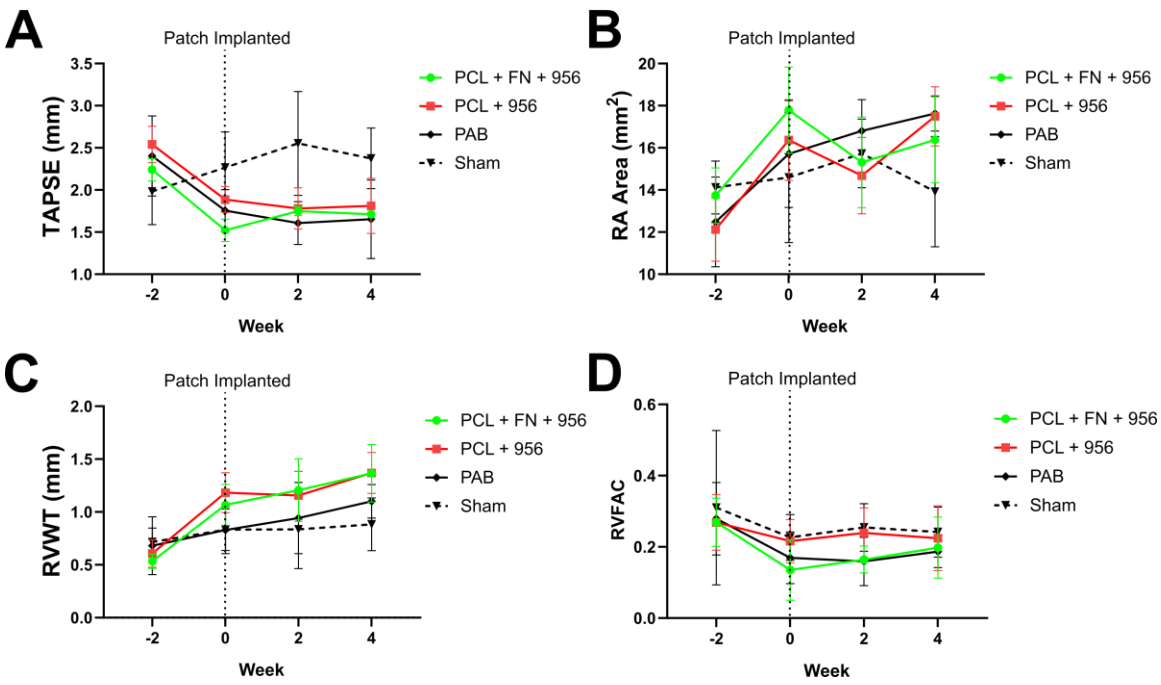

Figure 30. Raw values for (A) TAPSE, (B) RA Area, (C) RVWT and (D) RVFAC in rats treated with PCL + 956 patches, PCL + FN + 956 patches, and PAB only or Sham rats over time. (n = 8 for Sham, n = 5 for PAB, n = 5-8 for PCL, n = 5-6 for PCL + FN)

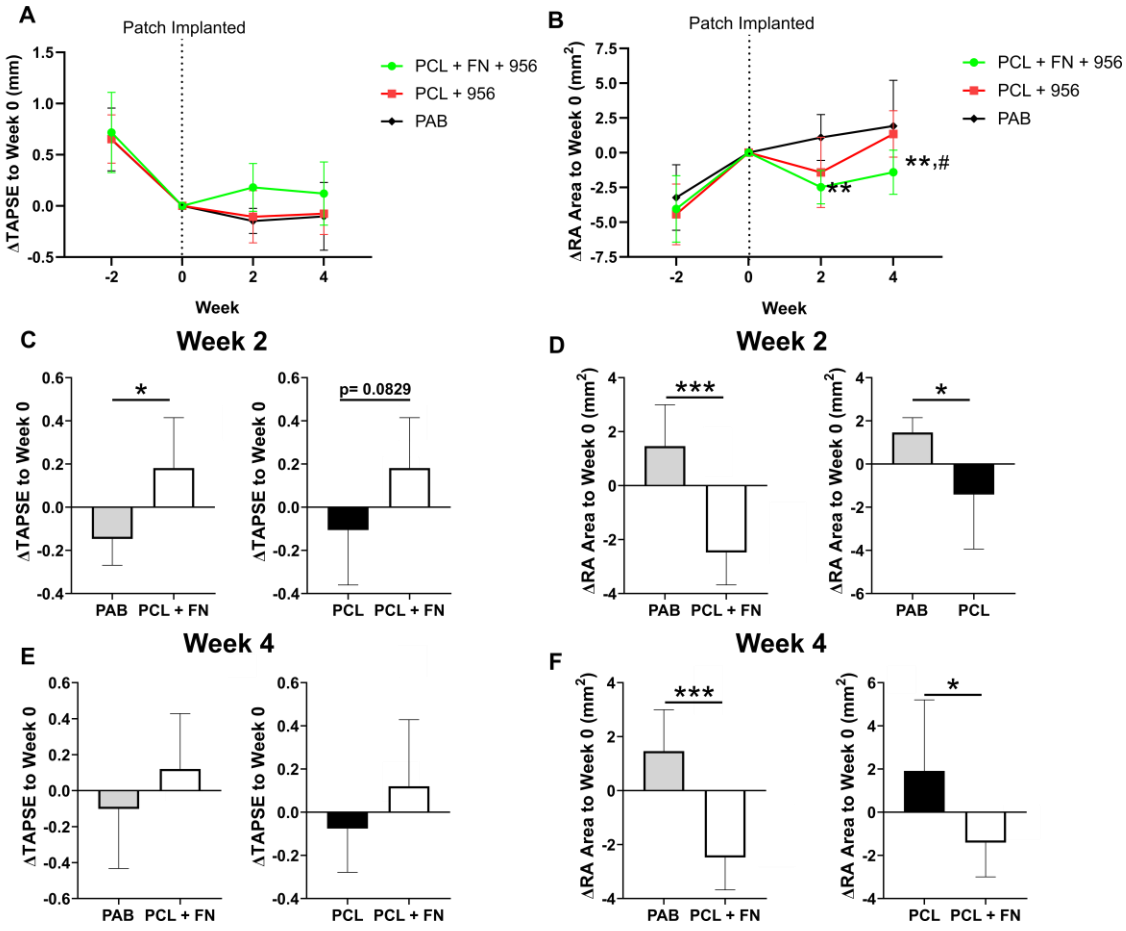

Figure 31. RV in PAB rats function measured by echocardiography following patch implantation. A) TAPSE and B) RA area values in rats treated with PCL + 956 patches, PCL + FN patches, or PAB only rats over time. (n = 5 for PAB, n = 5-8 for PCL, n = 5-6 for PCL + FN, $^{**}p < 0.01$ vs PAB, $\#p < 0.05$ vs PCL by two-way ANOVA with Tukey's post-hoc test) C) TAPSE and D) RA area values in rats treated with PCL + 956 patches, PCL + FN patches, or PAB only at 2 weeks following patch implantation. ($^{*}p < 0.05$, $^{***}p < 0.001$ by Student's t-test) E) TAPSE and F) RA area values in rats treated with PCL + 956 patches, PCL + FN patches, or PAB only at 4 weeks following patch implantation. ($^{*}p < 0.05$, $^{***}p < 0.001$ by Student's t-test) All values are reported as a change (Δ) to Week 0 values.

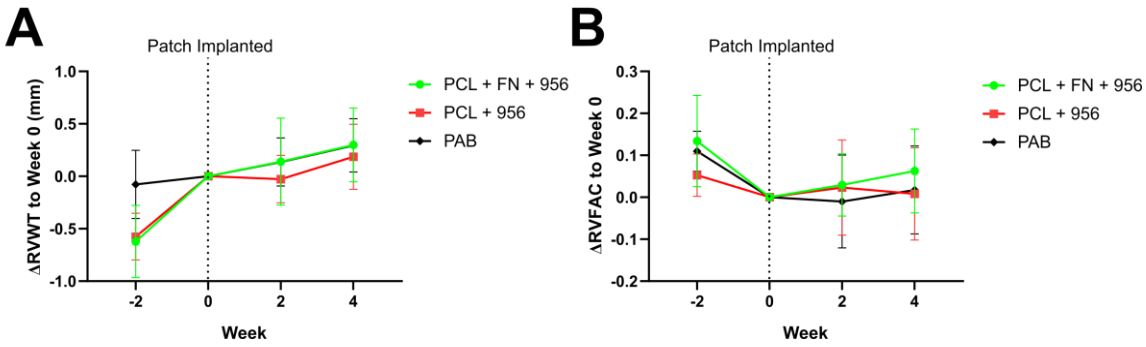

Figure 32. A) RVWT and B) RVFAC values (change to Week 0) in rats treated with PCL + 956 patches, PCL + FN + 956 patches, or PAB only rats over time. (n = 5 for PAB, n = 5-8 for PCL, n = 5-6 for PCL + FN)

4.4.9 Histological changes to the RV myocardium following patch implantation

Pressure overload in the RV is marked by increased fibrosis, decreased vessel density, and myocyte hypertrophy[41,260]. Therefore, we examined the cellular effects of treatment with PCL + 956 or PCL + FN + 956 patches on the hearts of PAB animals through immunohistochemistry. Both PCL and PCL + FN patch groups increased fibrosis compared to the PAB ($p < 0.01$) and Sham groups ($p < 0.001$) (Figure 33).

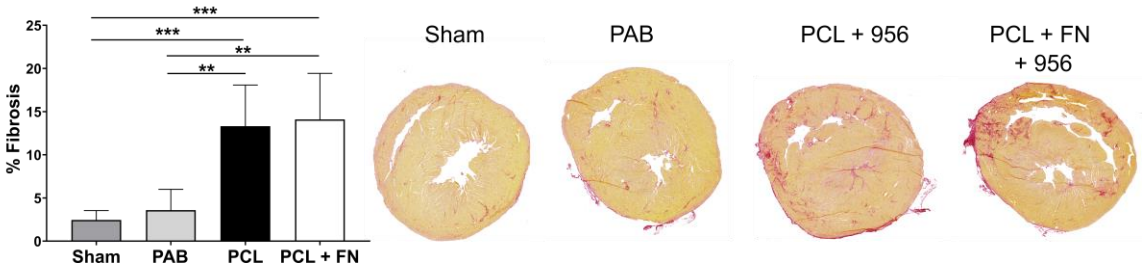

Figure 33. Fibrosis content in the RV of Sham and PAB animals and animals treated with PCL + 956 patches or PCL + FN + 956 patches. Brightfield images of picrosirius red-stained sections are shown to the right and quantified fibrosis is shown to the left. (n = 6 Sham, n = 5 PAB, n = 8 PCL, n = 6 PCL + FN)

Vessel density was significantly decreased in the PAB ($p < 0.05$) and PCL + 956 ($p < 0.01$) patch groups compared to the Sham group. However, we observed no significant difference in vessel density between the Sham and PCL + FN + 956 group (Figure 7A). Similarly, myocyte hypertrophy was significantly increased for the PAB ($p < 0.05$) and PCL + FN ($p < 0.01$) patch groups, but no significant changes in myocyte hypertrophy between the Sham and PCL + FN + 956 groups were present (Figure 7B). In total, implantation of PCL + FN + 956 led to improved *in vivo* outcomes in a PAB rat model of RVHF while PCL + 956 patches did not.

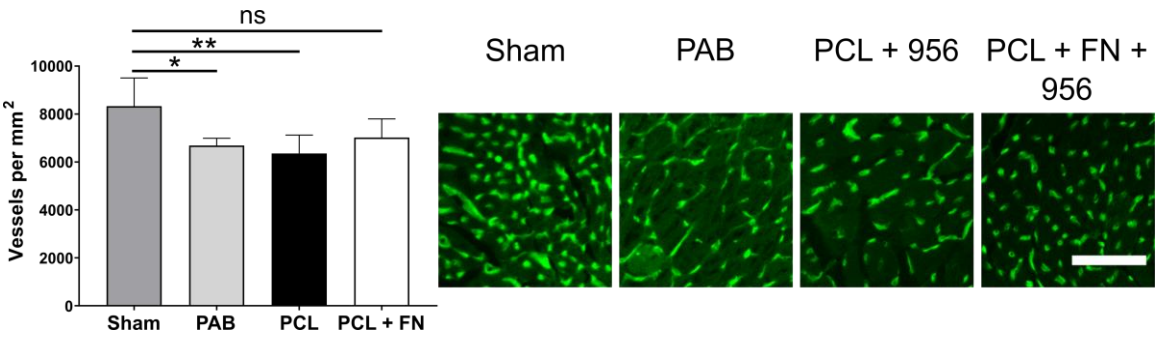

Figure 34. Vessel density in the RV of Sham animals, PAB animals, and animals treated with PCL + 956 or PCL + FN + 956 patches. Quantification is shown to the left of representative IB4 staining shown in green. Scale bar = 50 µm. (n = 6 Sham, n = 5 PAB, n = 7-8 PCL, n = 6 PCL + FN, *$p < 0.05$, **$p < 0.01$ by one-way ANOVA with Tukey's post-hoc test)

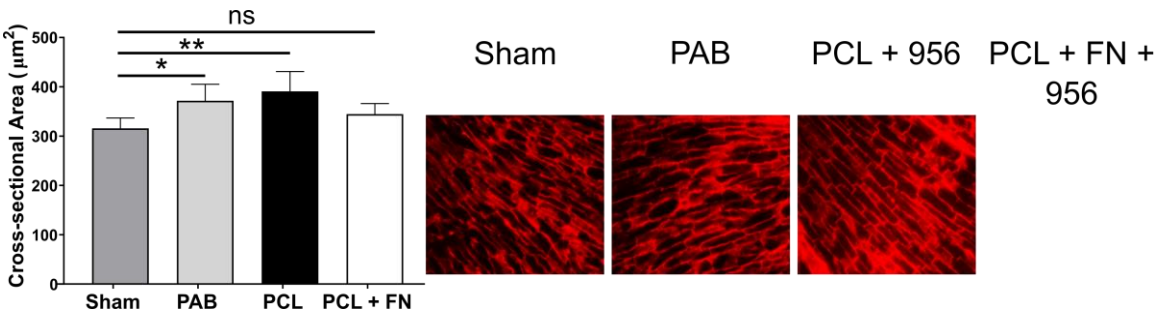

Figure 35. Myocyte hypertrophy in the RV of Sham animals, PAB animals, and animals treated with PCL + 956 or PCL + FN + 956 patches. Quantification is shown to the left of representative wheat germ agglutinin (WGA) staining shown in red. Scale bar = 50 µm. Scale bar = 50 µm. (n = 6 Sham, n = 5 PAB, n = 7-8 PCL, n = 6 PCL + FN, $*p < 0.05$, $**p < 0.01$ by one-way ANOVA with Tukey's post-hoc test)

4.5 Discussion

CHD remains the number one cause of birth-defect related death despite advances in surgical techniques and treatments over the past several decades[261,262]. Cell therapy has emerged as potential treatment to overcome RVHF that often develops following palliative surgery[214,252]. Currently being investigated in the clinic, autologous CPC therapy has shown to be safe and feasible and provide modest functional benefits in HLHS patients (CHILD Trial, NCT03406884). However, cardiac cell therapy is plagued by low cell retention and lack of engraftment and differentiation following injection[15,16]. Further, autologous cell therapy suffers from variability in the quality and efficacy of donor cells, leading to inconsistent outcomes[13,14,219]. Because of these issues, there is a need to deliver therapeutic cells *in vivo* more effectively and to improve autologous cells with diminished reparative capacity so that they can still confer functional benefit following implantation. Here, we fill these needs by using computational methods to identify mechanisms of

improved function in CPCs with low reparative capacity. We then exploit those mechanisms to improve CPC quality in a patient-specific manner by tailoring the design of an electrospun PCL-based cardiac patch.

A host of factors including donor age and disease can influence the reparative capacity of CPCs. Several studies from our laboratory have shown that there is an age-dependence on CPC reparative capacity, both in *in vivo* outcomes following direct injection and in response to biomaterials[10,147,263]. Computational sequencing studies have shown that changes in mRNA and microRNA (miRNA) in both the cells and in secreted extracellular vesicles (EVs) are largely responsible for improved function in younger CPCs compared to older CPCs[14,218]**.** We have also previously shown that these changes in mRNA and miRNA expression can be modified using different methods *ex vivo,* such as CPC spherical aggregation, electrical stimulation, and culture in hypoxia, to improve CPC function[13,219,224]. The disease of the patient from whom the CPCs are isolated can also play a role in their reparative capacity. For example, previous studies have shown that high glucose levels caused by maternal diabetes can induce apoptosis in pediatric CPCs and that patients with HLHS, Tetralogy of Fallot, or dilated cardiomyopathy having varying degrees of regenerative capacity[220,264]. These patient-to-patient differences further highlight the need to design patient-specific therapies for CHD.

Integrins are cell surface receptors that play major roles in cell adhesion to the surrounding ECM. They are composed of an α-class and a β-class subunit and in different combinations of these subunits bind ECM proteins such as collagen, fibronectin, and laminin[259]. Previous studies have shown that the $\alpha_5\beta_1$ integrin as well as the $\alpha_V\beta_5$ integrins are important for improved reparative function in different populations of CPCs[224,243].

Based on the computational approaches previously discussed, we used a PLSR model to make predictions on functional outcomes of treatment with CPCs from over 30 different donors (Figure 17A). We identified that expression of the integrin subunit α_V (ITGAV) was predicted to be important for improved outcomes in a subset of CPCs, those that are inherently low in reparative capacity (Figure 17B). Therefore, we used CPCs from 4 different donors (896, 903, 924, 956) in PCL and PCL + FN patches to examine patient-specific differences in patch performance (Figure 18A and B). Because paracrine secretion is likely the major mechanism by which CPC therapy improves function *in vivo*, we measured the ability of our different CPC-patch combinations to secrete anti-fibrotic (Figure 19) and pro-angiogenic (Figure 20) paracrine factors[12]. As suggested by the computational data, only the CPC that was low in reparative capacity and high in ITGAV expression (956) had increased anti-fibrotic (Figure 19A) and pro-angiogenic (Figure 20A) paracrine secretion on PCL + FN patches. We also knocked down the expression of ITGAV in cells from patient 956 and found that the improved paracrine secretion on PCL + FN patches was lost (Figure 21). However, knock-in of ITGAV in the CPC^{low}, low-ITGAV-expressing patient 896 did not lead to improved paracrine secretion on PCL + FN patches. These results demonstrate that for CPCs that are low in reparative capacity, high levels of ITGAV are necessary but not sufficient to have the CPCs' reparative function improved by addition of FN to the PCL patch.

Cardiac patches have been studied extensively in recent literature as a means to more effectively deliver therapeutic cells and improve ventricular function[70,253]. Specifically, electrospun patches have been explored due to their ease of production, low-cost, and ability to be easily modified with other components[179,181]. Like our approach here,

previous studies have functionalized the surface of electrospun patches with ECM proteins such as fibronectin and laminin[190,265]. However, cardiac patches are often designed non-specifically for a line of cells, rather than in a patient-specific manner, and often used as a therapy for ischemic injuries in the left ventricle, rather than as a treatment for RVHF[181]. To address these needs, we tested the efficacy of our patient-specific PCL + FN + patient 956 patches in a PAB rat model of RVHF. Our patches remained cellularized and attached to the RV 4 weeks following implantation (Figure 25B and C). Non-specific patches that we implanted into PAB rats did not improve RV function, even when they contained the highly reparative neonatal CPCs (Figure 27 and 28). In contrast, the patient-specific PCL + FN + patient 956 patches were able to both increase TAPSE and decrease RA area at both 2- and 4-weeks post-implantation while the same cells within the same patch lacking fibronectin did not (Figure 31). RVHF in CHD patients is marked by myocyte hypertrophy and a reduction in capillary density in the RV[266,267]. Therefore, we examined the ability of our implanted patches to decrease myocyte hypertrophy and increase vessel formation in the RV. Animals receiving PCL + patient 956 patches had significantly less vessels and significantly more myocyte hypertrophy than the Sham group, while animals receiving PCL + FN + patient 956 patches did not. In total, the patient-specific PCL + FN + patient 956 patches improved the RV at both the overall functional level and at the cellular level, while the non-specific PCL + patient 956 patches provided no benefit following implantation. These data reveal the importance of tailoring the biomaterial design of cardiac patches in a patient-specific manner to improve autologous cell therapy.

4.6 Conclusions

We have shown that computational methods can be used to identify important mechanisms of improving CPC reparative capacity and that we can use biomaterials that specifically target these mechanisms to improve cardiac patch performance. We identified that ITGAV is a mediator of improved reparative paracrine signaling in CPCs that are inherently low in reparative capacity. We then used a PCL + FN patch to induce binding of α_V to the patch surface, leading to improvements in anti-fibrotic and pro-angiogenic signaling. Importantly, these improvements occurred in a CPC-patient-specific manner, with improvements only present in a CPC patient line that was low in reparative capacity and high in ITGAV signaling (956). We found that *in vivo*, only PCL + FN + 956 patches could improve RV function. This study provides a framework that can be used for other subsets of therapeutic cells used in cardiac cell therapy. Employing these methods can be used to improve the design of patient-specific cardiac tissue-engineered products.

CHAPTER 5. CONCLUSIONS AND FUTURE DIRECTIONS

5.1 Conclusions

Congenital heart disease (CHD) is the most common congenital disease, is the leading cause of birth defect-related death, and inflicts immense emotional strain on the families of patients[21,22]. Corrective surgery has improved patient outcomes in recent years, but right ventricular heart failure (RVHF) can still occur in patients with more complex forms of CHD[57]. To address this issue, cell therapy has emerged as a viable therapy that may be able to improve RV function and stave off RVHF. In this dissertation, we engineered a therapeutic cardiac patch composed of electrospun polycaprolactone (PCL) nanofibers and cardiac-derived c-Kit$^+$ cells (CPCs) isolated from pediatric CHD patients. We were able to optimize the formulation of our patch in a CPC donor-specific manner, by including extracellular matrix (ECM) protein fibronectin (FN) and used these patient-specific patches to improve RV function in a pulmonary artery band (PAB) rat model of RVHF. The results presented here lay the foundation for future studies that use computational methods to identify important mechanisms of cell-to-ECM binding. The insights gleaned from these computational analyses can be used to enhance the therapeutic capacity of cell populations used for cardiac cell therapy and to improve the design of patient-specific cardiac patches for RVHF.

5.1.1 Aim 1: To determine the CPC age-dependent effects and underlying mechanisms of PCL patch parameters on CPC behavior and reparative capacity

In chapter 3, we investigated the CPC response to culture on eight different electrospun nanofibrous scaffolds: random PCL nanofibers, random PCL/gelatin nanofibers (PCL + Gel), random PCL nanofibers with fibronectin (PCL + FN), random PCL/gelatin nanofibers with fibronectin (PCL + Gel + FN), aligned PCL nanofibers, aligned PCL + Gel nanofibers, aligned PCL + FN nanofibers, and aligned PCL + Gel + FN nanofibers. We first investigated the mechanics of each scaffold and found that aligned-fiber scaffolds had higher tensile strengths and Young's moduli than random-fiber scaffolds, and that including fibronectin and/or gelatin improved the hydrophilicity of the scaffolds. Further, we found that for all scaffolds, the diameter of each fiber was in the nanometer range, mimicking what has been observed for collagen fibers in the myocardium[268]. We then measured changes in CPC morphology, metabolism, and reparative paracrine secretion on each scaffold. Importantly, when neonatal or child CPCs were seeded onto our different PCL scaffolds, we found that CPC changes on each scaffold were age-dependent in many instances. In patches seeded with neonatal CPCs, there were no improvements in angiogenic paracrine signaling when gelatin or fibronectin was included. However, child CPCs showed improved angiogenic paracrine secretion on aligned PCL + FN scaffolds. Further, child CPCs had increased cell metabolism on PCL + FN and PCL + Gel + FN scaffolds. Our PCL/CPC patches also exhibited anti-fibrotic paracrine secretion that was able to decrease fibrotic gene expression in rat cardiac fibroblasts (RCFs).

In the beginning of chapter 4, the age-dependent difference we observed in CPC phenotype on each electrospun scaffold led to us to use computational methods to elucidate how FN-coated scaffolds were improving the function of child (low reparative capacity)

CPCs but not neonatal (high reparative capacity) CPCs. Using these methods, we identified the α_V integrin subunit (ITGAV) as one of the necessary mediators of improved low reparative CPC (CPC^{low}) paracrine secretion on PCL + FN patches. Further, we identified a CPC patient, 956, who was low in reparative capacity and high in ITGAV signaling and showed that this specific CPC had improved angiogenic and anti-fibrotic paracrine secretion on PCL + FN patches. Knockdown of ITGAV in CPCs from patient 956 eliminated this improved paracrine secretion on PCL + FN patches. These results demonstrated that we could use computational methods to identify a CPC from a specific patient and design an improved cardiac patch by tailoring a biomaterial to improve that specific CPC's reparative capacity.

5.1.2 To determine if a PCL/CPC patch implanted onto a failing RV improves cardiac function

In the second half of chapter 4, we investigated if implantation of our PCL/CPC patches improved RV function in a PAB rat model. We first tested whether random- and aligned-fiber PCL alone patches seeded with pooled lines of neonatal or child CPCs could be implanted onto the epicardium of the RV and improve RV function. At 4 weeks post-implantation, our patches remained cellularized and attached to the epicardium of the RV. However, the non-specific PCL patches with pooled lines of cells were not able to improve any of the echocardiographic parameters of RV function that we measured. Therefore, we used the knowledge we gained from Aim 1's results to design a patient-specific patch. We used PCL + FN patches loaded with CPCs from patient 956 (PCL + FN + 956) and implanted them into our PAB rats. These patches increased tricuspid annular plane systolic excursion (TAPSE) and right atrial (RA) area at 2- and 4-weeks post-implantation.

Implantation of these patient-specific patches also led to increased vessel formation and decreased myocyte hypertrophy in the RV free wall. Implantation of PCL alone patches seeded with CPCs from patient 956 did not yield the functional or histological improvements of the PCL + FN + 956 patches. Taken together, these data illustrate that cardiac patches can be tailored in a CPC-patient-specific manner, and these patient-specific patches are able to improve RV function *in vivo* in a rat model of RVHF. This computational analysis to *in vivo* implantation workflow (Figure 36) may be applicable to other cardiac patch studies and may improve the function of other tissue-engineered devices.

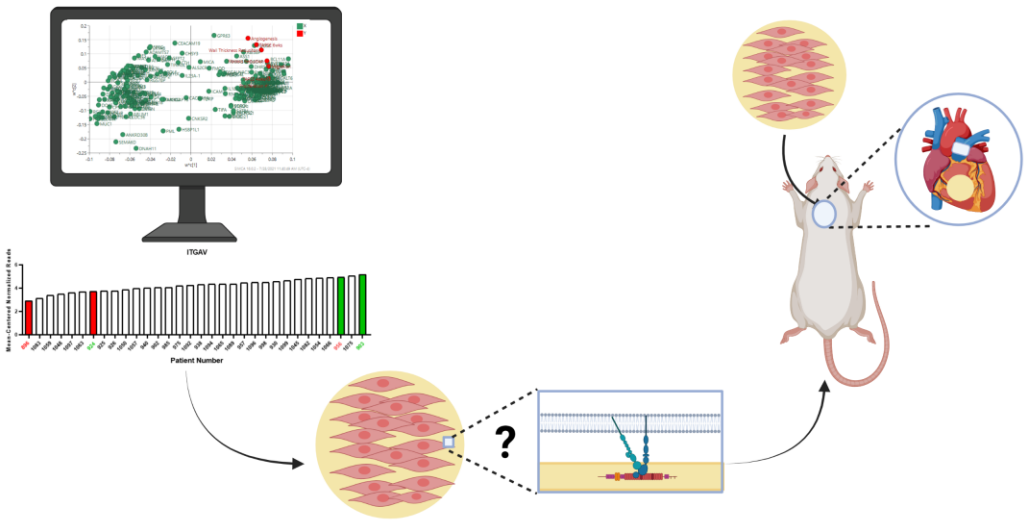

Figure 36. A proposed workflow for designing patient-specific cardiac patches. Computational modeling is used to identify an integrin that correlates highly with improved functional outcomes following cell therapy. A biomaterial is then designed to engage that integrin, leading to further improved functional outcomes following implantation.

5.2 Future Directions

5.2.1 Improving PCL scaffold design

Although our PCL + FN + 956 patches were successful in improving RV function in PAB rats, future directions may focus on further improving and optimizing the patch design. Our patches have Young's moduli in the 15-75 MPA range, while the heart's Young's modulus ranges from 20-500 kPA[150]. Therefore, there may be a large mechanical mismatch between our patches the native heart tissue on which they are implanted. This could be restrictive and hinder the pumping function of the RV. To measure whether this constriction is occurring, echocardiographic techniques like those used to measure constrictive pericarditis may be employed[269]. To reconcile the mechanical mismatch, other materials could be added to the electrospun polymer to decrease the Young's modulus of the patches and make the patches more compliant, such as by inclusion of an elastomer like poly(glycerol sebacate)[182,270].

Another way to improve our patch's design is by altering the FN concentration that is used to functionalize the patch surface. Previous studies have used FN concentrations of 10 µg/mL or 50 µg/mL to functionalized electrospun scaffolds[188,189], while in our study, the concentration of FN was only 1 µg/mL. Future experiments could be conducted to better understand if there are FN concentration-dependent changes in CPC function on PCL + FN scaffolds, with a higher concentration further increasing CPC reparative capacity. Functionalizing our patches with other ECM proteins such as laminin, collagen, or vitronectin may also improve CPC function by engaging other integrins that mediate improved reparative capacity. Functionalizing electrospun patches with decellularized

ECM may also help to more closely mimic the mechanical properties of the myocardium while also allowing binding of all the integrins that are important in CPCs[271]. Although not explored in depth in this dissertation, changes in cell morphology caused by our electrospun scaffolds may impart mechanical stimuli that alter CPC reparative function. Cell shape and elongation has been successfully controlled in a precise manner in several other previous studies[272,273], and these techniques may also be applied to the CPCs used here to more methodically examine the role of cell morphology in CPC reparative capacity.

5.2.2 Further understanding the mechanisms of integrin-mediated improvement of CPC reparative capacity

Also of interest for future research is uncovering how the binding of integrin subunit α_V to FN on the patch surface leads to improved CPC function. Integrins are a large family of proteins that complex with each other in several different combinations to bind different ECM proteins (Figure 37)[259]. Therefore, it is important to identify with which β subunit α_V complexes when binding to PCL + FN patches.

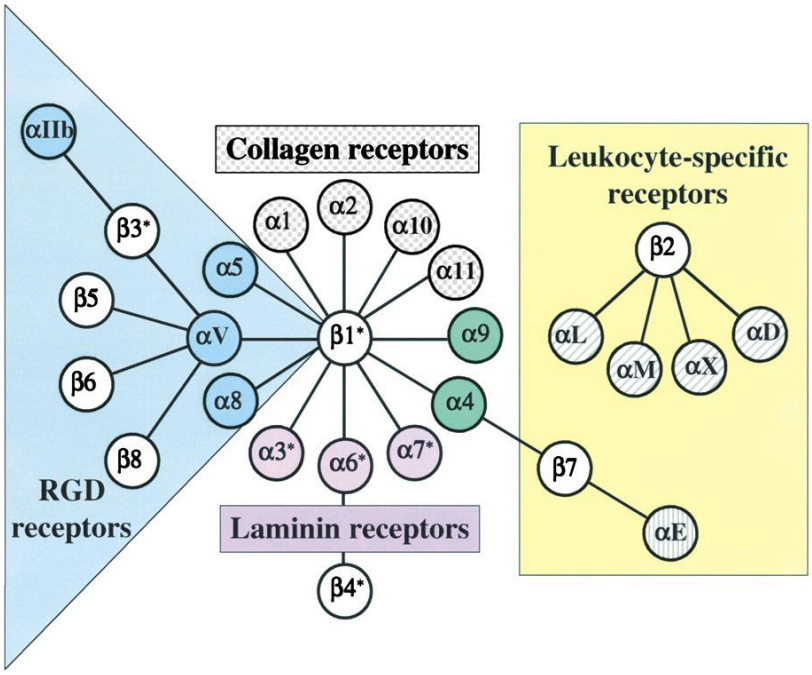

Figure 37. The family of α and β integrin subunits and in which combinations they bind different ECM proteins (RGD, laminin, collagen) and leukocytes. Reproduced from Hynes[259] with permission.

We observed that while high expression of the α_V subunit is necessary for improved reparative capacity in low reparative capacity CPCs, upregulation of α_V alone was not enough to rescue CPC function. Therefore, there may be interplay between α_V and other integrins that leads to the improvement in CPC function. Previous studies suggest α_V both binds FN as well as recruits other integrins, such as $\alpha_5\beta_1$, to the adhesion complex, which may be occurring on our patches[274]. Additionally, the only patient whose CPCs had improved reparative paracrine secretion on PCL + FN patches, patient 956, also has relatively high expression of the $\alpha_5\beta_1$ integrin (Figure 38D), further lending credence to the hypothesis that there is some interplay between the α_V subunit and $\alpha_5\beta_1$. We have observed that the α_5 subunit is upregulated in both the more reparative neonatal CPCs (Figure 38C) and in CPCs cultured on PCL + FN patches (Figure 38F). However, the α_V and β_1 subunit

is not upregulated in neonates (Figure 38A and B) or on PCL + FN scaffolds (Figure 38E). This suggests that the α_5 subunit may be the most important component of the $\alpha_5\beta_1$ for improving CPC reparative capacity. The downstream signaling that occurs after binding to FN can also be investigated, employing methods like those in previous studies[243].

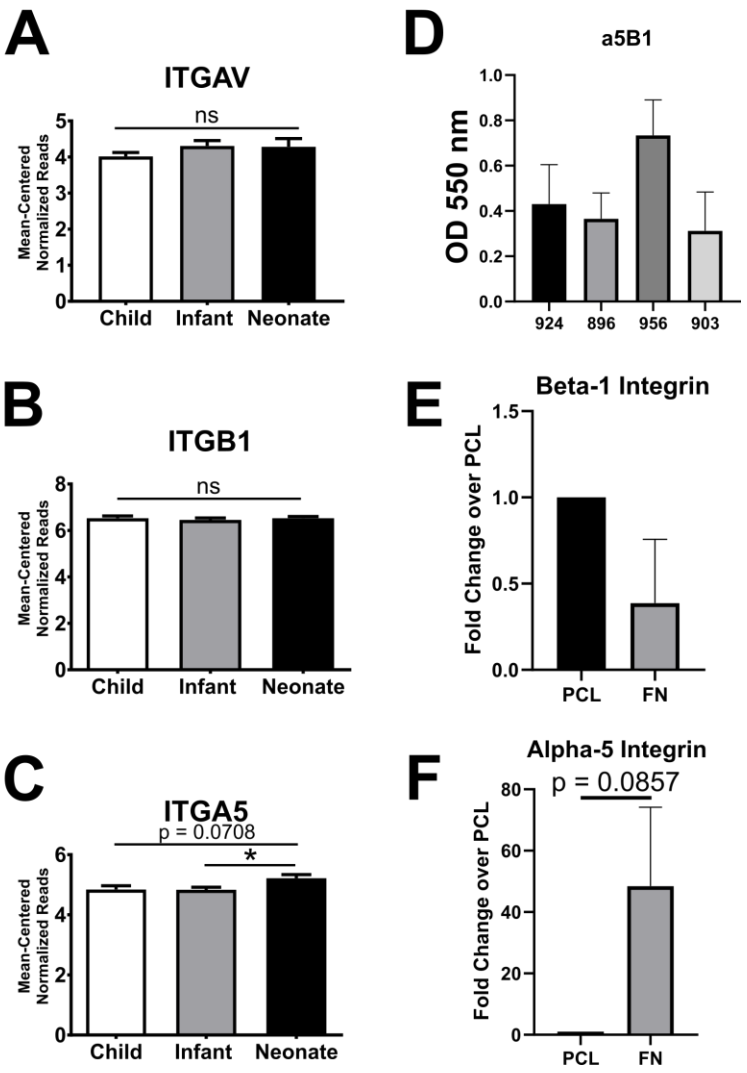

Figure 38. The role of the α_5 (ITGA5) and β_1 (ITGB1) integrins in CPC reparative capacity. Expression of (A) ITGAV, (B) ITB1, and (C) ITGA5 in child, infant, and neonatal CPCs as measured by RNA-seq. (D) Expression of the $\alpha_5\beta_1$ integrin protein in each of four CPC patients (924, 896, 956, 903) measured by ELISA. (n = 3-5). Expression of (E) ITGB1 and (F) ITGA5 in neonatal cells cultured on PCL or PCL + FN patches as measured by RT-PCR. (n = 3)

In this study, we used computational modeling to identify important integrins in the low-reparative-capacity subset of CPCs. Other future studies may use a similar approach with other subsets of CPCs based on age, disease, or sex to identify other patient-specific mechanisms that can better inform cardiac patch design. For example, we ran the same correlations with the male and female patient subsets of CPCs in Table 3. While integrin expression does not seem to be highly correlated with improved functional outcomes in CPCs from male patients, ITGA1 and ITGB3 are clearly very important for reparative capacity in CPCs isolated from female patients. Therefore, biomaterials could be designed with collagen and fibronectin to engage these integrins and further improve the reparative capacity of CPCs from female patients[259]. Further, although here we focus on a single integrin, it may also be of benefit to take into consideration the entire profile of integrin expression in each patient and modify the cardiac patch's biomaterial with ECM proteins accordingly. This integrin profile is easily measurable at the transcript level using techniques such as RNA-seq (Figure 39A and B) and at the protein using techniques like integrin adhesion assays (Figure 39C and D).

Table 3. Significance values for linear regressions of outcomes and expressions of integrins as measured by RNA-seq for CPCs from male patients (top) and CPCs from female patients (bottom). The expression of 11 integrin subunits (ITGA1, ITGA2, ITGA3, ITGA4, ITGA5, ITGAV, ITGB1, ITGB2, ITGB3, ITGB4, and ITGB5) were correlated with the 7 outcomes listed in the tables.

Male Patients		
Outcome	*p<0.05	**p<0.01
Angiogenesis		ITGB3
Fibrosis Reduction	ITGA5	
Migration		
Proliferation		
TAPSE 2w		
TAPSE 4w	ITGB3	
Wall Thickness Reduction	ITGA5, ITGB3	

Female Patients		
Outcome	*p<0.05	**p<0.01
Angiogenesis	ITGA1	
Fibrosis Reduction	ITGB2	ITGA1, ITGB3
Migration		ITGA1, ITGB3
Proliferation		ITGA1, ITGB3
TAPSE 2w		ITGA1, ITGB3
TAPSE 4w	ITGA1, ITGB3	
Wall Thickness		ITGA1, ITGB3

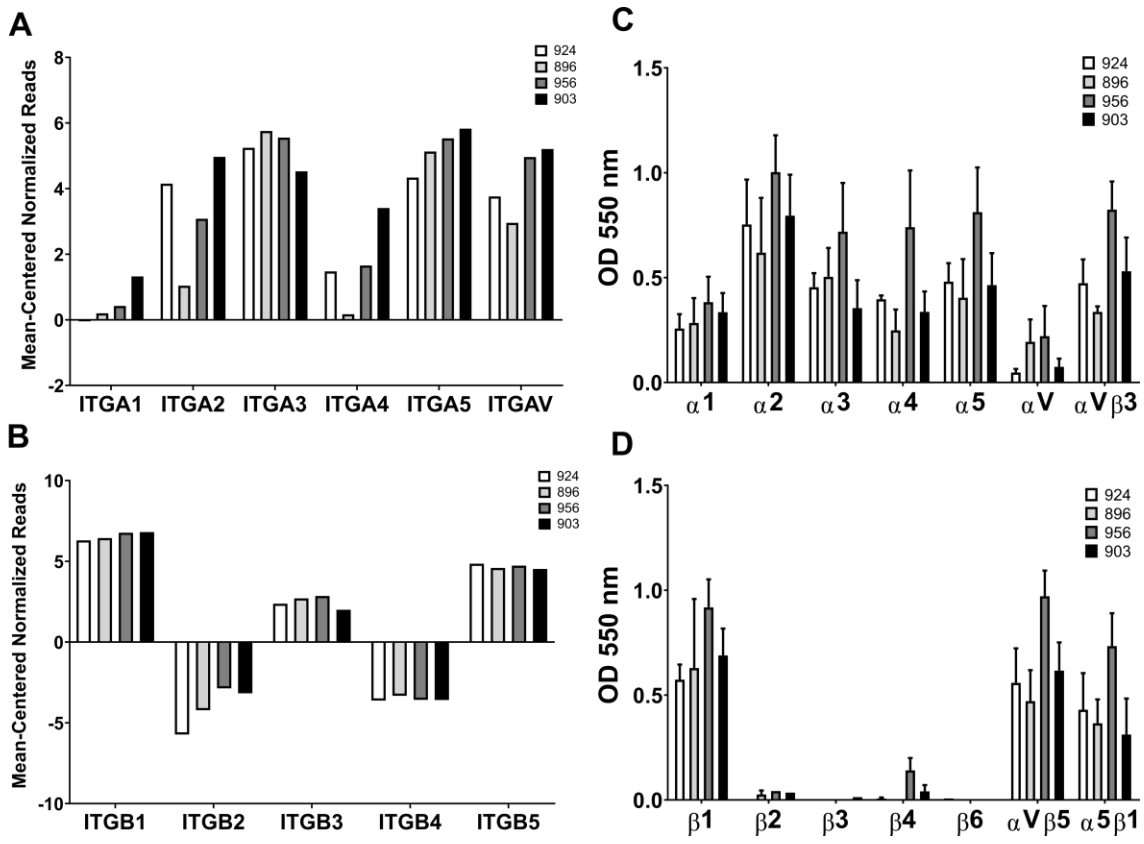

Figure 39. Total integrin expression profile of the four CPC patients (924, 896, 956, 903) used in this study. The α subunit RNA and protein expression measured by (A) RNA-seq and (B) integrin adhesion assay, respectively, and the β subunit RNA and protein expression measured by (A) RNA-seq and (B) integrin adhesion assay, respectively, are shown. (n = 3-5 for the ELISA data)

Finally, it may be necessary to incorporate other outcomes into our computational analysis to identify the most reparative CPC patients and the most important integrins/signaling pathways most accurately for improving CPC reparative capacities. Although not investigated here, previous studies have suggested that immune response majorly contributes to the improvements seen from cell therapy[147,275]. Therefore, it may be pertinent to include immune response-based outcomes (e.g., macrophage infiltration) in our models. It has also been suggested that this immune response is wholly responsible for functional improvements gained from cardiac cell therapy. It is therefore important to

further research the precise mechanism by which cardiac cell therapy is conferring benefit *in vivo*. More sophisticated methods, such as measuring circulating exosomes in blood plasma following cell injection[276], may able to more precisely identify the paracrine mechanisms of injected cells. In total, statistical modeling is a powerful tool to identify the mechanisms that underly functional benefit from cardiac cell therapy. More research in this area will not only improve cell therapy but also will improve cardiac biomaterials and patches. The insight gained from these studies will allow for the design of materials that engage the underlying mechanisms of improved reparative capacity in therapeutic cells and therefore, better ensure the success of reparative myocardial therapies.

APPENDIX A. LIST OF RT-PCR PRIMERS

Table A1. List of human and rat primer sequences used for RT-PCR.

Gene Symbol	Description	Forward 5'-3'	Reverse 5'-3'
Human Genes			
ITGAV	α_V Integrin Subunit	GCAGTGTGAGGAATTGATAGCG	AAGTAGAATGTGAGCCTGTCG
MEF2C	Myocyte-Specific Enhancer Factor 2C	TAACTTCTTTTCACTGTTGTGCTCCTT	GCCGCTTTTGGCAAATGTT
GATA4	GATA Binding Protein 4	GGAGATGCGTCCCATCAAGAC	GGAGACGCATAGCCTTGTGG
Nkx2.5	NK2 Homeobox 5, Cardiac-Specific Homeobox	ACCCTGAGTCCCCTGGATTT	TCACTCATTGCACGCTGCAT
CD-31	Platelet Endothelial Cell Adhesion Molecule 1	TCTATGACCTCGCCCTCCACAAA	GAACGGTGTCTTCAGGTTGTTATTTCA
FLT1	Vascular Endothelial Growth Factor Receptor 1	GACTAGATAGCGTCACCAGCAG	GAAACCGTCAGAATCCTCCTC
FLK1	Vascular Endothelial Growth Factor Receptor 2	ATAGAAGGTGCCCAGGAAAAG	GTCTTCAGTTCCCCTCCATTG
vWF	Von Willebrand Factor	TGTCTGGCTGAGGGAGGTAA	GTACATGGCTTTGCTGGCAC

veCAD	Vascular Endothelial Cadherin	TTTCCAGCAGCCTTTCTACCA	GGAAGAACTGGCCCTTGTCA
GAPDH	Glyceraldehyde 3-phosphate dehydrogenase	GTGGACCTGACCTGCCGTCT	GGAGGAGTGGGTGTCGCTGT
Rat Genes			
CTGF	Connective Tissue Growth Factor	TGAAGCTGACCTAGAGGAAAAC	GCACACCCCACAGAACTTAG
VIM	Vimentin	CATTGAGATCGCCACCTACAG	AGGAGTGTTCTTTTGGAGTGG
COL1A1	Collagen Type I Alpha 1 Chain	CATTGAGATCGCCACCTACAG	AGGAGTGTTCTTTTGGAGTGG
GAPDH	Glyceraldehyde 3-phosphate dehydrogenase	TCCAGTATGACTCTACCCACG	CACGACATACTCAGCACCAG

APPENDIX B. PERMISSIONS FOR PREVIOUSLY PUBLISHED MATERIAL

Permission for the use of Figure 37 from Hynes[259]

Printable Details

License Number	5167770520423
License date	Oct 14, 2021

Licensed Content

Licensed Content Publisher	Elsevier
Licensed Content Publication	Cell
Licensed Content Title	Integrins Bidirectional, Allosteric Signaling Machines
Licensed Content Author	Richard O. Hynes
Licensed Content Date	Sep 20, 2002
Licensed Content Volume	110
Licensed Content Issue	6
Licensed Content Pages	15

Order Details

Type of Use	reuse in a thesis/dissertation
Portion	figures/tables/illustrations
Number of figures/tables/illustrations	1
Format	electronic
Are you the author of this Elsevier article?	No
Will you be translating?	No

About Your Work

Title	ELECTROSPUN NANOFIBROUS SCAFFOLDS FOR THE DELIVERY OF CARDIAC-DERIVED C-KIT+ CELLS
Institution name	Emory University
Expected presentation date	Nov 2021

Additional Data

Portions	Figure 1

REFERENCES

(1) Jenkins, K. J.; Correa, A.; Feinstein, J. A.; Botto, L.; Britt, A. E.; Daniels, S. R.; Elixson, M.; Warnes, C. A.; Webb, C. L. Noninherited Risk Factors and Congenital Cardiovascular Defects: Current Knowledge: A Scientific Statement From the American Heart Association Council on Cardiovascular Disease in the Young: Endorsed by the American Academy of Pediatrics. *Circulation* **2007**, *115* (23), 2995–3014. https://doi.org/10.1161/CIRCULATIONAHA.106.183216.

(2) Sun, R.; Liu, M.; Lu, L.; Zheng, Y.; Zhang, P. Congenital Heart Disease: Causes, Diagnosis, Symptoms, and Treatments. *Cell Biochem Biophys* **2015**, *72* (3), 857–860. https://doi.org/10.1007/s12013-015-0551-6.

(3) Khoshnood, B.; Lelong, N.; Houyel, L.; Thieulin, A.-C.; Jouannic, J.-M.; Magnier, S.; Delezoide, A.-L.; Magny, J.-F.; Rambaud, C.; Bonnet, D.; Goffinet, F.; Group, on behalf of the E. S. Prevalence, Timing of Diagnosis and Mortality of Newborns with Congenital Heart Defects: A Population-Based Study. *Heart* **2012**, *98* (22), 1667–1673. https://doi.org/10.1136/heartjnl-2012-302543.

(4) Ohye, R. G.; Schranz, D.; D'Udekem, Y. Current Therapy for Hypoplastic Left Heart Syndrome and Related Single Ventricle Lesions. *Circulation* **2016**, *134* (17), 1265–1279. https://doi.org/10.1161/CIRCULATIONAHA.116.022816.

(5) Bernstein, H. S.; Srivastava, D. Stem Cell Therapy for Cardiac Disease. *Pediatric Research* **2012**, *71* (4–2), 491–499. https://doi.org/10.1038/pr.2011.61.

(6) Gao, Y.; Jacot, J. G. Stem Cells and Progenitor Cells for Tissue-Engineered Solutions to Congenital Heart Defects: Supplementary Issue: Stem Cell Biology. *Biomark Insights* **2015**, *10s1*, BMI.S20058. https://doi.org/10.4137/BMI.S20058.

(7) Ghafarzadeh, M.; Namdari, P.; Tarhani, M.; Tarhani, F. A Review of Application of Stem Cell Therapy in the Management of Congenital Heart Disease. *The Journal of Maternal-Fetal & Neonatal Medicine* **2018**, *0* (ja), 1–221. https://doi.org/10.1080/14767058.2018.1520829.

(8) Bhutani, S.; Nachlas, A. L. Y.; Brown, M. E.; Pete, T.; Johnson, C. T.; García, A. J.; Davis, M. E. Evaluation of Hydrogels Presenting Extracellular Matrix-Derived Adhesion Peptides and Encapsulating Cardiac Progenitor Cells for Cardiac Repair. *ACS Biomater. Sci. Eng.* **2018**, *4* (1), 200–210. https://doi.org/10.1021/acsbiomaterials.7b00502.

(9) Bejleri, D.; Streeter, B. W.; Nachlas, A. L. Y.; Brown, M. E.; Gaetani, R.; Christman, K. L.; Davis, M. E. A Bioprinted Cardiac Patch Composed of Cardiac-Specific Extracellular Matrix and Progenitor Cells for Heart Repair. *Advanced Healthcare Materials* **2018**, 1800672. https://doi.org/10.1002/adhm.201800672.

(10) Streeter, B. W.; Xue, J.; Xia, Y.; Davis, M. E. Electrospun Nanofiber-Based Patches for the Delivery of Cardiac Progenitor Cells. *ACS Applied Materials & Interfaces* **2019**, *11* (20), 18242–18253. https://doi.org/10.1021/acsami.9b04473.

(11) Trac, D.; Maxwell, J. T.; Brown, M. E.; Xu, C.; Davis, M. E. Aggregation of Child Cardiac Progenitor Cells into Spheres Activates Notch Signaling and Improves Treatment of Right Ventricular Heart Failure. *Circulation Research* **2018**. https://doi.org/10.1161/CIRCRESAHA.118.313845.

(12) Sharma, S.; Mishra, R.; Bigham, G. E.; Wehman, B.; Khan, M. M.; Xu, H.; Saha, P.; Goo, Y. A.; Datla, S. R.; Chen, L.; Tulapurkar, M. E.; Taylor, B. S.; Yang, P.; Karathanasis, S.; Goodlett, D. R.; Kaushal, S. A Deep Proteome Analysis Identifies the Complete Secretome as the Functional Unit of Human Cardiac Progenitor CellsNovelty and Significance. *Circulation Research* **2017**, *120* (5), 816–834. https://doi.org/10.1161/CIRCRESAHA.116.309782.

(13) Gray, W. D.; French, K. M.; Ghosh-Choudhary, S.; Maxwell, J. T.; Brown, M. E.; Platt, M. O.; Searles, C. D.; Davis, M. E. Identification of Therapeutic Covariant MicroRNA Clusters in Hypoxia-Treated Cardiac Progenitor Cell Exosomes Using Systems Biology. *Circulation Research* **2015**, *116* (2), 255–263. https://doi.org/10.1161/CIRCRESAHA.116.304360.

(14) Agarwal, U.; George, A.; Bhutani, S.; Ghosh-Choudhary, S.; Maxwell, J. T.; Brown, M. E.; Mehta, Y.; Platt, M. O.; Liang, Y.; Sahoo, S.; Davis, M. E. Experimental, Systems, and Computational Approaches to Understanding the MicroRNA-Mediated Reparative Potential of Cardiac Progenitor Cell–Derived Exosomes From Pediatric PatientsNovelty and Significance. *Circulation Research* **2017**, *120* (4), 701–712. https://doi.org/10.1161/CIRCRESAHA.116.309935.

(15) Zhang, M.; Methot, D.; Poppa, V.; Fujio, Y.; Walsh, K.; Murry, C. E. Cardiomyocyte Grafting for Cardiac Repair: Graft Cell Death and Anti-Death Strategies. *Journal of Molecular and Cellular Cardiology* **2001**, *33* (5), 907–921. https://doi.org/10.1006/jmcc.2001.1367.

(16) Terrovitis, J. V.; Smith, R. R.; Marbán, E. Assessment and Optimization of Cell Engraftment After Transplantation Into the Heart. *Circulation Research* **2010**, *106* (3), 479–494. https://doi.org/10.1161/CIRCRESAHA.109.208991.

(17) Wu, K. H.; Mo, X. M.; Han, Z. C.; Zhou, B. Stem Cell Engraftment and Survival in the Ischemic Heart. *The Annals of Thoracic Surgery* **2011**, *92* (5), 1917–1925. https://doi.org/10.1016/j.athoracsur.2011.07.012.

(18) Huyer, L. D.; Montgomery, M.; Zhao, Y.; Xiao, Y.; Conant, G.; Korolj, A.; Milica Radisic. Biomaterial Based Cardiac Tissue Engineering and Its Applications. *Biomed. Mater.* **2015**, *10* (3), 034004. https://doi.org/10.1088/1748-6041/10/3/034004.

(19) Radisic, M. Biomaterials for Cardiac Tissue Engineering. *Biomed. Mater.* **2015**, *10* (3), 030301. https://doi.org/10.1088/1748-6041/10/3/030301.

(20) Hoffman, J. I. E.; Kaplan, S. The Incidence of Congenital Heart Disease. *J Am Coll Cardiol* **2002**, *39* (12), 1890–1900. https://doi.org/10.1016/s0735-1097(02)01886-7.

(21) Benjamin, E. J.; Virani, S. S.; Callaway, C. W.; Chamberlain, A. M.; Chang, A. R.; Cheng, S.; Chiuve, S. E.; Cushman, M.; Delling, F. N.; Deo, R.; de Ferranti, S. D.; Ferguson, J. F.; Fornage, M.; Gillespie, C.; Isasi, C. R.; Jiménez, M. C.; Jordan, L. C.; Judd, S. E.; Lackland, D.; Lichtman, J. H.; Lisabeth, L.; Liu, S.; Longenecker, C. T.; Lutsey, P. L.; Mackey, J. S.; Matchar, D. B.; Matsushita, K.; Mussolino, M. E.; Nasir, K.; O'Flaherty, M.; Palaniappan, L. P.; Pandey, A.; Pandey, D. K.; Reeves, M. J.; Ritchey, M. D.; Rodriguez, C. J.; Roth, G. A.; Rosamond, W. D.; Sampson, U. K. A.; Satou, G. M.; Shah, S. H.; Spartano, N. L.; Tirschwell, D. L.; Tsao, C. W.; Voeks, J. H.; Willey, J. Z.; Wilkins, J. T.; Wu, J. HY.; Alger, H. M.; Wong, S. S.; Muntner, P. Heart Disease and Stroke Statistics—2018 Update: A Report From the American Heart Association. *Circulation* **2018**, *137* (12). https://doi.org/10.1161/CIR.0000000000000558.

(22) Moons, P.; Bovijn, L.; Budts, W.; Belmans, A.; Gewillig, M. Temporal Trends in Survival to Adulthood Among Patients Born With Congenital Heart Disease From 1970 to 1992 in Belgium. *Circulation* **2010**, *122* (22), 2264–2272. https://doi.org/10.1161/CIRCULATIONAHA.110.946343.

(23) Erikssen, G.; Liestøl, K.; Seem, E.; Birkeland, S.; Saatvedt, K. J.; Hoel, T. N.; Døhlen, G.; Skulstad, H.; Svennevig, J. L.; Thaulow, E.; Lindberg, H. L. Achievements in Congenital Heart Defect Surgery: A Prospective, 40-Year Study of 7038 Patients. *Circulation* **2015**, *131* (4), 337–346. https://doi.org/10.1161/CIRCULATIONAHA.114.012033.

(24) Gilboa, S. M.; Salemi, J. L.; Nembhard, W. N.; Fixler, D. E.; Correa, A. Mortality Resulting From Congenital Heart Disease Among Children and Adults in the United States, 1999 to 2006. *Circulation* **2010**, *122* (22), 2254–2263. https://doi.org/10.1161/CIRCULATIONAHA.110.947002.

(25) Tobler, D.; Greutmann, M. Simple Cardiac Shunts in Adults: Atrial Septal Defects, Ventricular Septal Defects, Patent Ductus Arteriosus. *Heart* **2020**, *106* (4), 307–314. https://doi.org/10.1136/heartjnl-2019-314700.

(26) Walker, R. E.; Moran, A. M.; Gauvreau, K.; Colan, S. D. Evidence of Adverse Ventricular Interdependence in Patients with Atrial Septal Defects. *The American Journal of Cardiology* **2004**, *93* (11), 1374–1377. https://doi.org/10.1016/j.amjcard.2004.02.033.

(27) Masutani, S.; Senzaki, H. Left Ventricular Function in Adult Patients With Atrial Septal Defect: Implication for Development of Heart Failure After Transcatheter

Closure. *Journal of Cardiac Failure* **2011**, *17* (11), 957–963. https://doi.org/10.1016/j.cardfail.2011.07.003.

(28) Arslani, K.; Roffler, N.; Zurek, M.; Greutmann, M.; Schwerzmann, M.; Bouchardy, J.; Rutz, T.; Ehl, N. F.; Jost, C. A.; Tobler, D. Patterns of Incidence Rates of Cardiac Complications in Patients With Congenital Heart Disease. *Canadian Journal of Cardiology* **2018**, *34* (12), 1624–1630. https://doi.org/10.1016/j.cjca.2018.09.010.

(29) Kidd, L.; Driscoll, D. J.; Gersony, W. M.; Hayes, C. J.; Keane, J. F.; O'Fallon, W. M.; Pieroni, D. R.; Wolfe, R. R.; Weidman, W. H. Second Natural History Study of Congenital Heart Defects. Results of Treatment of Patients with Ventricular Septal Defects. *Circulation* **1993**, *87* (2 Suppl), I38-51.

(30) Geva, T.; Martins, J. D.; Wald, R. M. Atrial Septal Defects. *The Lancet* **2014**, *383* (9932), 1921–1932. https://doi.org/10.1016/S0140-6736(13)62145-5.

(31) Murphy, J. G.; Gersh, B. J.; McGoon, M. D.; Mair, D. D.; Porter, C. J.; Ilstrup, D. M.; McGoon, D. C.; Puga, F. J.; Kirklin, J. W.; Danielson, G. K. Long-Term Outcome after Surgical Repair of Isolated Atrial Septal Defect: Follow-up at 27 to 32 Years. *N Engl J Med* **1990**, *323* (24), 1645–1650. https://doi.org/10.1056/NEJM199012133232401.

(32) Schneider, D. J.; Moore, J. W. Patent Ductus Arteriosus. *Circulation* **2006**, *114* (17), 1873–1882. https://doi.org/10.1161/CIRCULATIONAHA.105.592063.

(33) Marquis, R. M.; Miller, H. C.; McCormack, R. J.; Matthews, M. B.; Kitchin, A. H. Persistence of Ductus Arteriosus with Left to Right Shunt in the Older Patient. *Heart* **1982**, *48* (5), 469–484. https://doi.org/10.1136/hrt.48.5.469.

(34) O'Brien, P.; Marshall, A. C. Tetralogy of Fallot. *Circulation* **2014**, *130* (4). https://doi.org/10.1161/CIRCULATIONAHA.113.005547.

(35) Bailliard, F.; Anderson, R. H. Tetralogy of Fallot. *Orphanet J Rare Dis* **2009**, *4* (1), 2. https://doi.org/10.1186/1750-1172-4-2.

(36) Gatzoulis, M. A.; Till, J. A.; Somerville, J.; Redington, A. N. Mechanoelectrical Interaction in Tetralogy of Fallot: QRS Prolongation Relates to Right Ventricular Size and Predicts Malignant Ventricular Arrhythmias and Sudden Death. *Circulation* **1995**, *92* (2), 231–237. https://doi.org/10.1161/01.CIR.92.2.231.

(37) Nollert, G.; Fischlein, T.; Bouterwek, S.; Böhmer, C.; Klinner, W.; Reichart, B. Long-Term Survival in Patients With Repair of Tetralogy of Fallot: 36-Year Follow-Up of 490 Survivors of the First Year After Surgical Repair. *Journal of the American College of Cardiology* **1997**, *30* (5), 1374–1383. https://doi.org/10.1016/S0735-1097(97)00318-5.

(38) Khairy, P.; Fernandes, S. M.; Mayer, J. E.; Triedman, J. K.; Walsh, E. P.; Lock, J. E.; Landzberg, M. J. Long-Term Survival, Modes of Death, and Predictors of

Mortality in Patients With Fontan Surgery. *Circulation* **2008**, *117* (1), 85–92. https://doi.org/10.1161/CIRCULATIONAHA.107.738559.

(39) Grossfeld, P.; Nie, S.; Lin, L.; Wang, L.; Anderson, R. Hypoplastic Left Heart Syndrome: A New Paradigm for an Old Disease? *JCDD* **2019**, *6* (1), 10. https://doi.org/10.3390/jcdd6010010.

(40) Barron, D. J.; Kilby, M. D.; Davies, B.; Wright, J. G.; Jones, T. J.; Brawn, W. J. Hypoplastic Left Heart Syndrome. *The Lancet* **2009**, *374* (9689), 551–564. https://doi.org/10.1016/S0140-6736(09)60563-8.

(41) Saraf, A.; Book, W. M.; Nelson, T. J.; Xu, C. Hypoplastic Left Heart Syndrome: From Bedside to Bench and Back. *J. Mol. Cell. Cardiol.* **2019**, *135*, 109–118. https://doi.org/10.1016/j.yjmcc.2019.08.005.

(42) Norwood, W. I.; Lang, P.; Hansen, D. D. Physiologic Repair of Aortic Atresia-Hypoplastic Left Heart Syndrome. *N Engl J Med* **1983**, *308* (1), 23–26. https://doi.org/10.1056/NEJM198301063080106.

(43) Glenn, W. W. L. Circulatory Bypass of the Right Side of the Heart: Shunt between Superior Vena Cava and Distal Right Pulmonary Artery —Report of Clinical Application. *N Engl J Med* **1958**, *259* (3), 117–120. https://doi.org/10.1056/NEJM195807172590304.

(44) Fontan, F.; Baudet, E. Surgical Repair of Tricuspid Atresia. *Thorax* **1971**, *26* (3), 240–248. https://doi.org/10.1136/thx.26.3.240.

(45) Siffel, C.; Riehle-Colarusso, T.; Oster, M. E.; Correa, A. Survival of Children With Hypoplastic Left Heart Syndrome. *PEDIATRICS* **2015**, *136* (4), e864–e870. https://doi.org/10.1542/peds.2014-1427.

(46) Piran, S.; Veldtman, G.; Siu, S.; Webb, G. D.; Liu, P. P. Heart Failure and Ventricular Dysfunction in Patients With Single or Systemic Right Ventricles. *Circulation* **2002**, *105* (10), 1189–1194. https://doi.org/10.1161/hc1002.105182.

(47) Bae, J. M.; Jeon, T. Y.; Kim, J. S.; Kim, S.; Hwang, S. M.; Yoo, S.-Y.; Kim, J. H. Fontan-Associated Liver Disease: Spectrum of US Findings. *European Journal of Radiology* **2016**, *85* (4), 850–856. https://doi.org/10.1016/j.ejrad.2016.02.002.

(48) Wu, F. M.; Kogon, B.; Earing, M. G.; Aboulhosn, J. A.; Broberg, C. S.; John, A. S.; Harmon, A.; Sainani, N. I.; Hill, A. J.; Odze, R. D.; Johncilla, M. E.; Ukomadu, C.; Gauvreau, K.; Valente, A. M.; Landzberg, M. J. Liver Health in Adults with Fontan Circulation: A Multicenter Cross-Sectional Study. *The Journal of Thoracic and Cardiovascular Surgery* **2017**, *153* (3), 656–664. https://doi.org/10.1016/j.jtcvs.2016.10.060.

(49) Carins, T. A.; Shi, W. Y.; Iyengar, A. J.; Nisbet, A.; Forsdick, V.; Zannino, D.; Gentles, T.; Radford, D. J.; Justo, R.; Celermajer, D. S.; Bullock, A.; Winlaw, D.;

Wheaton, G.; Grigg, L.; d'Udekem, Y. Long-Term Outcomes after First-Onset Arrhythmia in Fontan Physiology. *The Journal of Thoracic and Cardiovascular Surgery* **2016**, *152* (5), 1355-1363.e1. https://doi.org/10.1016/j.jtcvs.2016.07.073.

(50) Atz, A. M.; Feinstein, J. A.; Jonas, R. A.; Perry, S. B.; Wessel, D. L. Preoperative Management of Pulmonary Venous Hypertension in Hypoplastic Left Heart Syndrome with Restrictive Atrial Septal Defect. *The American Journal of Cardiology* **1999**, *83* (8), 1224–1228. https://doi.org/10.1016/S0002-9149(99)00087-9.

(51) Caruthers, R. L.; Kempa, M.; Loo, A.; Gulbransen, E.; Kelly, E.; Erickson, S. R.; Hirsch, J. C.; Schumacher, K. R.; Stringer, K. A. Demographic Characteristics and Estimated Prevalence of Fontan-Associated Plastic Bronchitis. *Pediatr Cardiol* **2013**, *34* (2), 256–261. https://doi.org/10.1007/s00246-012-0430-5.

(52) Schumacher, K. R.; Gossett, J.; Guleserian, K.; Naftel, D. C.; Pruitt, E.; Dodd, D.; Carboni, M.; Lamour, J.; Pophal, S.; Zamberlan, M.; Gajarski, R. J. Fontan-Associated Protein-Losing Enteropathy and Heart Transplant: A Pediatric Heart Transplant Study Analysis. *The Journal of Heart and Lung Transplantation* **2015**, *34* (9), 1169–1176. https://doi.org/10.1016/j.healun.2015.03.022.

(53) Alsaied, T.; Alsidawi, S.; Allen, C. C.; Faircloth, J.; Palumbo, J. S.; Veldtman, G. R. Strategies for Thromboprophylaxis in Fontan Circulation: A Meta-Analysis. *Heart* **2015**, *101* (21), 1731–1737. https://doi.org/10.1136/heartjnl-2015-307930.

(54) Haddad, F.; Hunt, S. A.; Rosenthal, D. N.; Murphy, D. J. Right Ventricular Function in Cardiovascular Disease, Part I: Anatomy, Physiology, Aging, and Functional Assessment of the Right Ventricle. *Circulation* **2008**, *117* (11), 1436–1448. https://doi.org/10.1161/CIRCULATIONAHA.107.653576.

(55) Lorenz, C.; Walker, E.; Morgan, V.; Klein, S.; Graham, T. Normal Human Right and Left Ventricular Mass, Systolic Function, and Gender Differences by Cine Magnetic Resonance Imaging. *J. of Cardiovascular Magnetic Resonance* **1999**, *1* (1), 7–21. https://doi.org/10.3109/10976649909080829.

(56) Dell'Italia, L. J. The Right Ventricle: Anatomy, Physiology, and Clinical Importance. *Current Problems in Cardiology* **1991**, *16* (10), 658–720. https://doi.org/10.1016/0146-2806(91)90009-Y.

(57) Hsu, D. T.; Pearson, G. D. Heart Failure in Children: Part I: History, Etiology, and Pathophysiology. *Circulation: Heart Failure* **2009**, *2* (1), 63–70. https://doi.org/10.1161/CIRCHEARTFAILURE.108.820217.

(58) Friedberg, M. K.; Reddy, S. Right Ventricular Failure in Congenital Heart Disease: *Current Opinion in Pediatrics* **2019**, *31* (5), 604–610. https://doi.org/10.1097/MOP.0000000000000804.

(59) Taegtmeyer, H.; Golfman, L.; Sharma, S.; Razeghi, P.; Arsdall, M. Linking Gene Expression to Function: Metabolic Flexibility in the Normal and Diseased Heart. *Annals of the New York Academy of Sciences* **2004**, *1015* (1), 202–213. https://doi.org/10.1196/annals.1302.017.

(60) Dias, C. A.; Assad, R. S.; Caneo, L. F.; Abduch, M. C. D.; Aiello, V. D.; Dias, A. R.; Marcial, M. B.; Oliveira, S. A. Reversible Pulmonary Trunk Banding. II. An Experimental Model for Rapid Pulmonary Ventricular Hypertrophy. *The Journal of Thoracic and Cardiovascular Surgery* **2002**, *124* (5), 999–1006. https://doi.org/10.1067/mtc.2002.124234.

(61) Schwartz, A.; Lee, K. S. Study of Heart Mitochondria and Glycolytic Metabolism in Experimentally Induced Cardiac Failure. *Circulation Research* **1962**, *10* (3), 321–332. https://doi.org/10.1161/01.RES.10.3.321.

(62) Partovian, C.; Adnot, S.; Eddahibi, S.; Teiger, E.; Levame, M.; Dreyfus, P.; Raffestin, B.; Frelin, C. Heart and Lung VEGF MRNA Expression in Rats with Monocrotaline- or Hypoxia-Induced Pulmonary Hypertension. *American Journal of Physiology-Heart and Circulatory Physiology* **1998**, *275* (6), H1948–H1956. https://doi.org/10.1152/ajpheart.1998.275.6.H1948.

(63) Bogaard, H. J.; Natarajan, R.; Henderson, S. C.; Long, C. S.; Kraskauskas, D.; Smithson, L.; Ockaili, R.; McCord, J. M.; Voelkel, N. F. Chronic Pulmonary Artery Pressure Elevation Is Insufficient to Explain Right Heart Failure. *Circulation* **2009**, *120* (20), 1951–1960. https://doi.org/10.1161/CIRCULATIONAHA.109.883843.

(64) Gómez, A.; Bialostozky, D.; Zajarias, A.; Santos, E.; Palomar, A.; Martínez, M. L.; Sandoval, J. Right Ventricular Ischemia in Patients with Primary Pulmonary Hypertension. *Journal of the American College of Cardiology* **2001**, *38* (4), 1137–1142. https://doi.org/10.1016/S0735-1097(01)01496-6.

(65) Reddy, S.; Bernstein, D. Molecular Mechanisms of Right Ventricular Failure. *Circulation* **2015**, *132* (18), 1734–1742. https://doi.org/10.1161/CIRCULATIONAHA.114.012975.

(66) Weber, K. T.; Brilla, C. G. Pathological Hypertrophy and Cardiac Interstitium. Fibrosis and Renin-Angiotensin-Aldosterone System. *Circulation* **1991**, *83* (6), 1849–1865. https://doi.org/10.1161/01.CIR.83.6.1849.

(67) Eschenhagen, T.; Bolli, R.; Braun, T.; Field, L. J.; Fleischmann, B. K.; Frisén, J.; Giacca, M.; Hare, J. M.; Houser, S.; Lee, R. T.; Marbán, E.; Martin, J. F.; Molkentin, J. D.; Murry, C. E.; Riley, P. R.; Ruiz-Lozano, P.; Sadek, H. A.; Sussman, M. A.; Hill, J. A. Cardiomyocyte Regeneration: A Consensus Statement. *Circulation* **2017**, *136* (7), 680–686. https://doi.org/10.1161/CIRCULATIONAHA.117.029343.

(68) Hsieh, P. C.; Segers, V. F.; Davis, M. E.; MacGillivray, C.; Gannon, J.; Molkentin, J. D.; Robbins, J.; Lee, R. T. Evidence from a Genetic Fate-Mapping Study That

Stem Cells Refresh Adult Mammalian Cardiomyocytes after Injury. *Nat Med* **2007**, *13* (8), 970–974. https://doi.org/10.1038/nm1618.

(69) Dimmeler, S.; Burchfield, J.; Zeiher, A. M. Cell-Based Therapy of Myocardial Infarction. *Arteriosclerosis, Thrombosis, and Vascular Biology* **2007**, *28* (2), 208–216. https://doi.org/10.1161/ATVBAHA.107.155317.

(70) Zhang, J.; Zhu, W.; Radisic, M.; Vunjak-Novakovic, G. Can We Engineer a Human Cardiac Patch for Therapy? *Circulation Research* **2018**, *123* (2), 244–265. https://doi.org/10.1161/CIRCRESAHA.118.311213.

(71) Chavakis, E.; Koyanagi, M.; Dimmeler, S. Enhancing the Outcome of Cell Therapy for Cardiac Repair: Progress From Bench to Bedside and Back. *Circulation* **2010**, *121* (2), 325–335. https://doi.org/10.1161/CIRCULATIONAHA.109.901405.

(72) Menasché, P.; Hagège, A. A.; Scorsin, M.; Pouzet, B.; Desnos, M.; Duboc, D.; Schwartz, K.; Vilquin, J.-T.; Marolleau, J.-P. Myoblast Transplantation for Heart Failure. *The Lancet* **2001**, *357* (9252), 279–280. https://doi.org/10.1016/S0140-6736(00)03617-5.

(73) Menasche, P.; Alfieri, O.; Janssens, S.; McKenna, W.; Reichenspurner, H.; Trinquart, L.; Vilquin, J.-T.; Marolleau, J.-P.; Seymour, B.; Larghero, J.; Lake, S.; Chatellier, G.; Solomon, S.; Desnos, M.; Hagege, A. A. The Myoblast Autologous Grafting in Ischemic Cardiomyopathy (MAGIC) Trial: First Randomized Placebo-Controlled Study of Myoblast Transplantation. *Circulation* **2008**, *117* (9), 1189–1200. https://doi.org/10.1161/CIRCULATIONAHA.107.734103.

(74) Abraham, M. R.; Henrikson, C. A.; Tung, L. Antiarrhythmic Engineering of Skeletal Myoblasts for Cardiac Transplantation. *Circulation Research* **2005**, *97* (2), 159–167. https://doi.org/10.1161/01.RES.0000174794.22491.a0.

(75) Antanavičiūtė, I.; Ereminienė, E.; Vysockas, V.; Račkauskas, M.; Skipskis, V.; Rysevaitė, K.; Treinys, R.; Benetis, R.; Jurevičius, J.; Skeberdis, V. A. Exogenous Connexin43-Expressing Autologous Skeletal Myoblasts Ameliorate Mechanical Function and Electrical Activity of the Rabbit Heart after Experimental Infarction. *Int J Exp Pathol* **2015**, *96* (1), 42–53. https://doi.org/10.1111/iep.12109.

(76) Kolanowski, T. J.; Rozwadowska, N.; Malcher, A.; Szymczyk, E.; Kasprzak, J. D.; Mietkiewski, T.; Kurpisz, M. In Vitro and in Vivo Characteristics of Connexin 43-Modified Human Skeletal Myoblasts as Candidates for Prospective Stem Cell Therapy for the Failing Heart. *International Journal of Cardiology* **2014**, *173* (1), 55–64. https://doi.org/10.1016/j.ijcard.2014.02.009.

(77) Siepe, M.; Golsong, P.; Poppe, A.; Blumenthal, B.; von Wattenwyl, R.; Heilmann, C.; Förster, K.; Schlensak, C.; Beyersdorf, F. Scaffold-Based Transplantation of Akt1-Overexpressing Skeletal Myoblasts: Functional Regeneration Is Associated with Angiogenesis and Reduced Infarction Size. *Tissue Engineering Part A* **2010**, *17* (1–2), 205–212. https://doi.org/10.1089/ten.tea.2009.0721.

(78) Blumenthal, B.; Golsong, P.; Poppe, A.; Heilmann, C.; Schlensak, C.; Beyersdorf, F.; Siepe, M. Polyurethane Scaffolds Seeded With Genetically Engineered Skeletal Myoblasts: A Promising Tool to Regenerate Myocardial Function. *Artificial Organs* **2010**, *34* (2), E46–E54. https://doi.org/10.1111/j.1525-1594.2009.00937.x.

(79) Yoshikawa, Y.; Miyagawa, S.; Toda, K.; Saito, A.; Sakata, Y.; Sawa, Y. Myocardial Regenerative Therapy Using a Scaffold-Free Skeletal-Muscle-Derived Cell Sheet in Patients with Dilated Cardiomyopathy Even under a Left Ventricular Assist Device: A Safety and Feasibility Study. *Surg Today* **2018**, *48* (2), 200–210. https://doi.org/10.1007/s00595-017-1571-1.

(80) Sawa, Y.; Yoshikawa, Y.; Toda, K.; Fukushima, S.; Yamazaki, K.; Ono, M.; Sakata, Y.; Hagiwara, N.; Kinugawa, K.; Miyagawa, S. Safety and Efficacy of Autologous Skeletal Myoblast Sheets (TCD-51073) for the Treatment of Severe Chronic Heart Failure Due to Ischemic Heart Disease. *Circ. J.* **2015**, *79* (5), 991–999. https://doi.org/10.1253/circj.CJ-15-0243.

(81) Yoon, C. H.; Koyanagi, M.; Iekushi, K.; Seeger, F.; Urbich, C.; Zeiher, A. M.; Dimmeler, S. Mechanism of Improved Cardiac Function After Bone Marrow Mononuclear Cell Therapy: Role of Cardiovascular Lineage Commitment. *Circulation* **2010**, *121* (18), 2001–2011. https://doi.org/10.1161/CIRCULATIONAHA.109.909291.

(82) Strauer, B. E.; Brehm, M.; Zeus, T.; Gattermann, N.; Hernandez, A.; Sorg, R. V.; Kögler, G.; Wernet, P. Myocardial regeneration after intracoronary transplantation of human autologous stem cells following acute myocardial infarction. *Dtsch med Wochenschr* **2001**, *126* (34/35), 932–938. https://doi.org/10.1055/s-2001-16579-2.

(83) Wollert, K. C.; Meyer, G. P.; Lotz, J.; Ringes Lichtenberg, S.; Lippolt, P.; Breidenbach, C.; Fichtner, S.; Korte, T.; Hornig, B.; Messinger, D.; Arseniev, L.; Hertenstein, B.; Ganser, A.; Drexler, H. Intracoronary Autologous Bone-Marrow Cell Transfer after Myocardial Infarction: The BOOST Randomised Controlled Clinical Trial. *The Lancet* **2004**, *364* (9429), 141–148. https://doi.org/10.1016/S0140-6736(04)16626-9.

(84) Traverse, J. H.; Henry, T. D.; Pepine, C. J.; Willerson, J. T.; Zhao, D. X. M.; Ellis, S. G.; Forder, J. R.; Anderson, R. D.; Hatzopoulos, A. K.; Penn, M. S.; Perin, E. C.; Chambers, J.; Baran, K. W.; Raveendran, G.; Lambert, C.; Lerman, A.; Simon, D. I.; Vaughan, D. E.; Lai, D.; Gee, A. P.; Taylor, D. A.; Cogle, C. R.; Thomas, J. D.; Olson, R. E.; Bowman, S.; Francescon, J.; Geither, C.; Handberg, E.; Kappenman, C.; Westbrook, L.; Piller, L. B.; Simpson, L. M.; Baraniuk, S.; Loghin, C.; Aguilar, D.; Richman, S.; Zierold, C.; Spoon, D. B.; Bettencourt, J.; Sayre, S. L.; Vojvodic, R. W.; Skarlatos, S. I.; Gordon, D. J.; Ebert, R. F.; Kwak, M.; Moyé, L. A.; Simari, R. D.; Network (CCTRN), for the C. C. T. R. Effect of the Use and Timing of Bone Marrow Mononuclear Cell Delivery on Left Ventricular Function After Acute Myocardial Infarction: The TIME Randomized Trial. *JAMA* **2012**, *308* (22), 2380–2389. https://doi.org/10.1001/jama.2012.28726.

(85) Wollert, K. C.; Meyer, G. P.; Müller-Ehmsen, J.; Tschöpe, C.; Bonarjee, V.; Larsen, A. I.; May, A. E.; Empen, K.; Chorianopoulos, E.; Tebbe, U.; Waltenberger, J.; Mahrholdt, H.; Ritter, B.; Pirr, J.; Fischer, D.; Korf-Klingebiel, M.; Arseniev, L.; Heuft, H.-G.; Brinchmann, J. E.; Messinger, D.; Hertenstein, B.; Ganser, A.; Katus, H. A.; Felix, S. B.; Gawaz, M. P.; Dickstein, K.; Schultheiss, H.-P.; Ladage, D.; Greulich, S.; Bauersachs, J. Intracoronary Autologous Bone Marrow Cell Transfer after Myocardial Infarction: The BOOST-2 Randomised Placebo-Controlled Clinical Trial. *Eur Heart J* **2017**, *38* (39), 2936–2943. https://doi.org/10.1093/eurheartj/ehx188.

(86) Traverse, J. H.; Henry, T. D.; Ellis, S. G.; Pepine, C. J.; Willerson, J. T.; Zhao, D. X. M.; Forder, J. R.; Byrne, B. J.; Hatzopoulos, A. K.; Penn, M. S.; Perin, E. C.; Baran, K. W.; Chambers, J.; Lambert, C.; Raveendran, G.; Simon, D. I.; Vaughan, D. E.; Simpson, L. M.; Gee, A. P.; Taylor, D. A.; Cogle, C. R.; Thomas, J. D.; Silva, G. V.; Jorgenson, B. C.; Olson, R. E.; Bowman, S.; Francescon, J.; Geither, C.; Handberg, E.; Smith, D. X.; Baraniuk, S.; Piller, L. B.; Loghin, C.; Aguilar, D.; Richman, S.; Zierold, C.; Bettencourt, J.; Sayre, S. L.; Vojvodic, R. W.; Skarlatos, S. I.; Gordon, D. J.; Ebert, R. F.; Kwak, M.; Moyé, L. A.; Simari, R. D.; ResearchNetwork (CCTRN), for the C. C. T. Effect of Intracoronary Delivery of Autologous Bone Marrow Mononuclear Cells 2 to 3 Weeks Following Acute Myocardial Infarction on Left Ventricular Function: The LateTIME Randomized Trial. *JAMA* **2011**, *306* (19), 2110–2119. https://doi.org/10.1001/jama.2011.1670.

(87) Perin, E. C.; Dohmann, H. F. R.; Borojevic, R.; Silva, S. A.; Sousa, A. L. S.; Mesquita, C. T.; Rossi, M. I. D.; Carvalho, A. C.; Dutra, H. S.; Dohmann, H. J. F.; Silva, G. V.; Belém, L.; Vivacqua, R.; Rangel, F. O. D.; Esporcatte, R.; Geng, Y. J.; Vaughn, W. K.; Assad, J. A. R.; Mesquita, E. T.; Willerson, J. T. Transendocardial, Autologous Bone Marrow Cell Transplantation for Severe, Chronic Ischemic Heart Failure. *Circulation* **2003**, *107* (18), 2294–2302. https://doi.org/10.1161/01.CIR.0000070596.30552.8B.

(88) Perin, E. C.; Dohmann, H. F. R.; Borojevic, R.; Silva, S. A.; Sousa, A. L. S.; Silva, G. V.; Mesquita, C. T.; Belém, L.; Vaughn, W. K.; Rangel, F. O. D.; Assad, J. A. R.; Carvalho, A. C.; Branco, R. V. C.; Rossi, M. I. D.; Dohmann, H. J. F.; Willerson, J. T. Improved Exercise Capacity and Ischemia 6 and 12 Months after Transendocardial Injection of Autologous Bone Marrow Mononuclear Cells for Ischemic Cardiomyopathy. *Circulation* **2004**, *110* (11 Suppl 1), II213-218. https://doi.org/10.1161/01.CIR.0000138398.77550.62.

(89) Assmus, B.; Honold, J.; Schächinger, V.; Britten, M. B.; Fischer-Rasokat, U.; Lehmann, R.; Teupe, C.; Pistorius, K.; Martin, H.; Abolmaali, N. D.; Tonn, T.; Dimmeler, S.; Zeiher, A. M. Transcoronary Transplantation of Progenitor Cells after Myocardial Infarction. *New England Journal of Medicine* **2006**, *355* (12), 1222–1232. https://doi.org/10.1056/NEJMoa051779.

(90) Perin, E. C.; Willerson, J. T.; Pepine, C. J.; Henry, T. D.; Ellis, S. G.; Zhao, D. X. M.; Silva, G. V.; Lai, D.; Thomas, J. D.; Kronenberg, M. W.; Martin, A. D.;

Anderson, R. D.; Traverse, J. H.; Penn, M. S.; Anwaruddin, S.; Hatzopoulos, A. K.; Gee, A. P.; Taylor, D. A.; Cogle, C. R.; Smith, D.; Westbrook, L.; Chen, J.; Handberg, E.; Olson, R. E.; Geither, C.; Bowman, S.; Francescon, J.; Baraniuk, S.; Piller, L. B.; Simpson, L. M.; Loghin, C.; Aguilar, D.; Richman, S.; Zierold, C.; Bettencourt, J.; Sayre, S. L.; Vojvodic, R. W.; Skarlatos, S. I.; Gordon, D. J.; Ebert, R. F.; Kwak, M.; Moyé, L. A.; Simari, R. D.; Network (CCTRN), for the C. C. T. R. Effect of Transendocardial Delivery of Autologous Bone Marrow Mononuclear Cells on Functional Capacity, Left Ventricular Function, and Perfusion in Chronic Heart Failure: The FOCUS-CCTRN Trial. *JAMA* **2012**, *307* (16), 1717–1726. https://doi.org/10.1001/jama.2012.418.

(91) Heldman, A. W.; DiFede, D. L.; Fishman, J. E.; Zambrano, J. P.; Trachtenberg, B. H.; Karantalis, V.; Mushtaq, M.; Williams, A. R.; Suncion, V. Y.; McNiece, I. K.; Ghersin, E.; Soto, V.; Lopera, G.; Miki, R.; Willens, H.; Hendel, R.; Mitrani, R.; Pattany, P.; Feigenbaum, G.; Oskouei, B.; Byrnes, J.; Lowery, M. H.; Sierra, J.; Pujol, M. V.; Delgado, C.; Gonzalez, P. J.; Rodriguez, J. E.; Bagno, L. L.; Rouy, D.; Altman, P.; Foo, C. W. P.; Silva, J. da; Anderson, E.; Schwarz, R.; Mendizabal, A.; Hare, J. M. Transendocardial Mesenchymal Stem Cells and Mononuclear Bone Marrow Cells for Ischemic Cardiomyopathy: The TAC-HFT Randomized Trial. *JAMA* **2014**, *311* (1), 62–73. https://doi.org/10.1001/jama.2013.282909.

(92) Martino, H.; Brofman, P.; Greco, O.; Bueno, R.; Bodanese, L.; Clausell, N.; Maldonado, J. A.; Mill, J.; Braile, D.; Moraes, J.; Silva, S.; Bozza, A.; Santos, B.; Campos de Carvalho, A. Multicentre, Randomized, Double-Blind Trial of Intracoronary Autologous Mononuclear Bone Marrow Cell Injection in Non-Ischaemic Dilated Cardiomyopathy (the Dilated Cardiomyopathy Arm of the MiHeart Study). *Eur Heart J* **2015**, *36* (42), 2898–2904. https://doi.org/10.1093/eurheartj/ehv477.

(93) Fischer-Rasokat, U.; Assmus, B.; Seeger, F. H.; Honold, J.; Leistner, D.; Fichtlscherer, S.; Schachinger, V.; Tonn, T.; Martin, H.; Dimmeler, S.; Zeiher, A. M. A Pilot Trial to Assess Potential Effects of Selective Intracoronary Bone Marrow-Derived Progenitor Cell Infusion in Patients With Nonischemic Dilated Cardiomyopathy: Final 1-Year Results of the Transplantation of Progenitor Cells and Functional Regeneration Enhancement Pilot Trial in Patients With Nonischemic Dilated Cardiomyopathy. *Circulation: Heart Failure* **2009**, *2* (5), 417–423. https://doi.org/10.1161/CIRCHEARTFAILURE.109.855023.

(94) Seth, S.; Bhargava, B.; Narang, R.; Ray, R.; Mohanty, S.; Gulati, G.; Kumar, L.; Airan, B.; Venugopal, P. The ABCD (Autologous Bone Marrow Cells in Dilated Cardiomyopathy) Trial. *Journal of the American College of Cardiology* **2010**, *55* (15), 1643–1644. https://doi.org/10.1016/j.jacc.2009.11.070.

(95) Xiao, W.; Guo, S.; Gao, C.; Dai, G.; Yongjv Gao; Li, M.; Wang, X.; Hu, D. A Randomized Comparative Study on the Efficacy of Intracoronary Infusion of Autologous Bone Marrow Mononuclear Cells and Mesenchymal Stem Cells in

Patients With Dilated Cardiomyopathy. *Int. Heart J.* **2017**, *58* (2), 238–244. https://doi.org/10.1536/ihj.16-328.

(96) Sürder, D.; Manka, R.; Moccetti, T.; Lo Cicero, V.; Emmert, M. Y.; Klersy, C.; Soncin, S.; Turchetto, L.; Radrizzani, M.; Zuber, M.; Windecker, S.; Moschovitis, A.; Bühler, I.; Kozerke, S.; Erne, P.; Lüscher, T. F.; Corti, R. Effect of Bone Marrow–Derived Mononuclear Cell Treatment, Early or Late After Acute Myocardial Infarction: Twelve Months CMR and Long-Term Clinical Results. *Circulation Research* **2016**, *119* (3), 481–490. https://doi.org/10.1161/CIRCRESAHA.116.308639.

(97) Simari, R. D.; Pepine, C. J.; Traverse, J. H.; Henry, T. D.; Bolli, R.; Spoon, D. B.; Yeh, E.; Hare, J. M.; Schulman, I. H.; Anderson, R. D.; Lambert, C.; Sayre, S. L.; Taylor, D. A.; Ebert, R. F.; Moye, L. A. Bone Marrow Mononuclear Cell Therapy for Acute Myocardial Infarction: A Perspective From the Cardiovascular Cell Therapy Research Network. *Circulation Research* **2014**, *114* (10), 1564–1568. https://doi.org/10.1161/CIRCRESAHA.114.303720.

(98) Lin, Y.-D.; Yeh, M.-L.; Yang, Y.-J.; Tsai, D.-C.; Chu, T.-Y.; Shih, Y.-Y.; Chang, M.-Y.; Liu, Y.-W.; Tang, A. C. L.; Chen, T.-Y.; Luo, C.-Y.; Chang, K.-C.; Chen, J.-H.; Wu, H.-L.; Hung, T.-K.; Hsieh, P. C. H. Intramyocardial Peptide Nanofiber Injection Improves Postinfarction Ventricular Remodeling and Efficacy of Bone Marrow Cell Therapy in Pigs. *Circulation* **2010**, *122* (11_suppl_1), S132–S141. https://doi.org/10.1161/CIRCULATIONAHA.110.939512.

(99) Liu, Y.; Xu, Y.; Wang, Z.; Wen, D.; Zhang, W.; Schmull, S.; Li, H.; Chen, Y.; Xue, S. Electrospun Nanofibrous Sheets of Collagen/Elastin/Polycaprolactone Improve Cardiac Repair after Myocardial Infarction. *Am J Transl Res* **2016**, *8* (4), 1678–1694.

(100) Quijada, P.; Toko, H.; Fischer, K. M.; Bailey, B.; Reilly, P.; Hunt, K. D.; Gude, N. A.; Avitabile, D.; Sussman, M. A. Preservation of Myocardial Structure Is Enhanced by Pim-1 Engineering of Bone Marrow Cells. *Circulation Research* **2012**, *111* (1), 77–86. https://doi.org/10.1161/CIRCRESAHA.112.265207.

(101) Dominici, M.; Blanc, K. le; Müller, I.; Slaper-Cortenbach, I. C. M.; Marini, F. C.; Krause, D. S.; Deans, R. J.; Keating, A.; Prockop, D.; Horwitz, E. H. Minimal Criteria for Defining Multipotent Mesenchymal Stromal Cells. The International Society for Cellular Therapy Position Statement. *Cytotherapy* **2006**, *8* (4), 315–317.

(102) Golpanian, S.; Wolf, A.; Hatzistergos, K. E.; Hare, J. M. Rebuilding the Damaged Heart: Mesenchymal Stem Cells, Cell-Based Therapy, and Engineered Heart Tissue. *Physiological Reviews* **2016**, *96* (3), 1127–1168. https://doi.org/10.1152/physrev.00019.2015.

(103) Bahr, L. von; Batsis, I.; Moll, G.; Hägg, M.; Szakos, A.; Sundberg, B.; Uzunel, M.; Ringden, O.; Blanc, K. L. Analysis of Tissues Following Mesenchymal Stromal

Cell Therapy in Humans Indicates Limited Long-Term Engraftment and No Ectopic Tissue Formation. *STEM CELLS* **2012**, *30* (7), 1575–1578. https://doi.org/10.1002/stem.1118.

(104) Banerjee, M. N.; Bolli, R.; Hare, J. M. Clinical Studies of Cell Therapy in Cardiovascular Medicine: Recent Developments and Future Directions. *Circulation Research* **2018**, *123* (2), 266–287. https://doi.org/10.1161/CIRCRESAHA.118.311217.

(105) Hare, J. M.; Fishman, J. E.; Gerstenblith, G.; Velazquez, D. L. D.; Zambrano, J. P.; Suncion, V. Y.; Tracy, M.; Ghersin, E.; Johnston, P. V.; Brinker, J. A.; Breton, E.; Davis-Sproul, J.; Byrnes, J.; George, R.; Lardo, A.; Schulman, I. H.; Mendizabal, A. M.; Lowery, M. H.; Rouy, D.; Altman, P.; Foo, C. W. P.; Ruiz, P.; Amador, A.; Silva, J. D.; McNiece, I. K.; Heldman, A. W. Comparison of Allogeneic vs Autologous Bone Marrow–Derived Mesenchymal Stem Cells Delivered by Transendocardial Injection in Patients With Ischemic Cardiomyopathy: The POSEIDON Randomized Trial. *JAMA* **2012**, *308* (22), 2369–2379. https://doi.org/10.1001/jama.2012.25321.

(106) Quijada, P.; Salunga, H. T.; Hariharan, N.; Cubillo, J. D.; El-Sayed, F. G.; Moshref, M.; Bala, K. M.; Emathinger, J. M.; De La Torre, A.; Ormachea, L.; Alvarez, R.; Gude, N. A.; Sussman, M. A. Cardiac Stem Cell Hybrids Enhance Myocardial RepairNovelty and Significance. *Circulation Research* **2015**, *117* (8), 695–706. https://doi.org/10.1161/CIRCRESAHA.115.306838.

(107) Bolli, R.; Hare, J. M.; March, K. L.; Pepine, C. J.; Willerson, J. T.; Perin, E. C.; Yang, P. C.; Henry, T. D.; Traverse, J. H.; Mitrani, R. D.; Khan, A.; Hernandez-Schulman, I.; Taylor, D. A.; DiFede, D. L.; Lima, J. A. C.; Chugh, A.; Loughran, J.; Vojvodic, R. W.; Sayre, S. L.; Bettencourt, J.; Cohen, M.; Moyé, L.; Ebert, R. F.; Simari, R. D. Rationale and Design of the CONCERT-HF Trial (Combination of Mesenchymal and c-Kit $^{+}$ Cardiac Stem Cells As Regenerative Therapy for Heart Failure). *Circulation Research* **2018**, *122* (12), 1703–1715. https://doi.org/10.1161/CIRCRESAHA.118.312978.

(108) Mayourian, J.; Savizky, R. M.; Sobie, E. A.; Costa, K. D. Modeling Electrophysiological Coupling and Fusion between Human Mesenchymal Stem Cells and Cardiomyocytes. *PLOS Computational Biology* **2016**, *12* (7), e1005014. https://doi.org/10.1371/journal.pcbi.1005014.

(109) Mayourian, J.; Cashman, T. J.; Ceholski, D. K.; Johnson, B. V.; Sachs, D.; Kaji, D. A.; Sahoo, S.; Hare, J. M.; Hajjar, R. J.; Sobie, E. A.; Costa, K. D. Experimental and Computational Insight Into Human Mesenchymal Stem Cell Paracrine Signaling and Heterocellular Coupling Effects on Cardiac Contractility and Arrhythmogenicity. *Circulation Research* **2017**, *121* (4), 411–423. https://doi.org/10.1161/CIRCRESAHA.117.310796.

(110) Evans, M. J.; Kaufman, M. H. Establishment in Culture of Pluripotential Cells from Mouse Embryos. *Nature* **1981**, *292* (5819), 154–156. https://doi.org/10.1038/292154a0.

(111) Kofidis, T.; Lebl, D. R.; Martinez, E. C.; Hoyt, G.; Tanaka, M.; Robbins, R. C. Novel Injectable Bioartificial Tissue Facilitates Targeted, Less Invasive, Large-Scale Tissue Restoration on the Beating Heart after Myocardial Injury. *Circulation* **2005**, *112* (9 Suppl), I173-177. https://doi.org/10.1161/CIRCULATIONAHA.104.526178.

(112) Zimmermann, W.-H. Embryonic and Embryonic-like Stem Cells in Heart Muscle Engineering. *Journal of Molecular and Cellular Cardiology* **2011**, *50* (2), 320–326. https://doi.org/10.1016/j.yjmcc.2010.10.027.

(113) Bellamy, V.; Vanneaux, V.; Bel, A.; Nemetalla, H.; Emmanuelle Boitard, S.; Farouz, Y.; Joanne, P.; Perier, M.-C.; Robidel, E.; Mandet, C.; Hagège, A.; Bruneval, P.; Larghero, J.; Agbulut, O.; Menasché, P. Long-Term Functional Benefits of Human Embryonic Stem Cell-Derived Cardiac Progenitors Embedded into a Fibrin Scaffold. *The Journal of Heart and Lung Transplantation* **2014**, *34* (9), 1198–1207. https://doi.org/10.1016/j.healun.2014.10.008.

(114) Menasché, P.; Vanneaux, V.; Hagège, A.; Bel, A.; Cholley, B.; Parouchev, A.; Cacciapuoti, I.; Al-Daccak, R.; Benhamouda, N.; Blons, H.; Agbulut, O.; Tosca, L.; Trouvin, J.-H.; Fabreguettes, J.-R.; Bellamy, V.; Charron, D.; Tartour, E.; Tachdjian, G.; Desnos, M.; Larghero, J. Transplantation of Human Embryonic Stem Cell–Derived Cardiovascular Progenitors for Severe Ischemic Left Ventricular Dysfunction. *Journal of the American College of Cardiology* **2018**, *71* (4), 429–438. https://doi.org/10.1016/j.jacc.2017.11.047.

(115) van Laake, L. W.; Passier, R.; Doevendans, P. A.; Mummery, C. L. Human Embryonic Stem Cell–Derived Cardiomyocytes and Cardiac Repair in Rodents. *Circulation Research* **2008**, *102* (9), 1008–1010. https://doi.org/10.1161/CIRCRESAHA.108.175505.

(116) Laflamme, M. A.; Chen, K. Y.; Naumova, A. V.; Muskheli, V.; Fugate, J. A.; Dupras, S. K.; Reinecke, H.; Xu, C.; Hassanipour, M.; Police, S.; O'Sullivan, C.; Collins, L.; Chen, Y.; Minami, E.; Gill, E. A.; Ueno, S.; Yuan, C.; Gold, J.; Murry, C. E. Cardiomyocytes Derived from Human Embryonic Stem Cells in Pro-Survival Factors Enhance Function of Infarcted Rat Hearts. *Nature Biotechnology* **2007**, *25* (9), 1015–1024. https://doi.org/10.1038/nbt1327.

(117) Shiba, Y.; Fernandes, S.; Zhu, W.-Z.; Filice, D.; Muskheli, V.; Kim, J.; Palpant, N. J.; Gantz, J.; Moyes, K. W.; Reinecke, H.; Biber, B. V.; Dardas, T.; Mignone, J. L.; Izawa, A.; Hanna, R.; Viswanathan, M.; Gold, J. D.; Kotlikoff, M. I.; Sarvazyan, N.; Kay, M. W.; Murry, C. E.; Laflamme, M. A. Human ES-Cell-Derived Cardiomyocytes Electrically Couple and Suppress Arrhythmias in Injured Hearts. *Nature* **2012**, *489* (7415), 322–325. https://doi.org/10.1038/nature11317.

(118) Chong, J. J. H.; Yang, X.; Don, C. W.; Minami, E.; Liu, Y.-W.; Weyers, J. J.; Mahoney, W. M.; Biber, B. V.; Cook, S. M.; Palpant, N. J.; Gantz, J. A.; Fugate, J. A.; Muskheli, V.; Gough, G. M.; Vogel, K. W.; Astley, C. A.; Hotchkiss, C. E.; Baldessari, A.; Pabon, L.; Reinecke, H.; Gill, E. A.; Nelson, V.; Kiem, H.-P.; Laflamme, M. A.; Murry, C. E. Human Embryonic-Stem-Cell-Derived Cardiomyocytes Regenerate Non-Human Primate Hearts. *Nature* **2014**, *510* (7504), 273–277. https://doi.org/10.1038/nature13233.

(119) Caspi, O.; Lesman, A.; Basevitch, Y.; Gepstein, A.; Arbel, G.; Habib, I. H. M.; Gepstein, L.; Levenberg, S. Tissue Engineering of Vascularized Cardiac Muscle From Human Embryonic Stem Cells. *Circulation Research* **2007**, *100* (2), 263–272. https://doi.org/10.1161/01.RES.0000257776.05673.ff.

(120) Jacot, J. G.; Kita-Matsuo, H.; Wei, K. A.; Chen, H. S. V.; Omens, J. H.; Mercola, M.; Mcculloch, A. D. Cardiac Myocyte Force Development during Differentiation and Maturation. *Ann N Y Acad Sci* **2010**, *1188*, 121–127. https://doi.org/10.1111/j.1749-6632.2009.05091.x.

(121) Martherus, R. S. R. M.; Vanherle, S. J. V.; Timmer, E. D. J.; Zeijlemaker, V. A.; Broers, J. L.; Smeets, H. J.; Geraedts, J. P.; Ayoubi, T. A. Y. Electrical Signals Affect the Cardiomyocyte Transcriptome Independently of Contraction. *Physiological Genomics* **2010**, *42A* (4), 283–289. https://doi.org/10.1152/physiolgenomics.00182.2009.

(122) Földes, G.; Mioulane, M.; Wright, J. S.; Liu, A. Q.; Novak, P.; Merkely, B.; Gorelik, J.; Schneider, M. D.; Ali, N. N.; Harding, S. E. Modulation of Human Embryonic Stem Cell-Derived Cardiomyocyte Growth: A Testbed for Studying Human Cardiac Hypertrophy? *J Mol Cell Cardiol* **2011**, *50* (2–4), 367–376. https://doi.org/10.1016/j.yjmcc.2010.10.029.

(123) Takahashi, K.; Tanabe, K.; Ohnuki, M.; Narita, M.; Ichisaka, T.; Tomoda, K.; Yamanaka, S. Induction of Pluripotent Stem Cells from Adult Human Fibroblasts by Defined Factors. *Cell* **2007**, *131* (5), 861–872. https://doi.org/10.1016/j.cell.2007.11.019.

(124) Mauritz, C.; Schwanke, K.; Reppel, M.; Neef, S.; Katsirntaki, K.; Maier, L. S.; Nguemo, F.; Menke, S.; Haustein, M.; Hescheler, J.; Hasenfuss, G.; Martin, U. Generation of Functional Murine Cardiac Myocytes From Induced Pluripotent Stem Cells. *Circulation* **2008**, *118* (5), 507–517. https://doi.org/10.1161/CIRCULATIONAHA.108.778795.

(125) Ye, L.; Chang, Y.-H.; Xiong, Q.; Zhang, P.; Zhang, L.; Somasundaram, P.; Lepley, M.; Swingen, C.; Su, L.; Wendel, J. S.; Guo, J.; Jang, A.; Rosenbush, D.; Greder, L.; Dutton, J. R.; Zhang, J.; Kamp, T. J.; Kaufman, D. S.; Ge, Y.; Zhang, J. Cardiac Repair in a Porcine Model of Acute Myocardial Infarction with Human Induced Pluripotent Stem Cell-Derived Cardiovascular Cell Populations. *Cell Stem Cell* **2014**, *15* (6), 750–761. https://doi.org/10.1016/j.stem.2014.11.009.

(126) Gao, L.; Gregorich, Z. R.; Zhu, W.; Mattapally, S.; Oduk, Y.; Lou, X.; Kannappan, R.; Borovjagin, A. V.; Walcott, G. P.; Pollard, A. E.; Fast, V. G.; Hu, X.; Lloyd, S. G.; Ge, Y.; Zhang, J. Large Cardiac Muscle Patches Engineered From Human Induced-Pluripotent Stem Cell–Derived Cardiac Cells Improve Recovery From Myocardial Infarction in Swine. *Circulation* **2018**, *137* (16), 1712–1730. https://doi.org/10.1161/CIRCULATIONAHA.117.030785.

(127) Khan, M.; Xu, Y.; Hua, S.; Johnson, J.; Belevych, A.; Janssen, P. M. L.; Gyorke, S.; Guan, J.; Angelos, M. G. Evaluation of Changes in Morphology and Function of Human Induced Pluripotent Stem Cell Derived Cardiomyocytes (HiPSC-CMs) Cultured on an Aligned-Nanofiber Cardiac Patch. *PLoS One* **2015**, *10* (5). https://doi.org/10.1371/journal.pone.0126338.

(128) Wang, Q.; Yang, H.; Bai, A.; Jiang, W.; Li, X.; Wang, X.; Mao, Y.; Lu, C.; Qian, R.; Guo, F.; Ding, T.; Chen, H.; Chen, S.; Zhang, J.; Liu, C.; Sun, N. Functional Engineered Human Cardiac Patches Prepared from Nature's Platform Improve Heart Function after Acute Myocardial Infarction. *Biomaterials* **2016**, *105*, 52–65. https://doi.org/10.1016/j.biomaterials.2016.07.035.

(129) Fong, A. H.; Romero-López, M.; Heylman, C. M.; Keating, M.; Tran, D.; Sobrino, A.; Tran, A. Q.; Pham, H. H.; Fimbres, C.; Gershon, P. D.; Botvinick, E. L.; George, S. C.; Hughes, C. C. W. Three-Dimensional Adult Cardiac Extracellular Matrix Promotes Maturation of Human Induced Pluripotent Stem Cell-Derived Cardiomyocytes. *Tissue Engineering Part A* **2016**, *22* (15–16), 1016–1025. https://doi.org/10.1089/ten.tea.2016.0027.

(130) Beauchamp, P.; Moritz, W.; Kelm, J. M.; Ullrich, N. D.; Agarkova, I.; Anson, B. D.; Suter, T. M.; Zuppinger, C. Development and Characterization of a Scaffold-Free 3D Spheroid Model of Induced Pluripotent Stem Cell-Derived Human Cardiomyocytes. *Tissue Engineering Part C: Methods* **2015**, *21* (8), 852–861. https://doi.org/10.1089/ten.tec.2014.0376.

(131) Wang, L.; Liu, Y.; Ye, G.; He, Y.; Li, B.; Guan, Y.; Gong, B.; Mequanint, K.; Xing, M. M. Q.; Qiu, X. Injectable and Conductive Cardiac Patches Repair Infarcted Myocardium in Rats and Minipigs. *Nat Biomed Eng* **2021**, 1–17. https://doi.org/10.1038/s41551-021-00796-9.

(132) Okano, H.; Nakamura, M.; Yoshida, K.; Okada, Y.; Tsuji, O.; Nori, S.; Ikeda, E.; Yamanaka, S.; Miura, K. Steps Toward Safe Cell Therapy Using Induced Pluripotent Stem Cells. *Circulation Research* **2013**, *112* (3), 523–533. https://doi.org/10.1161/CIRCRESAHA.111.256149.

(133) Beltrami, A. P.; Barlucchi, L.; Torella, D.; Baker, M.; Limana, F.; Chimenti, S.; Kasahara, H.; Rota, M.; Musso, E.; Urbanek, K.; Leri, A.; Kajstura, J.; Nadal-Ginard, B.; Anversa, P. Adult Cardiac Stem Cells Are Multipotent and Support Myocardial Regeneration. *Cell* **2003**, *114* (6), 763–776. https://doi.org/10.1016/S0092-8674(03)00687-1.

(134) Chugh, A. R.; Beache, G.; Loughran, J. H.; Mewton, N.; Elmore, J. B.; Kajstura, J.; Pappas, P.; Tatooles, A.; Stoddard, M. F.; Lima, J. A. C.; Slaughter, M. S.; Anversa, P.; Bolli, R. Administration of Cardiac Stem Cells in Patients with Ischemic Cardiomyopathy (the SCIPIO Trial): Surgical Aspects and Interim Analysis of Myocardial Function and Viability by Magnetic Resonance. *Circulation* **2012**, *126* (11 Suppl 1), S54–S64. https://doi.org/10.1161/CIRCULATIONAHA.112.092627.

(135) Bolli, R.; Chugh, A. R.; D'Amario, D.; Loughran, J. H.; Stoddard, M. F.; Ikram, S.; Beache, G. M.; Wagner, S. G.; Leri, A.; Hosoda, T.; Elmore, J. B.; Goihberg, P.; Cappetta, D.; Solankhi, N. K.; Fahsah, I.; Rokosh, D. G.; Slaughter, M. S.; Kajstura, J.; Anversa, P. Effect of Cardiac Stem Cells in Patients with Ischemic Cardiomyopathy: Initial Results of the SCIPIO Trial. *Lancet* **2011**, *378* (9806), 1847–1857. https://doi.org/10.1016/S0140-6736(11)61590-0.

(136) Ellison, G. M.; Vicinanza, C.; Smith, A. J.; Aquila, I.; Leone, A.; Waring, C. D.; Henning, B. J.; Stirparo, G. G.; Papait, R.; Scarfò, M.; Agosti, V.; Viglietto, G.; Condorelli, G.; Indolfi, C.; Ottolenghi, S.; Torella, D.; Nadal-Ginard, B. Adult C-Kitpos Cardiac Stem Cells Are Necessary and Sufficient for Functional Cardiac Regeneration and Repair. *Cell* **2013**, *154* (4), 827–842. https://doi.org/10.1016/j.cell.2013.07.039.

(137) Vicinanza, C.; Aquila, I.; Scalise, M.; Cristiano, F.; Marino, F.; Cianflone, E.; Mancuso, T.; Marotta, P.; Sacco, W.; Lewis, F. C.; Couch, L.; Shone, V.; Gritti, G.; Torella, A.; Smith, A. J.; Terracciano, C. M.; Britti, D.; Veltri, P.; Indolfi, C.; Nadal-Ginard, B.; Ellison-Hughes, G. M.; Torella, D. Adult Cardiac Stem Cells Are Multipotent and Robustly Myogenic: C-Kit Expression Is Necessary but Not Sufficient for Their Identification. *Cell Death and Differentiation* **2017**, *24* (12), 2101–2116. https://doi.org/10.1038/cdd.2017.130.

(138) Vicinanza, C.; Aquila, I.; Cianflone, E.; Scalise, M.; Marino, F.; Mancuso, T.; Fumagalli, F.; Giovannone, E. D.; Cristiano, F.; Iaccino, E.; Marotta, P.; Torella, A.; Latini, R.; Agosti, V.; Veltri, P.; Urbanek, K.; Isidori, A. M.; Saur, D.; Indolfi, C.; Nadal-Ginard, B.; Torella, D. *Kit^{cre}* Knock-in Mice Fail to Fate-Map Cardiac Stem Cells. *Nature* **2018**, *555* (7697), E1–E5. https://doi.org/10.1038/nature25771.

(139) Sultana, N.; Zhang, L.; Yan, J.; Chen, J.; Cai, W.; Razzaque, S.; Jeong, D.; Sheng, W.; Bu, L.; Xu, M.; Huang, G.-Y.; Hajjar, R. J.; Zhou, B.; Moon, A.; Cai, C.-L. Resident C-Kit+ Cells in the Heart Are Not Cardiac Stem Cells. *Nature Communications* **2015**, *6* (1), 8701. https://doi.org/10.1038/ncomms9701.

(140) van Berlo, J. H.; Kanisicak, O.; Maillet, M.; Vagnozzi, R. J.; Karch, J.; Lin, S.-C. J.; Middleton, R. C.; Marbán, E.; Molkentin, J. D. C-Kit^{+} Cells Minimally Contribute Cardiomyocytes to the Heart. *Nature* **2014**, *509* (7500), 337–341. https://doi.org/10.1038/nature13309.

(141) Gude, N. A.; Firouzi, F.; Broughton, K. M.; Ilves, K.; Nguyen, K. P.; Payne, C. R.; Sacchi, V.; Monsanto, M. M.; Casillas, A. R.; Khalafalla, F. G.; Wang, B. J.; Ebeid, D.; Alvarez, R.; Dembitsky, W. P.; Bailey, B. A.; Berlo, J. H. van; Sussman, M. A. Cardiac C-Kit Biology Revealed by Inducible Transgenesis. *Circulation Research* **2018**, 57–72. https://doi.org/10.1161/CIRCRESAHA.117.311828.

(142) Liu, Q.; Yang, R.; Huang, X.; Zhang, H.; He, L.; Zhang, L.; Tian, X.; Nie, Y.; Hu, S.; Yan, Y.; Zhang, L.; Qiao, Z.; Wang, Q.-D.; Lui, K. O.; Zhou, B. Genetic Lineage Tracing Identifies *in Situ* Kit-Expressing Cardiomyocytes. *Cell Research* **2016**, *26* (1), 119–130. https://doi.org/10.1038/cr.2015.143.

(143) Bolli, R.; Tang, X.-L.; Guo, Y.; Li, Q. After the Storm: An Objective Appraisal of the Efficacy of c-Kit+ Cardiac Progenitor Cells in Preclinical Models of Heart Disease. *Canadian Journal of Physiology and Pharmacology* **2020**. https://doi.org/10.1139/cjpp-2020-0406.

(144) The Lancet Editors. Retraction—Cardiac Stem Cells in Patients with Ischaemic Cardiomyopathy (SCIPIO): Initial Results of a Randomised Phase 1 Trial. *The Lancet* **2019**, *393* (10176), 1084. https://doi.org/10.1016/S0140-6736(19)30542-2.

(145) Le, T.; Chong, J. Cardiac Progenitor Cells for Heart Repair. *Cell Death Discov* **2016**, *2*, 16052. https://doi.org/10.1038/cddiscovery.2016.52.

(146) Makkar, R. R.; Smith, R. R.; Cheng, K.; Malliaras, K.; Thomson, L. E. J.; Berman, D.; Czer, L. S. C.; Marbán, L.; Mendizabal, A.; Johnston, P. V.; Russell, S. D.; Schuleri, K. H.; Lardo, A. C.; Gerstenblith, G.; Marbán, E. Intracoronary Cardiosphere-Derived Cells for Heart Regeneration after Myocardial Infarction (CADUCEUS): A Prospective, Randomised Phase 1 Trial. *Lancet* **2012**, *379* (9819), 895–904. https://doi.org/10.1016/S0140-6736(12)60195-0.

(147) Agarwal, U.; Smith, A. W.; French, K. M.; Boopathy, A. V.; George, A.; Trac, D.; Brown, M. E.; Shen, M.; Jiang, R.; Fernandez, J. D.; Kogon, B. E.; Kanter, K. R.; Alsoufi, B.; Wagner, M. B.; Platt, M. O.; Davis, M. E. Age-Dependent Effect of Pediatric Cardiac Progenitor Cells After Juvenile Heart Failure: Age-Dependent Pediatric CPC Therapy. *STEM CELLS Translational Medicine* **2016**, *5* (7), 883–892. https://doi.org/10.5966/sctm.2015-0241.

(148) Fischer, K. M.; Cottage, C. T.; Wu, W.; Din, S.; Gude, N. A.; Avitabile, D.; Quijada, P.; Collins, B. L.; Fransioli, J.; Sussman, M. A. Enhancement of Myocardial Regeneration Through Genetic Engineering of Cardiac Progenitor Cells Expressing Pim-1 Kinase. *Circulation* **2009**, *120* (21), 2077–2087. https://doi.org/10.1161/CIRCULATIONAHA.109.884403.

(149) Avolio, E.; Meloni, M.; Spencer, H. L.; Riu, F.; Katare, R.; Mangialardi, G.; Oikawa, A.; Rodriguez-Arabaolaza, I.; Dang, Z.; Mitchell, K.; Reni, C.; Alvino, V. V.; Rowlinson, J.; Livi, U.; Cesselli, D.; Angelini, G.; Emanueli, C.; Beltrami, A. P.; Madeddu, P. Combined Intramyocardial Delivery of Human Pericytes and Cardiac Stem Cells Additively Improves the Healing of Mouse Infarcted Hearts

Through Stimulation of Vascular and Muscular Repair. *Circulation Research* **2015**, *116* (10), e81–e94. https://doi.org/10.1161/CIRCRESAHA.115.306146.

(150) Reis, L. A.; Chiu, L. L. Y.; Feric, N.; Fu, L.; Radisic, M. Biomaterials in Myocardial Tissue Engineering. *Journal of Tissue Engineering and Regenerative Medicine* **2016**, *10* (1), 11–28. https://doi.org/10.1002/term.1944.

(151) Su, T.; Huang, K.; Mathews, K. G.; Scharf, V. F.; Hu, S.; Li, Z.; Frame, B. N.; Cores, J.; Dinh, P.-U.; Daniele, M. A.; Ligler, F. S.; Cheng, K. Cardiac Stromal Cell Patch Integrated with Engineered Microvessels Improves Recovery from Myocardial Infarction in Rats and Pigs. *ACS Biomater Sci Eng* **2020**, *6* (11), 6309–6320. https://doi.org/10.1021/acsbiomaterials.0c00942.

(152) Singelyn, J. M.; Sundaramurthy, P.; Johnson, T. D.; Schup-Magoffin, P. J.; Hu, D. P.; Faulk, D. M.; Wang, J.; Mayle, K. M.; Bartels, K.; Salvatore, M.; Kinsey, A. M.; DeMaria, A. N.; Dib, N.; Christman, K. L. Catheter-Deliverable Hydrogel Derived From Decellularized Ventricular Extracellular Matrix Increases Endogenous Cardiomyocytes and Preserves Cardiac Function Post-Myocardial Infarction. *Journal of the American College of Cardiology* **2012**, *59* (8), 751–763. https://doi.org/10.1016/j.jacc.2011.10.888.

(153) Dai, W.; Gerczuk, P.; Zhang, Y.; Smith, L.; Kopyov, O.; Kay, G. L.; Jyrala, A. J.; Kloner, R. A. Intramyocardial Injection of Heart Tissue-Derived Extracellular Matrix Improves Postinfarction Cardiac Function in Rats. *J Cardiovasc Pharmacol Ther* **2013**, *18* (3), 270–279. https://doi.org/10.1177/1074248412472257.

(154) Seif-Naraghi, S. B.; Singelyn, J. M.; Salvatore, M. A.; Osborn, K. G.; Wang, J. J.; Sampat, U.; Kwan, O. L.; Strachan, G. M.; Wong, J.; Schup-Magoffin, P. J.; Braden, R. L.; Bartels, K.; DeQuach, J. A.; Preul, M.; Kinsey, A. M.; DeMaria, A. N.; Dib, N.; Christman, K. L. Safety and Efficacy of an Injectable Extracellular Matrix Hydrogel for Treating Myocardial Infarction. *Science Translational Medicine* **2013**, *5* (173), 173ra25-173ra25. https://doi.org/10.1126/scitranslmed.3005503.

(155) Wei, H.-J.; Chen, S.-C.; Chang, Y.; Hwang, S.-M.; Lin, W.-W.; Lai, P.-H.; Chiang, H. K.; Hsu, L.-F.; Yang, H.-H.; Sung, H.-W. Porous Acellular Bovine Pericardia Seeded with Mesenchymal Stem Cells as a Patch to Repair a Myocardial Defect in a Syngeneic Rat Model. *Biomaterials* **2006**, *27* (31), 5409–5419. https://doi.org/10.1016/j.biomaterials.2006.06.022.

(156) Wei, H.-J.; Chen, C.-H.; Lee, W.-Y.; Chiu, I.; Hwang, S.-M.; Lin, W.-W.; Huang, C.-C.; Yeh, Y.-C.; Chang, Y.; Sung, H.-W. Bioengineered Cardiac Patch Constructed from Multilayered Mesenchymal Stem Cells for Myocardial Repair. *Biomaterials* **2008**, *29* (26), 3547–3556. https://doi.org/10.1016/j.biomaterials.2008.05.009.

(157) Rajabi-Zeleti, S.; Jalili-Firoozinezhad, S.; Azarnia, M.; Khayyatan, F.; Vahdat, S.; Nikeghbalian, S.; Khademhosseini, A.; Baharvand, H.; Aghdami, N. The Behavior

of Cardiac Progenitor Cells on Macroporous Pericardium-Derived Scaffolds. *Biomaterials* **2014**, *35* (3), 970–982. https://doi.org/10.1016/j.biomaterials.2013.10.045.

(158) Vashi, A. V.; White, J. F.; McLean, K. M.; Neethling, W. M. L.; Rhodes, D. I.; Ramshaw, J. A. M.; Werkmeister, J. A. Evaluation of an Established Pericardium Patch for Delivery of Mesenchymal Stem Cells to Cardiac Tissue. *J Biomed Mater Res A* **2015**, *103* (6), 1999–2005. https://doi.org/10.1002/jbm.a.35335.

(159) Tan, M. Y.; Zhi, W.; Wei, R. Q.; Huang, Y. C.; Zhou, K. P.; Tan, B.; Deng, L.; Luo, J. C.; Li, X. Q.; Xie, H. Q.; Yang, Z. M. Repair of Infarcted Myocardium Using Mesenchymal Stem Cell Seeded Small Intestinal Submucosa in Rabbits. *Biomaterials* **2009**, *30* (19), 3234–3240. https://doi.org/10.1016/j.biomaterials.2009.02.013.

(160) Okada, M.; Payne, T. R.; Oshima, H.; Momoi, N.; Tobita, K.; Huard, J. Differential Efficacy of Gels Derived from Small Intestinal Submucosa as an Injectable Biomaterial for Myocardial Infarct Repair. *Biomaterials* **2010**, *31* (30), 7678–7683. https://doi.org/10.1016/j.biomaterials.2010.06.056.

(161) Kochupura, P. V.; Azeloglu, E. U.; Kelly, D. J.; Doronin, S. V.; Badylak, S. F.; Krukenkamp, I. B.; Cohen, I. S.; Gaudette, G. R. Tissue-Engineered Myocardial Patch Derived from Extracellular Matrix Provides Regional Mechanical Function. *Circulation* **2005**, *112* (9 Suppl), I144-149. https://doi.org/10.1161/CIRCULATIONAHA.104.524355.

(162) Robinson, K. A.; Li, J.; Mathison, M.; Redkar, A.; Cui, J.; Chronos, N. A. F.; Matheny, R. G.; Badylak, S. F. Extracellular Matrix Scaffold for Cardiac Repair. *Circulation* **2005**, *112* (9 Suppl), I135-143. https://doi.org/10.1161/CIRCULATIONAHA.104.525436.

(163) Ott, H. C.; Matthiesen, T. S.; Goh, S.-K.; Black, L. D.; Kren, S. M.; Netoff, T. I.; Taylor, D. A. Perfusion-Decellularized Matrix: Using Nature's Platform to Engineer a Bioartificial Heart. *Nature Medicine* **2008**, *14* (2), 213–221. https://doi.org/10.1038/nm1684.

(164) Singelyn, J. M.; DeQuach, J. A.; Seif-Naraghi, S. B.; Littlefield, R. B.; Schup-Magoffin, P. J.; Christman, K. L. Naturally Derived Myocardial Matrix as an Injectable Scaffold for Cardiac Tissue Engineering. *Biomaterials* **2009**, *30* (29), 5409–5416. https://doi.org/10.1016/j.biomaterials.2009.06.045.

(165) Traverse, J. H.; Henry, T. D.; Dib, N.; Patel, A. N.; Pepine, C.; Schaer, G. L.; DeQuach, J. A.; Kinsey, A. M.; Chamberlin, P.; Christman, K. L. First-in-Man Study of a Cardiac Extracellular Matrix Hydrogel in Early and Late Myocardial Infarction Patients. *JACC: Basic to Translational Science* **2019**, *4* (6), 659–669. https://doi.org/10.1016/j.jacbts.2019.07.012.

(166) Tang, J.; Wang, J.; Huang, K.; Ye, Y.; Su, T.; Qiao, L.; Hensley, M. T.; Caranasos, T. G.; Zhang, J.; Gu, Z.; Cheng, K. Cardiac Cell–Integrated Microneedle Patch for Treating Myocardial Infarction. *Science Advances* **2018**, *4* (11), eaat9365. https://doi.org/10.1126/sciadv.aat9365.

(167) Ishii, O.; Shin, M.; Sueda, T.; Vacanti, J. P. In Vitro Tissue Engineering of a Cardiac Graft Using a Degradable Scaffold with an Extracellular Matrix–like Topography. *The Journal of Thoracic and Cardiovascular Surgery* **2005**, *130* (5), 1358–1363. https://doi.org/10.1016/j.jtcvs.2005.05.048.

(168) Shin, M.; Ishii, O.; Sueda, T.; Vacanti, J. P. Contractile Cardiac Grafts Using a Novel Nanofibrous Mesh. *Biomaterials* **2004**, *25* (17), 3717–3723. https://doi.org/10.1016/j.biomaterials.2003.10.055.

(169) Wickham, A. M.; Islam, M. M.; Mondal, D.; Phopase, J.; Sadhu, V.; Tamás, É.; Polisetti, N.; Richter-Dahlfors, A.; Liedberg, B.; Griffith, M. Polycaprolactone-Thiophene-Conjugated Carbon Nanotube Meshes as Scaffolds for Cardiac Progenitor Cells. *J. Biomed. Mater. Res. Part B Appl. Biomater.* **2014**, *102* (7), 1553–1561. https://doi.org/10.1002/jbm.b.33136.

(170) Tallawi, M.; Dippold, D.; Rai, R.; D'Atri, D.; Roether, J. A.; Schubert, D. W.; Rosellini, E.; Engel, F. B.; Boccaccini, A. R. Novel PGS/PCL Electrospun Fiber Mats with Patterned Topographical Features for Cardiac Patch Applications. *Materials Science and Engineering: C* **2016**, *69*, 569–576. https://doi.org/10.1016/j.msec.2016.06.083.

(171) Pok, S.; Myers, J. D.; Madihally, S. V.; Jacot, J. G. A MULTI-LAYERED SCAFFOLD OF A CHITOSAN AND GELATIN HYDROGEL SUPPORTED BY A PCL CORE FOR CARDIAC TISSUE ENGINEERING. *Acta Biomater* **2013**, *9* (3), 5630–5642. https://doi.org/10.1016/j.actbio.2012.10.032.

(172) Kai, D.; Prabhakaran, M. P.; Jin, G.; Ramakrishna, S. Guided Orientation of Cardiomyocytes on Electrospun Aligned Nanofibers for Cardiac Tissue Engineering. *Journal of Biomedical Materials Research Part B: Applied Biomaterials* **2011**, *98B* (2), 379–386. https://doi.org/10.1002/jbm.b.31862.

(173) Chen, Q.-Z.; Bismarck, A.; Hansen, U.; Junaid, S.; Tran, M. Q.; Harding, S. E.; Ali, N. N.; Boccaccini, A. R. Characterisation of a Soft Elastomer Poly(Glycerol Sebacate) Designed to Match the Mechanical Properties of Myocardial Tissue. *Biomaterials* **2008**, *29* (1), 47–57. https://doi.org/10.1016/j.biomaterials.2007.09.010.

(174) Chen, Q.-Z.; Ishii, H.; Thouas, G. A.; Lyon, A. R.; Wright, J. S.; Blaker, J. J.; Chrzanowski, W.; Boccaccini, A. R.; Ali, N. N.; Knowles, J. C.; Harding, S. E. An Elastomeric Patch Derived from Poly(Glycerol Sebacate) for Delivery of Embryonic Stem Cells to the Heart. *Biomaterials* **2010**, *31* (14), 3885–3893. https://doi.org/10.1016/j.biomaterials.2010.01.108.

(175) Murphy, S. V.; Atala, A. 3D Bioprinting of Tissues and Organs. *Nature Biotechnology* **2014**, *32* (8), 773–785. https://doi.org/10.1038/nbt.2958.

(176) Mosadegh, B.; Xiong, G.; Dunham, S.; Min, J. K. Current Progress in 3D Printing for Cardiovascular Tissue Engineering. *Biomed. Mater.* **2015**, *10* (3), 034002. https://doi.org/10.1088/1748-6041/10/3/034002.

(177) Gao, L.; Kupfer, M. E.; Jung, J. P.; Yang, L.; Zhang, P.; Da Sie, Y.; Tran, Q.; Ajeti, V.; Freeman, B. T.; Fast, V. G.; Campagnola, P. J.; Ogle, B. M.; Zhang, J. Myocardial Tissue Engineering With Cells Derived From Human-Induced Pluripotent Stem Cells and a Native-Like, High-Resolution, 3-Dimensionally Printed Scaffold. *Circulation Research* **2017**, *120* (8), 1318–1325. https://doi.org/10.1161/CIRCRESAHA.116.310277.

(178) Tijore, A.; Irvine, S. A.; Sarig, U.; Mhaisalkar, P.; Baisane, V.; Subbu Venkatraman. Contact Guidance for Cardiac Tissue Engineering Using 3D Bioprinted Gelatin Patterned Hydrogel. *Biofabrication* **2018**, *10* (2), 025003. https://doi.org/10.1088/1758-5090/aaa15d.

(179) Li, D.; Xia, Y. Electrospinning of Nanofibers: Reinventing the Wheel? *Advanced Materials* **2004**, *16* (14), 1151–1170. https://doi.org/10.1002/adma.200400719.

(180) Liu, W.; Thomopoulos, S.; Xia, Y. Electrospun Nanofibers for Regenerative Medicine. *Advanced Healthcare Materials* **2012**, *1* (1), 10–25. https://doi.org/10.1002/adhm.201100021.

(181) Kitsara, M.; Agbulut, O.; Kontziampasis, D.; Chen, Y.; Menasché, P. Fibers for Hearts: A Critical Review on Electrospinning for Cardiac Tissue Engineering. *Acta Biomaterialia* **2017**, *48*, 20–40. https://doi.org/10.1016/j.actbio.2016.11.014.

(182) Kharaziha, M.; Nikkhah, M.; Shin, S.-R.; Annabi, N.; Masoumi, N.; Gaharwar, A. K.; Camci-Unal, G.; Khademhosseini, A. PGS:Gelatin Nanofibrous Scaffolds with Tunable Mechanical and Structural Properties for Engineering Cardiac Tissues. *Biomaterials* **2013**, *34* (27), 6355–6366. https://doi.org/10.1016/j.biomaterials.2013.04.045.

(183) Fleischer, S.; Shevach, M.; Feiner, R.; Dvir, T. Coiled Fiber Scaffolds Embedded with Gold Nanoparticles Improve the Performance of Engineered Cardiac Tissues. *Nanoscale* **2014**, *6* (16), 9410–9414. https://doi.org/10.1039/C4NR00300D.

(184) Shevach, M.; Maoz, B. M.; Feiner, R.; Shapira, A.; Dvir, T. Nanoengineering Gold Particle Composite Fibers for Cardiac Tissue Engineering. *J. Mater. Chem. B* **2013**, *1* (39), 5210–5217. https://doi.org/10.1039/C3TB20584C.

(185) Ravichandran, R.; Sridhar, R.; Venugopal, J. R.; Sundarrajan, S.; Mukherjee, S.; Ramakrishna, S. Gold Nanoparticle Loaded Hybrid Nanofibers for Cardiogenic Differentiation of Stem Cells for Infarcted Myocardium Regeneration.

Macromolecular Bioscience **2014**, *14* (4), 515–525. https://doi.org/10.1002/mabi.201300407.

(186) Chung, H.-J.; Kim, J.-T.; Kim, H.-J.; Kyung, H.-W.; Katila, P.; Lee, J.-H.; Yang, T.-H.; Yang, Y.-I.; Lee, S.-J. Epicardial Delivery of VEGF and Cardiac Stem Cells Guided by 3-Dimensional PLLA Mat Enhancing Cardiac Regeneration and Angiogenesis in Acute Myocardial Infarction. *Journal of Controlled Release* **2015**, *205*, 218–230. https://doi.org/10.1016/j.jconrel.2015.02.013.

(187) Ravichandran, R.; Venugopal, J. R.; Mukherjee, S.; Sundarrajan, S.; Ramakrishna, S. Elastomeric Core/Shell Nanofibrous Cardiac Patch as a Biomimetic Support for Infarcted Porcine Myocardium. *Tissue Engineering Part A* **2015**, *21* (7–8), 1288–1298. https://doi.org/10.1089/ten.tea.2014.0265.

(188) Badrossamay, M. R.; McIlwee, H. A.; Goss, J. A.; Parker, K. K. Nanofiber Assembly by Rotary Jet-Spinning. *Nano Lett* **2010**, *10* (6), 2257–2261. https://doi.org/10.1021/nl101355x.

(189) Fleischer, S.; Miller, J.; Hurowitz, H.; Shapira, A.; Dvir, T. Effect of Fiber Diameter on the Assembly of Functional 3D Cardiac Patches. *Nanotechnology* **2015**, *26* (29), 291002. https://doi.org/10.1088/0957-4484/26/29/291002.

(190) Yu, J.; Lee, A.-R.; Lin, W.-H.; Lin, C.-W.; Wu, Y.-K.; Tsai, W.-B. Electrospun PLGA Fibers Incorporated with Functionalized Biomolecules for Cardiac Tissue Engineering. *Tissue Engineering Part A* **2014**, *20* (13–14), 1896–1907. https://doi.org/10.1089/ten.tea.2013.0008.

(191) Eschenhagen, T.; Fink, C.; Remmers, U.; Scholz, H.; Wattchow, J.; Weil, J.; Zimmermann, W.; Dohmen, H. H.; Schäfer, H.; Bishopric, N.; Wakatsuki, T.; Elson, E. L. Three-Dimensional Reconstitution of Embryonic Cardiomyocytes in a Collagen Matrix: A New Heart Muscle Model System. *FASEB J.* **1997**, *11* (8), 683–694.

(192) Naito, H. Optimizing Engineered Heart Tissue for Therapeutic Applications as Surrogate Heart Muscle. *Circulation* **2006**, *114* (1_suppl), I-72-I–78. https://doi.org/10.1161/CIRCULATIONAHA.105.001560.

(193) Riegler, J.; Tiburcy, M.; Ebert, A.; Tzatzalos, E.; Raaz, U.; Abilez, O. J.; Shen, Q.; Kooreman, N. G.; Neofytou, E.; Chen, V. C.; Wang, M.; Meyer, T.; Tsao, P. S.; Connolly, A. J.; Couture, L. A.; Gold, J. D.; Zimmermann, W. H.; Wu, J. C. Human Engineered Heart Muscles Engraft and Survive Long Term in a Rodent Myocardial Infarction ModelNovelty and Significance. *Circulation Research* **2015**, *117* (8), 720–730. https://doi.org/10.1161/CIRCRESAHA.115.306985.

(194) Jackman, C. P.; Ganapathi, A. M.; Asfour, H.; Qian, Y.; Allen, B. W.; Li, Y.; Bursac, N. Engineered Cardiac Tissue Patch Maintains Structural and Electrical Properties after Epicardial Implantation. *Biomaterials* **2018**, *159*, 48–58. https://doi.org/10.1016/j.biomaterials.2018.01.002.

(195) Sun, X.; Nunes, S. S. Overview of Hydrogel-Based Strategies for Application in Cardiac Tissue Regeneration. *Biomed. Mater.* **2015**, *10* (3), 034005. https://doi.org/10.1088/1748-6041/10/3/034005.

(196) Landa, N.; Miller, L.; Feinberg, M. S.; Holbova, R.; Shachar, M.; Freeman, I.; Cohen, S.; Leor, J. Effect of Injectable Alginate Implant on Cardiac Remodeling and Function After Recent and Old Infarcts in Rat. *Circulation* **2008**, *117* (11), 1388–1396. https://doi.org/10.1161/CIRCULATIONAHA.107.727420.

(197) Serpooshan, V.; Zhao, M.; Metzler, S. A.; Wei, K.; Shah, P. B.; Wang, A.; Mahmoudi, M.; Malkovskiy, A. V.; Rajadas, J.; Butte, M. J.; Bernstein, D.; Ruiz-Lozano, P. The Effect of Bioengineered Acellular Collagen Patch on Cardiac Remodeling and Ventricular Function Post Myocardial Infarction. *Biomaterials* **2013**, *34* (36). https://doi.org/10.1016/j.biomaterials.2013.08.017.

(198) Kerscher, P.; Turnbull, I. C.; Hodge, A. J.; Kim, J.; Seliktar, D.; Easley, C. J.; Costa, K. D.; Lipke, E. A. Direct Hydrogel Encapsulation of Pluripotent Stem Cells Enables Ontomimetic Differentiation and Growth of Engineered Human Heart Tissues. *Biomaterials* **2016**, *83*, 383–395. https://doi.org/10.1016/j.biomaterials.2015.12.011.

(199) Boopathy, A. V.; Che, P. L.; Somasuntharam, I.; Fiore, V. F.; Cabigas, E. B.; Ban, K.; Brown, M. E.; Narui, Y.; Barker, T. H.; Yoon, Y. S.; Salaita, K.; Garcia, A. J.; Davis, M. E. The Modulation of Cardiac Progenitor Cell Function by Hydrogel-Dependent Notch1 Activation. *Biomaterials* **2014**, *35* (28), 8103–8112. https://doi.org/10.1016/j.biomaterials.2014.05.082.

(200) Ruan, J.-L.; Tulloch, N. L.; Razumova, M. V.; Saiget, M.; Muskheli, V.; Pabon, L.; Reinecke, H.; Regnier, M.; Murry, C. E. Mechanical Stress Conditioning and Electrical Stimulation Promote Contractility and Force Maturation of Induced Pluripotent Stem Cell-Derived Human Cardiac Tissue. *Circulation* **2016**, *134* (20), 1557–1567. https://doi.org/10.1161/CIRCULATIONAHA.114.014998.

(201) Lux, M.; Andrée, B.; Horvath, T.; Nosko, A.; Manikowski, D.; Hilfiker-Kleiner, D.; Haverich, A.; Hilfiker, A. In Vitro Maturation of Large-Scale Cardiac Patches Based on a Perfusable Starter Matrix by Cyclic Mechanical Stimulation. *Acta Biomaterialia* **2016**, *30*, 177–187. https://doi.org/10.1016/j.actbio.2015.11.006.

(202) Tulloch, N. L.; Muskheli, V.; Razumova, M. V.; Korte, F. S.; Regnier, M.; Hauch, K. D.; Pabon, L.; Reinecke, H.; Murry, C. E. Growth of Engineered Human Myocardium With Mechanical Loading and Vascular Coculture. *Circulation Research* **2011**, *109* (1), 47–59. https://doi.org/10.1161/CIRCRESAHA.110.237206.

(203) Gwak, S.-J.; Bhang, S. H.; Kim, I.-K.; Kim, S.-S.; Cho, S.-W.; Jeon, O.; Yoo, K. J.; Putnam, A. J.; Kim, B.-S. The Effect of Cyclic Strain on Embryonic Stem Cell-Derived Cardiomyocytes. *Biomaterials* **2008**, *29* (7), 844–856. https://doi.org/10.1016/j.biomaterials.2007.10.050.

(204) Treskes, P.; Neef, K.; Srinivasan, S. P.; Halbach, M.; Stamm, C.; Cowan, D.; Scherner, M.; Madershahian, N.; Wittwer, T.; Hescheler, J.; Wahlers, T.; Choi, Y.-H. Preconditioning of Skeletal Myoblast-Based Engineered Tissue Constructs Enables Functional Coupling to Myocardium in Vivo. *J Thorac Cardiovasc Surg* **2015**, *149* (1), 348–356. https://doi.org/10.1016/j.jtcvs.2014.09.034.

(205) Ronaldson-Bouchard, K.; Ma, S. P.; Yeager, K.; Chen, T.; Song, L.; Sirabella, D.; Morikawa, K.; Teles, D.; Yazawa, M.; Vunjak-Novakovic, G. Advanced Maturation of Human Cardiac Tissue Grown from Pluripotent Stem Cells. *Nature* **2018**, *556* (7700), 239–243. https://doi.org/10.1038/s41586-018-0016-3.

(206) Garikipati, V. N. S.; Shoja-Taheri, F.; Davis, M. E.; Kishore, R. Extracellular Vesicles and the Application of System Biology and Computational Modeling in Cardiac Repair. *Circulation Research* **2018**, *123* (2), 188–204. https://doi.org/10.1161/CIRCRESAHA.117.311215.

(207) Zhu, D.; Li, Z.; Huang, K.; Caranasos, T. G.; Rossi, J. S.; Cheng, K. Minimally Invasive Delivery of Therapeutic Agents by Hydrogel Injection into the Pericardial Cavity for Cardiac Repair. *Nature Communications* **2021**, *12* (1), 1412. https://doi.org/10.1038/s41467-021-21682-7.

(208) Yao, J.; Huang, K.; Zhu, D.; Chen, T.; Jiang, Y.; Zhang, J.; Mi, L.; Xuan, H.; Hu, S.; Li, J.; Zhou, Y.; Cheng, K. A Minimally Invasive Exosome Spray Repairs Heart after Myocardial Infarction. *ACS Nano* **2021**, *15* (7), 11099–11111. https://doi.org/10.1021/acsnano.1c00628.

(209) Mayourian, J.; Ceholski, D. K.; Gorski, P. A.; Mathiyalagan, P.; Murphy, J. F.; Salazar, S. I.; Stillitano, F.; Hare, J. M.; Sahoo, S.; Hajjar, R. J.; Costa, K. D. Exosomal MicroRNA-21-5p Mediates Mesenchymal Stem Cell Paracrine Effects on Human Cardiac Tissue ContractilityNovelty and Significance. *Circulation Research* **2018**, *122* (7), 933–944. https://doi.org/10.1161/CIRCRESAHA.118.312420.

(210) Waters, R.; Alam, P.; Pacelli, S.; Chakravarti, A. R.; Ahmed, R. P. H.; Paul, A. Stem Cell-Inspired Secretome-Rich Injectable Hydrogel to Repair Injured Cardiac Tissue. *Acta Biomaterialia* **2018**, *69*, 95–106. https://doi.org/10.1016/j.actbio.2017.12.025.

(211) Tang, J.; Shen, D.; Caranasos, T. G.; Wang, Z.; Vandergriff, A. C.; Allen, T. A.; Hensley, M. T.; Dinh, P.-U.; Cores, J.; Li, T.-S.; Zhang, J.; Kan, Q.; Cheng, K. Therapeutic Microparticles Functionalized with Biomimetic Cardiac Stem Cell Membranes and Secretome. *Nature Communications* **2017**, *8*, 13724. https://doi.org/10.1038/ncomms13724.

(212) Luo, L.; Tang, J.; Nishi, K.; Yan, C.; Dinh, P.-U.; Cores, J.; Kudo, T.; Zhang, J.; Li, T.-S.; Cheng, K. Fabrication of Synthetic Mesenchymal Stem Cells for the Treatment of Acute Myocardial Infarction in MiceNovelty and Significance.

Circulation Research **2017**, *120* (11), 1768–1775. https://doi.org/10.1161/CIRCRESAHA.116.310374.

(213) Huang, K.; Ozpinar, E. W.; Su, T.; Tang, J.; Shen, D.; Qiao, L.; Hu, S.; Li, Z.; Liang, H.; Mathews, K.; Scharf, V.; Freytes, D. O.; Cheng, K. An Off-the-Shelf Artificial Cardiac Patch Improves Cardiac Repair after Myocardial Infarction in Rats and Pigs. *Science Translational Medicine* **2020**, *12* (538), eaat9683. https://doi.org/10.1126/scitranslmed.aat9683.

(214) Bittle, G. J.; Morales, D.; Deatrick, K. B.; Parchment, N.; Saha, P.; Mishra, R.; Sharma, S.; Pietris, N.; Vasilenko, A.; Bor, C.; Ambastha, C.; Gunasekaran, M.; Li, D.; Kaushal, S. Stem Cell Therapy for Hypoplastic Left Heart Syndrome: Mechanism, Clinical Application, and Future Directions. *Circulation Research* **2018**, *123* (2), 288–300. https://doi.org/10.1161/CIRCRESAHA.117.311206.

(215) Wehman, B.; Pietris, N.; Bigham, G.; Siddiqui, O.; Mishra, R.; Li, T.; Aiello, E.; Jack, G.; Wang, W.; Murthi, S.; Sharma, S.; Kaushal, S. Cardiac Progenitor Cells Enhance Neonatal Right Ventricular Function After Pulmonary Artery Banding. *Ann Thorac Surg* **2017**, *104* (6), 2045–2053. https://doi.org/10.1016/j.athoracsur.2017.04.058.

(216) French, K. M.; Davis, M. E. Isolation and Expansion of C-Kit-Positive Cardiac Progenitor Cells by Magnetic Cell Sorting. In *Cardiac Tissue Engineering*; Methods in Molecular Biology; Humana Press, New York, NY, 2014; pp 39–50. https://doi.org/10.1007/978-1-4939-1047-2_4.

(217) Simpson, D. L.; Mishra, R.; Sharma, S.; Goh, S. K.; Deshmukh, S.; Kaushal, S. A Strong Regenerative Ability of Cardiac Stem Cells Derived from Neonatal Hearts. *Circulation* **2012**, *126* (11 Suppl 1), S46-53. https://doi.org/10.1161/CIRCULATIONAHA.111.084699.

(218) Shoja-Taheri, F.; George, A.; Agarwal, U.; Platt, M. O.; Gibson, G.; Davis, M. E. Using Statistical Modeling to Understand and Predict Pediatric Stem Cell Function. *Circ Genom Precis Med* **2019**, *12* (6), e002403. https://doi.org/10.1161/CIRCGEN.118.002403.

(219) Trac, D.; Hoffman, J. R.; Bheri, S.; Maxwell, J. T.; Platt, M. O.; Davis, M. E. Predicting Functional Responses of Progenitor Cell Exosome Potential with Computational Modeling. *STEM CELLS Translational Medicine* **2019**. https://doi.org/10.1002/sctm.19-0059.

(220) Traister, A.; Patel, R.; Huang, A.; Patel, S.; Plakhotnik, J.; Lee, J. E.; Medina, M. G.; Welsh, C.; Ruparel, P.; Zhang, L.; Friedberg, M.; Maynes, J.; Coles, J. Cardiac Regenerative Capacity Is Age- and Disease-Dependent in Childhood Heart Disease. *PLOS ONE* **2018**, *13* (7), e0200342. https://doi.org/10.1371/journal.pone.0200342.

(221) Kang, K.; Chuai, J.-B.; Xie, B.-D.; Li, J.-Z.; Qu, H.; Wu, H.; Fang, S.-H.; Cui, J.-J.; Xiu, L.-L.; Han, J.-C.; Cao, T.-H.; Leng, X.-P.; Tian, H.; Li, R.-K.; Jiang, S.-L. Mesenchymal Stromal Cells from Patients with Cyanotic Congenital Heart Disease Are Optimal Candidate for Cardiac Tissue Engineering. *Biomaterials* **2020**, *230*, 119574. https://doi.org/10.1016/j.biomaterials.2019.119574.

(222) French, K. M.; Maxwell, J. T.; Bhutani, S.; Ghosh-Choudhary, S.; Fierro, M. J.; Johnson, T. D.; Christman, K. L.; Taylor, W. R.; Davis, M. E. Fibronectin and Cyclic Strain Improve Cardiac Progenitor Cell Regenerative Potential *In Vitro*. *Stem Cells International* **2016**, *2016*, 1–11. https://doi.org/10.1155/2016/8364382.

(223) Maxwell, J. T.; Wagner, M. B.; Davis, M. E. Electrically Induced Calcium Handling in Cardiac Progenitor Cells. *Stem Cells Int* **2016**, *2016*, 8917380. https://doi.org/10.1155/2016/8917380.

(224) Maxwell, J. T.; Trac, D.; Shen, M.; Brown, M. E.; Davis, M. E.; Chao, M. S.; Supapannachart, K. J.; Zaladonis, C. A.; Baker, E.; Li, M. L.; Zhao, J.; Jacobs, D. I. Electrical Stimulation of Pediatric Cardiac-Derived c-Kit+ Progenitor Cells Improves Retention and Cardiac Function in Right Ventricular Heart Failure. *Stem Cells* **2019**, *37* (12), 1528–1541. https://doi.org/10.1002/stem.3088.

(225) Trac, D.; Maxwell, J. T.; Brown, M. E.; Xu, C.; Davis, M. E. Aggregation of Child Cardiac Progenitor Cells Into Spheres Activates Notch Signaling and Improves Treatment of Right Ventricular Heart Failure. *Circulation Research* **2019**, *124* (4), 526–538. https://doi.org/10.1161/CIRCRESAHA.118.313845.

(226) Davies, B.; Elwood, N. J.; Li, S.; Cullinane, F.; Edwards, G. A.; Newgreen, D. F.; Brizard, C. P. Human Cord Blood Stem Cells Enhance Neonatal Right Ventricular Function in an Ovine Model of Right Ventricular Training. *Ann Thorac Surg* **2010**, *89* (2), 585–593, 593.e1-4. https://doi.org/10.1016/j.athoracsur.2009.10.035.

(227) Oommen, S.; Yamada, S.; Cantero Peral, S.; Campbell, K. A.; Bruinsma, E. S.; Terzic, A.; Nelson, T. J. Human Umbilical Cord Blood-Derived Mononuclear Cells Improve Murine Ventricular Function upon Intramyocardial Delivery in Right Ventricular Chronic Pressure Overload. *Stem Cell Res Ther* **2015**, *6*, 50. https://doi.org/10.1186/s13287-015-0044-y.

(228) Liufu, R.; Shi, G.; He, X.; Lv, J.; Liu, W.; Zhu, F.; Wen, C.; Zhu, Z.; Chen, H. The Therapeutic Impact of Human Neonatal BMSC in a Right Ventricular Pressure Overload Model in Mice. *Stem Cell Res Ther* **2020**, *11* (1), 96. https://doi.org/10.1186/s13287-020-01593-y.

(229) Wehman, B.; Sharma, S.; Pietris, N.; Mishra, R.; Siddiqui, O. T.; Bigham, G.; Li, T.; Aiello, E.; Murthi, S.; Pittenger, M.; Griffith, B.; Kaushal, S. Mesenchymal Stem Cells Preserve Neonatal Right Ventricular Function in a Porcine Model of Pressure Overload. *Am J Physiol Heart Circ Physiol* **2016**, *310* (11), H1816-1826. https://doi.org/10.1152/ajpheart.00955.2015.

(230) Ishigami, S.; Ohtsuki, S.; Tarui, S.; Ousaka, D.; Eitoku, T.; Kondo, M.; Okuyama, M.; Kobayashi, J.; Baba, K.; Arai, S.; Kawabata, T.; Yoshizumi, K.; Tateishi, A.; Kuroko, Y.; Iwasaki, T.; Sato, S.; Kasahara, S.; Sano, S.; Oh, H. Intracoronary Autologous Cardiac Progenitor Cell Transfer in Patients With Hypoplastic Left Heart Syndrome: The TICAP Prospective Phase 1 Controlled Trial. *Circulation Research* **2015**, *116* (4), 653–664. https://doi.org/10.1161/CIRCRESAHA.116.304671.

(231) Tarui, S.; Ishigami, S.; Ousaka, D.; Kasahara, S.; Ohtsuki, S.; Sano, S.; Oh, H. Transcoronary Infusion of Cardiac Progenitor Cells in Hypoplastic Left Heart Syndrome: Three-Year Follow-up of the Transcoronary Infusion of Cardiac Progenitor Cells in Patients With Single-Ventricle Physiology (TICAP) Trial. *The Journal of Thoracic and Cardiovascular Surgery* **2015**, *150* (5), 1198-1208.e2. https://doi.org/10.1016/j.jtcvs.2015.06.076.

(232) Ishigami, S.; Ohtsuki, S.; Eitoku, T.; Ousaka, D.; Kondo, M.; Kurita, Y.; Hirai, K.; Fukushima, Y.; Baba, K.; Goto, T.; Horio, N.; Kobayashi, J.; Kuroko, Y.; Kotani, Y.; Arai, S.; Iwasaki, T.; Sato, S.; Kasahara, S.; Sano, S.; Oh, H. Intracoronary Cardiac Progenitor Cells in Single Ventricle Physiology: The PERSEUS (Cardiac Progenitor Cell Infusion to Treat Univentricular Heart Disease) Randomized Phase 2 Trial. *Circ. Res.* **2017**, *120* (7), 1162–1173. https://doi.org/10.1161/CIRCRESAHA.116.310253.

(233) Oh, H. Cell Therapy Trials in Congenital Heart Disease. *Circ Res* **2017**, *120* (8), 1353–1366. https://doi.org/10.1161/CIRCRESAHA.117.309697.

(234) Burkhart, H. M.; Qureshi, M. Y.; Rossano, J. W.; Cantero Peral, S.; O'Leary, P. W.; Hathcock, M.; Kremers, W.; Nelson, T. J.; Breuer, A.; Cavanaugh, K.; Cetta, F.; Dearani, J. A.; Dietz, A.; Edwards, B.; Hirsch, S.; Holst, K.; Krucker, K.; Lenn, K.; Martineau, S.; Mascio, C. E.; Majerus, A.; Miller, A.; Miller, J.; Miller, K.; Mir, A.; Olson, T. M.; Radel, D.; Reece, C.; Riess, L.; Said, S. M.; Taylor, J.; Thebiay, J.; Thompson, J. L.; Wentworth, M.; Wobig, J. Autologous Stem Cell Therapy for Hypoplastic Left Heart Syndrome: Safety and Feasibility of Intraoperative Intramyocardial Injections. *The Journal of Thoracic and Cardiovascular Surgery* **2019**, *158* (6), 1614–1623. https://doi.org/10.1016/j.jtcvs.2019.06.001.

(235) Kaushal, S.; Wehman, B.; Pietris, N.; Naughton, C.; Bentzen, S. M.; Bigham, G.; Mishra, R.; Sharma, S.; Vricella, L.; Everett, A. D.; Deatrick, K. B.; Huang, S.; Mehta, H.; Ravekes, W. A.; Hibino, N.; Difede, D. L.; Khan, A.; Hare, J. M. Study Design and Rationale for ELPIS: A Phase I/IIb Randomized Pilot Study of Allogeneic Human Mesenchymal Stem Cell Injection in Patients with Hypoplastic Left Heart Syndrome. *American Heart Journal* **2017**, *192*, 48–56. https://doi.org/10.1016/j.ahj.2017.06.009.

(236) Chery, J.; Wong, J.; Huang, S.; Wang, S.; Si, M.-S. Regenerative Medicine Strategies for Hypoplastic Left Heart Syndrome. *Tissue Engineering Part B: Reviews* **2016**, *22* (6), 459–469. https://doi.org/10.1089/ten.teb.2016.0136.

(237) Patterson, J. T.; Gilliland, T.; Maxfield, M. W.; Church, S.; Naito, Y.; Shinoka, T.; Breuer, C. K. Tissue-Engineered Vascular Grafts for Use in the Treatment of Congenital Heart Disease: From the Bench to the Clinic and Back Again. *Regen Med* **2012**, *7* (3), 409–419. https://doi.org/10.2217/rme.12.12.

(238) Tennant, P. W.; Pearce, M. S.; Bythell, M.; Rankin, J. 20-Year Survival of Children Born with Congenital Anomalies: A Population-Based Study. *The Lancet* **2010**, *375* (9715), 649–656. https://doi.org/10.1016/S0140-6736(09)61922-X.

(239) Lamour, J. M.; Kanter, K. R.; Naftel, D. C.; Chrisant, M. R.; Morrow, W. R.; Clemson, B. S.; Kirklin, J. K. The Effect of Age, Diagnosis, and Previous Surgery in Children and Adults Undergoing Heart Transplantation for Congenital Heart Disease. *Journal of the American College of Cardiology* **2009**, *54* (2), 160–165. https://doi.org/10.1016/j.jacc.2009.04.020.

(240) Nguyen, P. K.; Rhee, J.-W.; Wu, J. C. Adult Stem Cell Therapy and Heart Failure, 2000 to 2016: A Systematic Review. *JAMA Cardiol* **2016**, *1* (7), 831–841. https://doi.org/10.1001/jamacardio.2016.2225.

(241) Xue, J.; Xie, J.; Liu, W.; Xia, Y. Electrospun Nanofibers: New Concepts, Materials, and Applications. *Accounts of Chemical Research* **2017**, *50* (8), 1976–1987. https://doi.org/10.1021/acs.accounts.7b00218.

(242) Pereira, I. H. L.; Ayres, E.; Averous, L.; Schlatter, G.; Hebraud, A.; de Paula, A. C. C.; Viana, P. H. L.; Goes, A. M.; Oréfice, R. L. Differentiation of Human Adipose-Derived Stem Cells Seeded on Mineralized Electrospun Co-Axial Poly(ε-Caprolactone) (PCL)/Gelatin Nanofibers. *J Mater Sci Mater Med* **2014**, *25* (4), 1137–1148. https://doi.org/10.1007/s10856-013-5133-9.

(243) Konstandin, M. H.; Toko, H.; Gastelum, G. M.; Quijada, P.; De La Torre, A.; Quintana, M.; Collins, B.; Din, S.; Avitabile, D.; Volkers, M.; Gude, N.; Fassler, R.; Sussman, M. A. Fibronectin Is Essential for Reparative Cardiac Progenitor Cell Response After Myocardial Infarction. *Circulation Research* **2013**, *113* (2), 115–125. https://doi.org/10.1161/CIRCRESAHA.113.301152.

(244) Charest, J. L.; Eliason, M. T.; García, A. J.; King, W. P. Combined Microscale Mechanical Topography and Chemical Patterns on Polymer Cell Culture Substrates. *Biomaterials* **2006**, *27* (11), 2487–2494. https://doi.org/10.1016/j.biomaterials.2005.11.022.

(245) Xue, J.; He, M.; Liu, H.; Niu, Y.; Crawford, A.; Coates, P. D.; Chen, D.; Shi, R.; Zhang, L. Drug Loaded Homogeneous Electrospun PCL/Gelatin Hybrid Nanofiber Structures for Anti-Infective Tissue Regeneration Membranes. *Biomaterials* **2014**, *35* (34), 9395–9405. https://doi.org/10.1016/j.biomaterials.2014.07.060.

(246) Guex, A. G.; Frobert, A.; Valentin, J.; Fortunato, G.; Hegemann, D.; Cook, S.; Carrel, T. P.; Tevaearai, H. T.; Giraud, M. N. Plasma-Functionalized Electrospun Matrix for Biograft Development and Cardiac Function Stabilization. *Acta Biomaterialia* **2014**, *10* (7), 2996–3006. https://doi.org/10.1016/j.actbio.2014.01.006.

(247) Joanne, P.; Kitsara, M.; Boitard, S.-E.; Naemetalla, H.; Vanneaux, V.; Pernot, M.; Larghero, J.; Forest, P.; Chen, Y.; Menasché, P.; Agbulut, O. Nanofibrous Clinical-Grade Collagen Scaffolds Seeded with Human Cardiomyocytes Induces Cardiac Remodeling in Dilated Cardiomyopathy. *Biomaterials* **2016**, *80*, 157–168. https://doi.org/10.1016/j.biomaterials.2015.11.035.

(248) Mishra, R.; Vijayan, K.; Colletti, E. J.; Harrington, D. A.; Matthiesen, T. S.; Simpson, D.; Goh, S. K.; Walker, B. L.; Almeida-Porada, G.; Wang, D.; Backer, C. L.; Dudley, S. C.; Wold, L. E.; Kaushal, S. Characterization and Functionality of Cardiac Progenitor Cells in Congenital Heart Patients. *Circulation* **2011**, *123* (4), 364–373. https://doi.org/10.1161/CIRCULATIONAHA.110.971622.

(249) Rathod, R. H.; Powell, A. J.; Geva, T. Myocardial Fibrosis in Congenital Heart Disease. *Circulation Journal* **2016**, *80* (6), 1300–1307. https://doi.org/10.1253/circj.CJ-16-0353.

(250) Franz, S.; Rammelt, S.; Scharnweber, D.; Simon, J. C. Immune Responses to Implants – A Review of the Implications for the Design of Immunomodulatory Biomaterials. *Biomaterials* **2011**, *32* (28), 6692–6709. https://doi.org/10.1016/j.biomaterials.2011.05.078.

(251) Bouma, B. J.; Mulder, B. J. M. Changing Landscape of Congenital Heart Disease. *Circ Res* **2017**, *120* (6), 908–922. https://doi.org/10.1161/CIRCRESAHA.116.309302.

(252) Burkhart, H. M.; Qureshi, M. Y.; Peral, S. C.; O'Leary, P. W.; Olson, T. M.; Cetta, F.; Nelson, T. J. Regenerative Therapy for Hypoplastic Left Heart Syndrome: First Report of Intraoperative Intramyocardial Injection of Autologous Umbilical-Cord Blood–Derived Cells. *The Journal of Thoracic and Cardiovascular Surgery* **2015**, *149* (3), e35–e37. https://doi.org/10.1016/j.jtcvs.2014.10.093.

(253) Streeter, B. W.; Davis, M. E. Therapeutic Cardiac Patches for Repairing the Myocardium. In *Cell Biology and Translational Medicine, Volume 5: Stem Cells: Translational Science to Therapy*; Turksen, K., Ed.; Springer International Publishing: Cham, 2018; pp 1–24. https://doi.org/10.1007/5584_2018_309.

(254) Su, T.; Huang, K.; Daniele, M. A.; Hensley, M. T.; Young, A. T.; Tang, J.; Allen, T. A.; Vandergriff, A. C.; Erb, P. D.; Ligler, F. S.; Cheng, K. Cardiac Stem Cell Patch Integrated with Microengineered Blood Vessels Promotes Cardiomyocyte Proliferation and Neovascularization after Acute Myocardial Infarction. *ACS Applied Materials & Interfaces* **2018**, *10* (39), 33088–33096. https://doi.org/10.1021/acsami.8b13571.

(255) Chi, N.-H.; Yang, M.-C.; Chung, T.-W.; Chen, J.-Y.; Chou, N.-K.; Wang, S.-S. Cardiac Repair Achieved by Bone Marrow Mesenchymal Stem Cells/Silk Fibroin/Hyaluronic Acid Patches in a Rat of Myocardial Infarction Model. *Biomaterials* **2012**, *33* (22), 5541–5551. https://doi.org/10.1016/j.biomaterials.2012.04.030.

(256) Doron, G.; Klontzas, M. E.; Mantalaris, A.; Guldberg, R. E.; Temenoff, J. S. Multiomics Characterization of Mesenchymal Stromal Cells Cultured in Monolayer and as Aggregates. *Biotechnology and Bioengineering* **2020**, *117* (6), 1761–1778. https://doi.org/10.1002/bit.27317.

(257) Sack, K. L.; Davies, N. H.; Guccione, J. M.; Franz, T. Personalised Computational Cardiology: Patient-Specific Modelling in Cardiac Mechanics and Biomaterial Injection Therapies for Myocardial Infarction. *Heart Fail Rev* **2016**, *21* (6), 815–826. https://doi.org/10.1007/s10741-016-9528-9.

(258) Jung, J. P.; Hu, D.; Domian, I. J.; Ogle, B. M. An Integrated Statistical Model for Enhanced Murine Cardiomyocyte Differentiation via Optimized Engagement of 3D Extracellular Matrices. *Sci Rep* **2015**, *5* (1), 18705. https://doi.org/10.1038/srep18705.

(259) Hynes, R. O. Integrins. *Cell* **2002**, *110* (6), 673–687. https://doi.org/10.1016/S0092-8674(02)00971-6.

(260) Souders, C. A.; Borg, T. K.; Banerjee, I.; Baudino, T. A. Pressure Overload Induces Early Morphological Changes in the Heart. *Am J Pathol* **2012**, *181* (4), 1226–1235. https://doi.org/10.1016/j.ajpath.2012.06.015.

(261) Lopez, K. N.; Morris, S. A.; Sexson Tejtel, S. K.; Espaillat, A.; Salemi, J. L. US Mortality Attributable to Congenital Heart Disease Across the Lifespan From 1999 Through 2017 Exposes Persistent Racial/Ethnic Disparities. *Circulation* **2020**, *142* (12), 1132–1147. https://doi.org/10.1161/CIRCULATIONAHA.120.046822.

(262) Feinstein, J. A.; Benson, D. W.; Dubin, A. M.; Cohen, M. S.; Maxey, D. M.; Mahle, W. T.; Pahl, E.; Villafañe, J.; Bhatt, A. B.; Peng, L. F.; Johnson, B. A.; Marsden, A. L.; Daniels, C. J.; Rudd, N. A.; Caldarone, C. A.; Mussatto, K. A.; Morales, D. L.; Ivy, D. D.; Gaynor, J. W.; Tweddell, J. S.; Deal, B. J.; Furck, A. K.; Rosenthal, G. L.; Ohye, R. G.; Ghanayem, N. S.; Cheatham, J. P.; Tworetzky, W.; Martin, G. R. Hypoplastic Left Heart Syndrome. *Journal of the American College of Cardiology* **2012**, *59* (1), S1–S42. https://doi.org/10.1016/j.jacc.2011.09.022.

(263) Bejleri, D.; Davis, M. E. Decellularized Extracellular Matrix Materials for Cardiac Repair and Regeneration. *Adv Healthc Mater* **2019**, *8* (5), e1801217. https://doi.org/10.1002/adhm.201801217.

(264) Zhong, J.; Wang, S.; Shen, W.-B.; Kaushal, S.; Yang, P. The Current Status and Future of Cardiac Stem/Progenitor Cell Therapy for Congenital Heart Defects from

Diabetic Pregnancy. *Pediatr Res* **2018**, *83* (1–2), 275–282. https://doi.org/10.1038/pr.2017.259.

(265) Fleischer, S.; Feiner, R.; Shapira, A.; Ji, J.; Sui, X.; Daniel Wagner, H.; Dvir, T. Spring-like Fibers for Cardiac Tissue Engineering. *Biomaterials* **2013**, *34* (34), 8599–8606. https://doi.org/10.1016/j.biomaterials.2013.07.054.

(266) Salih, C.; Sheppard, M. N.; Ho, S. Y. Morphometry of Coronary Capillaries in Hypoplastic Left Heart Syndrome. *The Annals of Thoracic Surgery* **2004**, *77* (3), 903–907. https://doi.org/10.1016/j.athoracsur.2003.07.046.

(267) Padalino, M. A.; Castellani, C.; Toffoli, S.; Barbera, M. D.; Milanesi, O.; Thiene, G.; Stellin, G.; Angelini, A. Pathological Changes and Myocardial Remodelling Related to the Mode of Shunting Following Surgical Palliation for Hypoplastic Left Heart Syndrome. *Cardiol Young* **2008**, *18* (4), 415–422. https://doi.org/10.1017/S1047951108002461.

(268) Mendes, A. B. L.; Ferro, M.; Rodrigues, B.; Souza, M. R. de; Araujo, R. C.; Souza, R. R. de. Quantification of Left Ventricular Myocardial Collagen System in Children, Young Adults, and the Elderly. *Medicina (B Aires)* **2012**, *72* (3), 216–220.

(269) Welch, T. D.; Ling, L. H.; Espinosa, R. E.; Anavekar, N. S.; Wiste, H. J.; Lahr, B. D.; Schaff, H. V.; Oh, J. K. Echocardiographic Diagnosis of Constrictive Pericarditis: Mayo Clinic Criteria. *Circ Cardiovasc Imaging* **2014**, *7* (3), 526–534. https://doi.org/10.1161/CIRCIMAGING.113.001613.

(270) Flaig, F.; Ragot, H.; Simon, A.; Revet, G.; Kitsara, M.; Kitasato, L.; Hébraud, A.; Agbulut, O.; Schlatter, G. Design of Functional Electrospun Scaffolds Based on Poly(Glycerol Sebacate) Elastomer and Poly(Lactic Acid) for Cardiac Tissue Engineering. *ACS Biomaterials Science & Engineering* **2020**, *6* (4), 2388–2400. https://doi.org/10.1021/acsbiomaterials.0c00243.

(271) D'Amore, A.; Yoshizumi, T.; Luketich, S. K.; Wolf, M. T.; Gu, X.; Cammarata, M.; Hoff, R.; Badylak, S. F.; Wagner, W. R. Bi-Layered Polyurethane – Extracellular Matrix Cardiac Patch Improves Ischemic Ventricular Wall Remodeling in a Rat Model. *Biomaterials* **2016**, *107*, 1–14. https://doi.org/10.1016/j.biomaterials.2016.07.039.

(272) Hu, Y.; You, J.-O.; Aizenberg, J. Micropatterned Hydrogel Surface with High-Aspect-Ratio Features for Cell Guidance and Tissue Growth. *ACS Appl. Mater. Interfaces* **2016**, *8* (34), 21939–21945. https://doi.org/10.1021/acsami.5b12268.

(273) Feaster, T. K.; Cadar, A. G.; Wang, L.; Williams, C. H.; Chun, Y. W.; Hempel, J. E.; Bloodworth, N.; Merryman, W. D.; Lim, C. C.; Wu, J. C.; Knollmann, B. C.; Hong, C. C. Matrigel Mattress: A Method for the Generation of Single Contracting Human-Induced Pluripotent Stem Cell–Derived Cardiomyocytes. *Circulation*

Research **2015**, *117* (12), 995–1000. https://doi.org/10.1161/CIRCRESAHA.115.307580.

(274) Bharadwaj, M.; Strohmeyer, N.; Colo, G. P.; Helenius, J.; Beerenwinkel, N.; Schiller, H. B.; Fässler, R.; Müller, D. J. AV-Class Integrins Exert Dual Roles on A5β1 Integrins to Strengthen Adhesion to Fibronectin. *Nature Communications* **2017**, *8* (1), 14348. https://doi.org/10.1038/ncomms14348.

(275) Vagnozzi, R. J.; Maillet, M.; Sargent, M. A.; Khalil, H.; Johansen, A. K. Z.; Schwanekamp, J. A.; York, A. J.; Huang, V.; Nahrendorf, M.; Sadayappan, S.; Molkentin, J. D. An Acute Immune Response Underlies the Benefit of Cardiac Stem Cell Therapy. *Nature* **2020**, *577* (7790), 405–409. https://doi.org/10.1038/s41586-019-1802-2.

(276) Saha, P.; Sharma, S.; Korutla, L.; Datla, S. R.; Shoja-Taheri, F.; Mishra, R.; Bigham, G. E.; Sarkar, M.; Morales, D.; Bittle, G.; Gunasekaran, M.; Ambastha, C.; Arfat, M. Y.; Li, D.; Habertheuer, A.; Hu, R.; Platt, M. O.; Yang, P.; Davis, M. E.; Vallabhajosyula, P.; Kaushal, S. Circulating Exosomes Derived from Transplanted Progenitor Cells Aid the Functional Recovery of Ischemic Myocardium. *Sci Transl Med* **2019**, *11* (493). https://doi.org/10.1126/scitranslmed.aau1168.